5-2018

Numerical Simulation of Combustion in the Ironmaking Blast Furnace Raceway

Tyamo Okosun
Purdue University

NUMERICAL SIMULATION OF COMBUSTION IN THE IRONMAKING BLAST FURNACE RACEWAY

by

Tyamo Okosun

A Dissertation

Submitted to the Faculty of Purdue University

In Partial Fulfillment of the Requirements for the degree of

Doctor of Philosophy

School of Mechanical Engineering

West Lafayette, Indiana

May 2018

THE PURDUE UNIVERSITY GRADUATE SCHOOL
STATEMENT OF DISSERTATION APPROVAL

Dr. Chenn Q. Zhou, Chair
School of Mechanical Engineering

Dr. Jay P. Gore
School of Mechanical Engineering

Dr. Jun Chen
School of Mechanical Engineering

Dr. Tom I. Shih
School of Aeronautics and Astronautics

Approved by:

Dr. Jay P. Gore
Head of the Departmental Graduate Program

To Dad, who made this possible.

ACKNOWLEDGMENTS

I am indebted to my advisor, Prof. Chenn Q. Zhou, for her continually guidance throughout much of my undergraduate and graduate studies. I would like to express my sincere gratitude to Prof. Jun Chen, Prof. Jay P. Gore, and Prof. Tom Shih for serving on my advisory committee. I would also like to acknowledge the late Prof. Sanford Fleeter, who served on my advisory committee for several years before his passing.

I must thank my parents for all of their support over the many years of my studies. There are not enough words to adequately express my gratitude for just how much they have given. I would like to thank all of my present and past colleagues and friends from the Center for Innovation through Visualization and Simulation (CIVS) at Purdue University Northwest for their support and friendship, including Steve Dubec, Nick Walla, Jack Moreland, Bin Wu, Jichao Wang, Don Lail, Luke Phillips, and many more. I would also like to thank Dr. Dong Fu for his insight into blast furnace modeling, and Dr. Armin Silaen for his input to the many aspects of this research.

I must also extend a special thank you to Dr. Stuart J. Street of AK Steel. Without his continual input and conversation, this research would have been considerably less impactful. Finally, I would like to acknowledge support from the collaborators at AK Steel, ArcelorMittal, U.S. Steel, Stelco Inc., Praxair, Union Gas, Cliffs Natural Resources, Steel Dynamics Inc., NIPSCO, NUCOR, SSAB, and other supporters of the Steel Manufacturing Simulation and Visualization Consortium (SMSVC) throughout the course of this research.

TABLE OF CONTENTS

LIST OF TABLES

LIST OF FIGURES

NOMENCLATURE

Symbol	Description
a_P	Variable coefficient at computational cell center
a_E	Variable coefficient at computational cell east
a_W	Variable coefficient at computational cell west
a_N	Variable coefficient at computational cell north
a_S	Variable coefficient at computational cell south
a_T	Variable coefficient at computational cell top
a_B	Variable coefficient at computational cell bottom
A_p	Particle surface area [m^2]
A, B	Pre-exponential factors [s^{-1}]
a	Specific surface area of coke [m^2/kg]
A, B, C	Cell surface areas [m^2]
B_i	Rate constant [s^{-1}]
C_μ,σ_k,σ_ε,$C_{1\varepsilon}$, and $C_{2\varepsilon}$	Constants for the k-ε turbulence model
C_p	Particle heat capacity [J/K or $(kg \cdot m^2)/(K \cdot s^2)$]
C_D	Coefficient of drag
C_{ps}	Heat capacity of the particle phase [J/kg·K]
C_i	Instantaneous concentration of coke [$kmol/m^3$]
d_p	Particle diameter [m]
E_i	Activation energy [kcal/mole]

e_{bgp}	Sum of emitted intensities for gas and particles [W·s/sr]
F	Additional acceleration term in particle force balance [m/s^2]
$F_D(\vec{u} - \overrightarrow{u_p})$	Drag force per unit particle mass [N/kg or m/s^2]
$F_{gas,} F_p$	External body force term (gas and particle) [N/m^3]
$F_{vm,gas}$, $F_{vm,p}$	Virtual mass force term (gas and particle) [N/m^3]
$F_{td,gas}$, $F_{td,p}$	Turbulent dispersion force term (gas and particle) [N/m^3]
$G_{k,m}$	Production of turbulence [J/kg·s]
G_R	Turbulent energy generation due to mass change of particle [J/kg·s]
G_p	Destruction or production term for turbulent kinetic energy [J/kg·s]
h	Convective heat transfer coefficient [W/m^2·K]
I_m	Radiation intensity in the direction Ω_m [W·s/sr]
I_s	In-scattering source term [W/sr]
k	Turbulent kinetic energy [J/kg or m^2/s^2]
K_{gs}, K_{sg}	Gas-solid momentum exchange coefficient [kg/(m^3·s)]
k_{fi}	Mass transfer coefficient [kg/(kmol·s)]
k_{mi}	Chemical rate constant
k_{ext}	Extinction coefficient [m^2/kg]
k_{ag}	Gas absorption coefficient [m^2/kg]
k_{ap}	Particle absorption coefficient [m^2/kg]
k_s	Particle scattering coefficient [m^2/kg]
m_p	Particle mass [kg]

m_{wc}	Moisture evaporation rate [kg/s]
$m_{c,i}$	Consumption rate of coke reaction *i* [kg/m^3·s]
Nu_p	Particle Nusselt number
P_{gas}	Gas phase pressure [Pa]
Q_{vap}	Heat of vaporization for water [J/kgH_2O]
R	Universal gas constant [J/(mol·K)]
Re	Relative Reynolds number
Re_p	Granular/particle phase particle Reynolds number
S_ϕ	General source term
$S_{\phi p}$	General source term for particle phase
Sh	Sherwood number
T_∞	Continuous phase temperature near particle [K]
T_p	Particle temperature [K]
T_m	Average temperature of gas/coke mixture [K]
$\vec{u}_i, \vec{v}_i, \vec{w}_i$	Components of phase *i* velocity [m/s]
$\vec{u}_i^t, \vec{v}_i^t, \vec{w}_i^t$	Fluctuating components of phase *i* velocity due to turbulence [m/s]
V_{rs}	Ratio of terminal velocity of a group of particles to that of an isolate particle
w_{EBU}	Reaction rate from Eddy Breakup Model [kg/m^3·s]
w_{Arr}	Reaction rate from Arrhenius rates [kg/m^3·s]
W_s	Combined reaction rates of EBU and Arrhenius [kg/m^3·s]
w_i	Angular quadrature weight

Y_i	Species mass fraction
$Y_{H2O,p}$	Water vapor mass fraction at coal particle surface
α_i	Volume fraction of phase *i*
β_{gc}	Gas-solid momentum exchange coefficient [kg/(m^3·s)]
Γ	Effective diffusivity [m^2/s]
Γ_t	Turbulent (eddy) diffusivity [m^2/s]
δ_{ij}	Kronecker delta
$(\delta x)_i$, $(\delta y)_i$, $(\delta z)_i$	Distances between cell nodes [m]
Δx, Δy, Δz	Cell length, height, and width [m]
ε	Turbulence dissipation rate [J/kg·s or m^2/s^3]
η_i	Effectiveness factor of catalytic reaction [m^3/(kmol·s)]
λ_{gas}	Bulk viscosity of the gas phase [Pa·s or kg/(m·s)]
λ_p	Thermal conductivity [W/(m·K)]
ϕ	General transported property
ϕ^t	Fluctuating component of general transported property due to turbulence
μ_t	Turbulent (eddy) viscosity [Pa·s or kg/(m·s)]
μ_{gas}	Shear viscosity of the gas phase [Pa·s or kg/(m·s)]
μ_m	Mixture viscosity [Pa·s or kg/(m·s)]
$\mu_{t,m}$	Mixture turbulent (eddy) viscosity [Pa·s or kg/(m·s)]
μ_m, η_m, ξ_m	Direction cosines for Ω_m
ρ	Density [kg/m^3]

ρ_i	Density of phase *i* [kg/m^3]
ρ_{eff}	Effective density [kg/m^3]
ρ_m	Mixture density [kg/m^3]
ρ_{bc}	Bulk density of coke bed [kg/m^3]
τ_i	Stress tensor of phase *i* [N/m^2]
τ_p	Particulate relaxation time [s]
Ω_m	Discrete angular direction

ABSTRACT

Author: Okosun, Tyamo. Ph.D.
Institution: Purdue University
Degree Received: May 2018
Title: Numerical Simulation of Combustion in the Ironmaking Blast Furnace Raceway.
Major Professor: Chenn Q. Zhou

As almost all conversion of raw iron ore to pig iron at the start of the ironmaking process currently takes place in a blast furnace, these furnaces remain a critical component in the iron and steelmaking industry. Enhancements in the efficiency of blast furnace operation have a significant effect on industrial energy consumption, as the process represents nearly 70% of the total energy consumption of the iron and steelmaking process. Over the past several decades, auxiliary fuel injection has been adopted as a method of reducing the total amount of coke necessary for furnace operation. Coke making is both energy intensive and environmentally unfriendly, and as such, any reduction in coke usage by the blast furnace is positive for the iron and steelmaking industry. However, the intricate variations in blast furnace raceway conditions and injected fuel combustion characteristics due to the method and conditions at which auxiliary fuels are injected into the furnace are still not fully understood.

The goal of this research is to utilize computational fluid dynamics (CFD) modeling to provide a deeper level of understanding of the complex relationships between blast furnace injection system designs and operating conditions on the combustion processes and phenomena within the raceway. In this vein, a multi-stage 3-D CFD model has been developed and applied to simulate combustion phenomena within several industrial blast furnace raceway regions. The three primary components of focus in this research are the tuyere and injection apparatus, raceway formation, and raceway combustion. A comprehensive CFD methodology for simulation operating conditions and combustion within the blast furnace raceway has been developed. This methodology utilizes CFD modeling to simulate conditions within the raceway region. A revised raceway formation model has been developed to better correspond to industrial observations, and new methodology for analysis and presentation of simulation results from these models have been developed. The models have been validated against industrial observation and measurements from three currently

operating industrial blast furnaces. The models have also been utilized to examine varied operating conditions in the aforementioned furnaces.

Two new methods of exploring raceway gas temperature using simulation modeling were developed in this research, namely a Topographical Flame Temperature (TOFT) and a Raceway Adiabatic Flame Temperature (RAFT) analogue. These methods allow for both better validation of computational modeling results against industrial observation and measurement, as well as providing a new path to explore raceway gas temperature distribution under unique conditions, including extremely high natural gas injection rates, which may present potential for significantly improving the economic and operational efficiency of the furnace.

The analyses of industry blast furnaces provide significant insight into the effects of injection conditions and apparatus designs upon combustion characteristics and reaction phenomena within the raceway. Previously unexplored novel fuel injection techniques were explored within this research, and simulations have indicated that injected fuel burnout rates could be improved by as much as 23% in specific scenarios and production could be increased by roughly 2.5%. While a switch to these injection techniques may pose some difficulties in practice, industrial project partners have already begun trials for implementation on a full-scale furnace.

Finally, this modeling revealed significant potential benefits to blast furnace operation through modification of natural gas and pulverized coal injection locations, pulverized coal carrier gas type, injection lance tip design, and other parameters. While these exact parameters cannot be implemented identically across all plant furnaces, they provide a baseline of fundamental understanding from which furnace operators and engineers can draw in their ongoing attempts to optimize combustion efficiency and reduce operational expenditures.

CHAPTER 1. INTRODUCTION

1.1 The Blast Furnace

Despite recent advances in processes throughout the iron and steelmaking industry, such as the advent of more efficient direct reduction ironmaking (DRI) technologies and the widespread application of electric arc furnaces (EAFs) to mini-mills, the blast furnace is still crucial to a majority of all ironmaking in the United States. A significant fraction of pig iron generated through the conversion of iron ore is made in blast furnaces, due to the robust nature of the process and how deeply ingrained it is within traditional steel mills. However, it is energy intensive, and operation of a blast furnace incurs significant capital expenditures, including maintenance, fuel, and raw material costs.

The blast furnace is a countercurrent moving packed bed chemical reactor designed with the purpose of reducing iron ore to liquid iron. This process involves various complex chemical reactions and flow phenomena that present a variety of unique challenges to experimentation and numerical modeling alike. During operation, the materials that make up the packed bed, namely pelletized iron ore, a processed form of coal known as coke, and various fluxes, are charged into the furnace in alternating layers. Below these layers, which are referred to as the burden, preheated air, referred to as the hot blast, is driven into the coke in the lower portion of the furnace through a ring of nozzles along the furnace annulus named tuyeres.

Within the cavities formed by the hot blast in the packed bed, known as raceways, coke combustion takes place, gasifying carbon and generating heat for furnace operation. Temperatures in this region of the furnace often exceed 2,000 ˚C, and the combustion process generates significant amounts of carbon monoxide (CO) gas. This reducing gas reacts with the oxygen present in the iron ore, removing it. As the ore is reduced, it descends through the furnace and its temperature rises. The material begins to melt at roughly 1,500 ˚C, and it drips through the packed coke bed to the furnace hearth, where it amasses into layers of ‘hot metal’ (liquid iron) and slag. The area in which this process begins to occur is called the cohesive zone, owing to the fact that the ore pellets within begin to coalesce, forcing gas flow through coke slits between the ore layers. After dripping

through the coke bed below the cohesive zone and reaching the hearth, liquid can then be removed from the furnace through the taphole and processed further to achieve the required chemical compositions. A diagram detailing the general flow patterns, inputs, and regions of a generic blast furnace is presented in Figure 1.

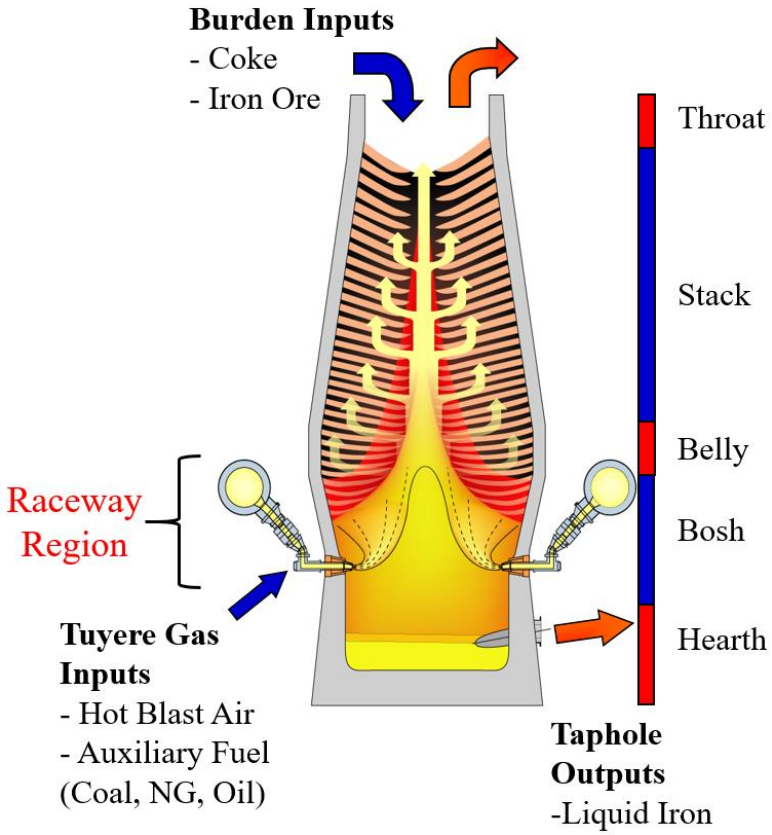

Figure 1. General schematic of the blast furnace process [1].

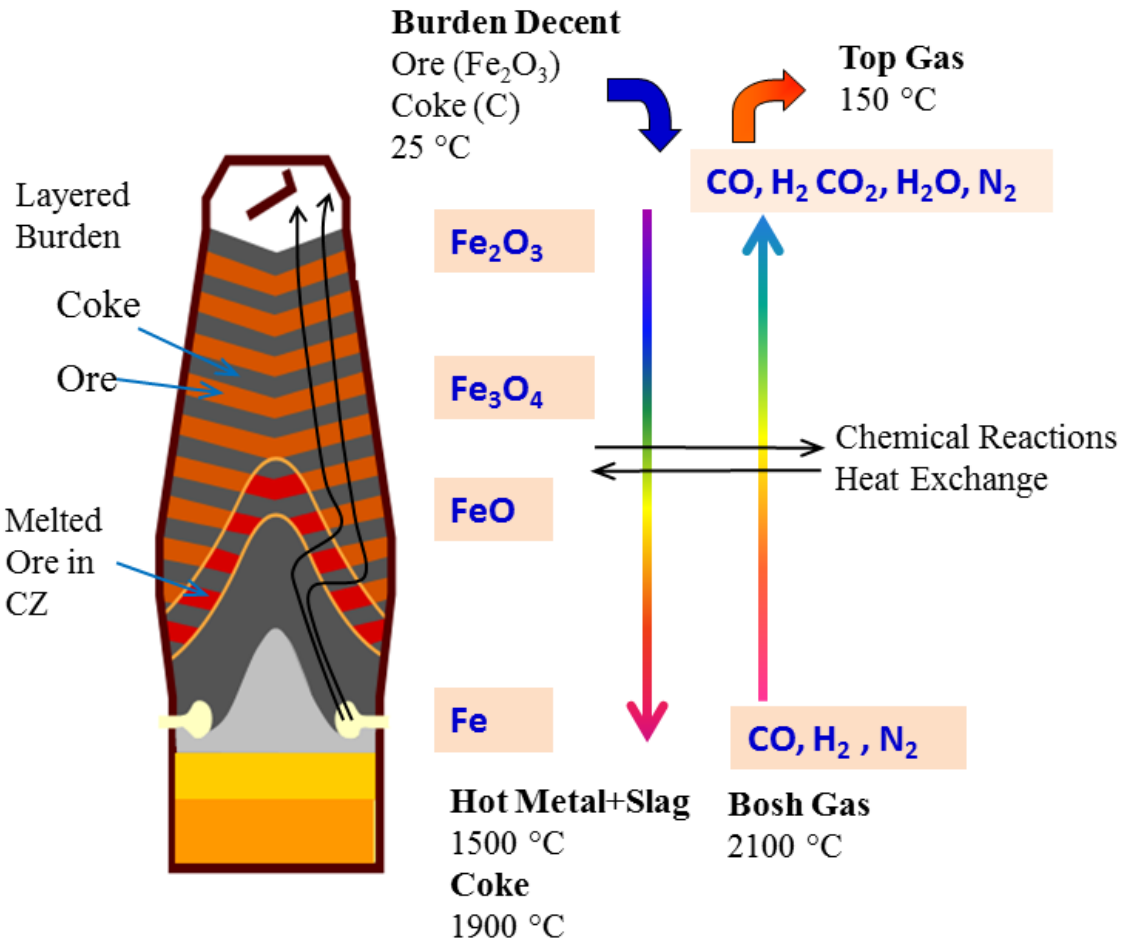

Figure 2. Countercurrent moving bed in blast furnace [1].

The distribution of solid materials within the blast furnace has a significant effect on gas flow patterns, as well as on the shape and location of the cohesive zone. These factors all have an impact upon the fuel economy, productivity, and stability of blast furnace operations. Reductions in fuel consumption rates result in energy and cost savings for furnace operators and reduce furnace emissions by significant amounts.

In addition to the hot blast, various types of auxiliary fuels, such as pulverized coal (PC), natural gas (NG), and fuel oil, are often injected into the blast furnace raceway. The combustion of these auxiliary fuels contributes to the generation of heat and reducing gases necessary for furnace operation, allowing for the replacement of varying amounts of coke. Coke has been integral to ironmaking within blast furnaces since the inception of the process. However, the creation of coke

from coal is an expensive and time-consuming activity with significant environmental impacts. In an effort to reduce coke consumption, the ironmaking industry began to adopt additional focus on injected fuels, beginning with pulverized coal injection (PCI) in the 1960s. PCI has been widely implemented throughout the ironmaking industry, and a significant fraction of blast furnaces operating today utilize some form of auxiliary fuel injection [2,3].

Recently, with the increased availability of natural gas in North America, the ironmaking industry within the United States has begun to explore the possible benefits of co-injecting natural gas and pulverized coal [4]. Based on available benchmarking data provided by the Association for Iron and Steel Technology (AIST), nearly 48% of all North American blast furnaces operated using the co-injection of natural gas and pulverized coal in 2015, with an average total fuel injection rate of 128 kilograms of injected fuel per metric ton of hot metal produced.

As previously mentioned, this injected fuel can partially take the place of coke for generating heat and reducing gases in the furnace. However, several difficulties can arise with the use of high rates of PCI. Reducing the total amount of coke charged into the furnace results in thinner coke layers within the burden. As coke has a higher permeability than ore layers, this can increase the overall gas resistance in the upper parts of the blast furnace. Additionally, as the PCI rate is increased, unburned char and particulate fines can build up within the coke bed, leading to reduced permeability and furnace instability.

When properly implemented, auxiliary fuel injection has positively affected blast furnace reduction gas utilization, furnace energy consumption, and operational efficiency. The amount of coke that can be replaced with a given amount of auxiliary fuel, known as the coke replacement ratio, is influenced by a wide variety of factors. With this in mind, researchers have placed heavy focus on the analysis of auxiliary fuel injection techniques.

The reaction phenomena taking place within the blast furnace raceway generate an extremely inhospitable environment (temperatures in excess of 2,500 ˚C) in which taking accurate measurements can prove extremely difficult. Direct measurement techniques are often entirely impossible within the raceway itself, leading to a lack of specific knowledge regarding the

characteristics of combustion inside. Because of this, studies investigating PCI combustion are typically limited to the use of either laboratory-based experimentation on simplified models or Computational Fluid Dynamics (CFD) simulation [5]. CFD modeling is often far less expensive to undertake than physical experimentation on test rigs in a laboratory, and advances in computer technology continue to allow for more direct examination of the extreme conditions within the blast furnace raceway. CFD can provide detailed data regarding fluid flow, heat transfer, and chemical reactions in the kinds of complex multi-phase flows observed within the raceway, allowing for the completion of parametric studies examining the effects of various factors upon the combustion characteristics within the raceway envelope. These studies can be utilized to investigate the effects of design and operational parameters involving auxiliary fuel injection, in an effort to enhance the positive impact of auxiliary fuel use on blast furnace performance and energy efficiency.

1.2 Literature Review

1.2.1 Experimental Blast Furnace Raceway Region Research

The primary goal of the blast furnace process is the reduction of iron ore into liquid iron. In order to accomplish this, reducing gases must first be generated in oxidizing zones at the lower regions of the furnace. These raceways are extreme environments containing high temperature gases, combustion reactions, and turbulent flow patterns. Inside, oxygen from the hot blast air reacts with coke and injected fuels to produce heat and reducing gases that then rise through the coke bed to supply the rest of the furnace. Because of its integral nature to the performance of the furnace, there is a long history of research regarding the furnace raceway region.

Studies of the reactions and combustion processes inside the raceway date back to as early as the late 1800s, and experimental analysis of the process has continued to the present day. However, despite this long history of research, there is still a lack of knowledge regarding parameters of the raceway, including shape and depth, and there is often poor understanding of the complexities of the processes that occur within the raceway envelope [6]. Industrial practice holds that coke particles recirculate inside the raceway with gas flow patterns in both horizontal and vertical axes, however, the exact size and position of this recirculation is unknown, and varies with furnace

geometry, operating conditions, and raw material inputs. Examinations of raceway properties have been conducted, with tests on both cold flow models and pilot plants revealing details regarding the natural transient variations in the raceway size [7]. Experimental studies and industrial practice have provided steady improvements in knowledge regarding the raceway, allowing operators to optimize operations over nearly a century and a half of use.

As PCI has become a more popular practice in blast furnace operation to reduce coke usage, research has begun to focus on establishing a fundamental understanding of the effects of auxiliary fuel injection on raceway combustion characteristics. Early research includes studies focusing on the variation of coal type, particle size, blast temperature, and injection lance position in scale test rigs [8,9]. Observations from these studies indicated that the flow pattern of pulverized coal particles after exiting the lace have a significant influence on combustibility. Studies have also been conducted on various methods of enhancing pulverized coal combustion through oxygen enrichment, novel fuel mixtures, pulverized coal grind size, pulverized coal grade, and other parameters [10]. In the late 1990s, a wide range of other research projects were undertaken by both academia and industry research teams with the intent of improving injected fuel combustion, though these studies focus primarily on the process-scale impacts of various injection technologies and fundamental understanding of PCI combustion characteristics was still somewhat limited [11-14].

Near the turn of the century, research projects were conducted regarding the possibility of injected alternative fuels in addition to pulverized coal. The most widely adopted co-injected fuel was natural gas. In contrast to injected solids, natural gas presents advantages related to ease of injection and maintenance of injection systems, as well as reduction in ash and other particulate loading in the raceway and coke bed. The development of co-injection practices revealed potential operational pitfalls relating to the high temperatures and temperature gradients experienced by injection apparatuses, as well as the possibility for abrasive wear due to solid substances in gas flows [15]. Recently, analyses of the effects of NG-PC co-injection in blast furnaces have been conducted, with particular focus on cost-effectiveness [16].

Additionally, research has indicated that placement of injection lances is critical to combustion efficiency and stability when dealing with co-injection designs [17-19]. In an effort to further enhance the benefits of natural gas injection, novel injection techniques have been proposed, such as heating injected natural gas by passing the flow through the cooled cavities of tuyere elements [20]. The theoretical benefits of such proposals are not insignificant; however, the ironmaking industry is often understandably reluctant to adopt these new approaches without significant data indicating a positive benefit to operations.

1.2.2 Numerical Blast Furnace Raceway Region Modeling

1.2.2.1 Pulverized Coal Injection

As the twenty-first century began, computational methods and technology had advanced to a state at which modeling of auxiliary fuel injection apparatuses had become possible. Early models made significant assumptions regarding flow physics and geometry, with many simulations focusing exclusively on one or two-dimensional representations of the raceway [21]. Some of the earliest attempts to model raceway conditions were conducted with the assumption of one-dimensional plug flow within the tuyere and raceway, ignoring mixing between pulverized coal particles and gas [2,22]. Two-dimensional modeling of the raceway was more advanced; however, turbulent features of the gas flow field were typically either ignored [23] or simplified [21], and the inherent limitations of working in two dimensions precludes the examination of complex geometries.

Specific techniques for the simulation of coal particles in multiphase flow regimes have been undertaken in focused, simplified geometries in an effort to enhance the accuracy and efficiency of numerical modeling. Studies of the combustion of pulverized coal within a tube-shaped combustor were conducted using an Eulerian treatment of both gas and particle phases, with allowances made for mass transfer due to moisture evaporation, devolatilization, and char reactions. This model was used to simulate 2-D gas-particle flows and was validated against experimental measurement results. The model indicated that smaller coal particles are heated and devolatilized more rapidly in the aforementioned combustor [24].

Through the early 2000s simulations were expanded to focus on three-dimensional numerical models of injected fuel combustion in the raceway. These studies began to examine the effects that

PCI has upon blast furnace operation, both positive and detrimental. Phenomena examined include coal particle flow, raceway residence time, with attention paid to examining the effects of coal particle size, coal injection rate, oxygen enrichment levels, and other factors [25].

One of the earliest mathematical studies examining the effects of pulverized coal and natural gas co-injection was conducted using a purely theoretical furnace design, not representative of any industrial furnace. Results focused on the operational impacts of a proposed co-injection setup on furnace operation, given a broad variety of assumptions regarding the materials considered and furnace operating regimes. Details such as productivity variations, silicon content, gas temperatures, coke rates, and carbon emissions were examined [26]. The authors of this research indicate that the mixing of natural gas and hot blast within the tuyere is critical to the efficiency of combustion.

The advancement of computer technology began to allow for more complex three-dimensional mathematical models of multiphase flow patterns, combustion, and heat transfer phenomena in the mid-2000s. An investigation of pulverized coal injection based on Mittal Steel's IH7 furnace was conducted in 2006 [27]. This model developed was capable of simulating pulverized coal transport, heat transfer, coal devolatilization, char combustion, and other parameters at varying hot blast temperatures and coal injection rates. It also provides additional capabilities for simulating more complex geometries, such as different lance configurations.

The late 2000s saw the publication of an increasing number of studies using numerical modeling techniques to simulate injected fuel combustion in the blast furnace blowpipe, tuyere, and raceway region. As numerical modeling grew more accurate and less computationally expensive, it began to supplant some of the more expensive procedures involved in experimental measurement of the harsh conditions within the blast furnace raceway environment [28,29].

1.2.2.2 Co-injection and Other Auxiliary Fuel Studies

As previously mentioned, various experimental studies have revealed possible benefits related to the co-injection of pulverized coal with additional oxygen and other auxiliary fuels. However, the complexities of co-injection and auxiliary fuel combustion both in the tuyere and the raceway are

not yet fully understood. Numerical modeling provides a method by which flow field interaction, turbulence, mixing, reaction rates, and other factors can be examined with specific focus on the influence of wide-ranging design and operational parameters.

A common implementation of CFD simulation to injected fuel analysis is troubleshooting. Numerical modeling has been utilized to supplement plant trials on a full-scale industrial furnace undertaken at Dofasco Steel, regarding a switch from single to dual oil injection lances [30]. After seven months, the plant trials were terminated due to a blowpipe refractory failure, and CFD modeling of the blowpipe and tuyere region was used to investigate the possibility of overheating associated with the new lance designs from the trial. This modeling did not include the raceway outside the tuyere, likely due to the level of computing power available for the project.

Simulations of the tuyere region of a blast furnace at Stelco Inc. Hamilton Works provided insight into the interactions between natural gas, pulverized coal, and pure O_2 during a range of standard operating conditions [31]. This study indicated that the location of the natural gas lance introduced a swirl effect in the gas flow inside the tuyere, possibly modifying fuel/air mixing. Further simulation studies on this furnace examined the effects of modifying parameters such as carrier gas flow rate, co-axial lance O_2 injection rate, blast temperature, and natural gas flow rate [32]. Additionally, this study expanded the computational domain to include the blast furnace raceway. It was reported that oxygen flow through the annular lance surrounding the pulverized coal plume can hinder coal combustion, as the coal particles are insulated from heating by the hot blast and natural gas plume.

Research has also been conducted in combined numerical/experimental stages, with CFD simulation being supported by and compared to experiments in pilot scale test rigs. Investigations conducted at Bluescope Operations indicated that numerical modeling could provide accurate prediction of pulverized coal combustion for many types of coal when simulating the test rig geometry [33]. A single co-axial lance was used to inject coal particles and oxygen, and several parameters were varied, including lance design, blast parameters, and coal type and grind. An examination was also made of the effects of tuyere length upon coal combustion and gas flow patterns. Lance design modifications were found to have a significant impact upon the segregation

of coal particles within the plume, and designs that enhanced particle dispersion resulted in higher levels of combustion in the raceway. Further exploration of this injection rig was conducted in a secondary project, with special focus on the effectiveness of lance tip design modifications [34]. Additionally, the CFD model was used to examine an issue of buildup inside the tuyere related to an increase in coal ash content in the Bluescope furnaces.

Further work regarding the Bluescope furnaces reports on a comparison of process parameters and their influence on coal combustion [35]. Parameters studied include coal size and type, blast temperature, and blast oxygen content. Once again, a co-axial lance was utilized. Two different methods were used to calculate total fuel consumption over the computational domain, one which only looked at the portion of the edge of the raceway in line with the tuyere axis, and the other which used the entire outer boundary of the raceway to calculate fuel burnout.

A recent analysis of natural gas and pulverized coal co-injection in the blowpipe and tuyere region examined the potential benefits of unique lance designs with respect to the costs incurred through the development and implementation of such lances [36]. Further examination of this work explored varied lance tip designs and configurations, including a single lance vs. dual lance design comparison [37]. Additional recent studies have explored the concept of coal injection methods using oxy-coal injection and cooling gases for improving injected fuel burnout and allowing for higher PCI rates [38,39].

Also of note is the work that has been done over the past several decades relating to raceway formation. Some efforts focused on developing basic relationships between gas flow velocities and raceway size using physical models and testing [40,41]. Other efforts assumed a spherical raceway shape, allowing for studies based on momentum balancing to predict the total size of the raceway envelope [42,43]. More recently, several research projects regarding raceway shape and size have been undertaken using two-phase Eulerian-Eulerian CFD modeling [44,45].

1.3 Research Objectives

This research has six primary objectives.

1. To develop and revise 3-D CFD models of gas flow, raceway formation, and chemical reactions under different hot blast and injection conditions and furnace geometries.
2. To develop a new method for presenting the spatial variations in raceway flame temperature, as an alternative to the industry standard Raceway Adiabatic Flame Temperature (RAFT) calculation.
3. To develop a new method for determining an analogue to RAFT from simulation modeling results to use for comparison with industrial data and simulation validation.
4. To utilize the aforementioned CFD models to analyze the feasibility and efficacy of previously unexplored techniques for blast furnace operation, and provide enhanced designs and operating conditions for adoption of such techniques at an industrial blast furnace.
5. To establish enhanced operating conditions for injection apparatuses in the blast furnace through numerical simulation by varying auxiliary fuel injection rates, lance designs, injection position within the tuyere, and injection methods, and to highlight specific guidelines that can lead to improved operation with respect to the influences of various parameters on combustion characteristics within the tuyere/raceway region of the blast furnace.
6. To develop practices and operating conditions with the aim of minimizing wear and degradation experienced in industrial blast furnaces with regards to the auxiliary fuel injection system, and by extension reduce required maintenance downtime.

1.4 Assessment of Benefits

As a carbon intensive process, consuming coke, pulverized coal, natural gas, and other hydrocarbon based fuels, the blast furnace has significant CO_2 emissions. Most of the carbon introduced into the furnace through either the burden or fuel injection will be transformed into gaseous form and will be released through the top of the furnace. The remainder of the carbon in the process is dissolved into the hot metal, and will be refined in various downstream processes in the steelmaking plant.

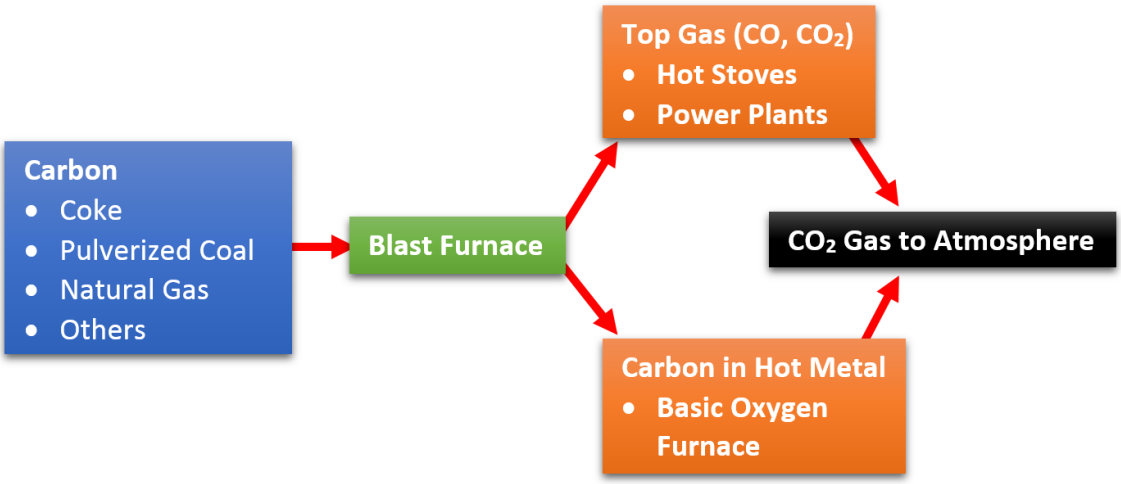

Figure 3. Carbon in the blast furnace process.

At the most simplistic level, mass and energy balance determines the total rate of carbon consumption by the blast furnace. The heat generated via carbon combustion is utilized to provide energy for the reactions in the furnace stack, such as the melting of hot metal and the direct reduction of FeO. Additionally, there must be enough carbon monoxide (and hydrogen gas in co-injection cases that utilize natural gas injection) generated through combustion for the indirect reduction reactions of Fe_3O_4 and Fe_2O_3. Reducing the overall furnace carbon rate will reduce CO_2 emissions while simultaneously reducing the operational cost of the blast furnace process.

With this in mind, the key benefit of increasing injected fuel rates has to do with coke replacement. Coke making is a process through which low-ash, low-sulfur bituminous coal is converted into a high-carbon content fuel through destructive distillation. This process requires the heating of coal to extremely high temperatures so that large molecules begin to break down. In addition to reducing the release of toxic gases from the coke making process, the energy saved through replacing coke with injected fuels is significant from an economic perspective. However, efficient coke replacement relies heavily on optimization of injected fuel combustion, so as not to waste carbon or energy. Un-combusted carbon will eventually exit the furnace dissolved into the hot metal, and will be released as CO_2 after processing in the Basic Oxygen Furnace and other downstream portions of the steelmaking process. Furnace operators also see un-combusted carbon as a negative because it is in essence nothing more than wasted fuel.

Raising the auxiliary fuel injection rate is of interest to industrial blast furnace operators, as it reduces total operating costs and helps to meet emissions standards. However, complications related to high PCI rates have been recognized throughout the industry, and in order to circumvent these difficulties, a better understanding of injected fuel combustion inside the raceway is required. Unique methods have been proposed to increase fuel injection, but without a full understanding of the effects that these proposed designs and operating conditions could have upon reaction conditions within the raceway, enthusiasm for direct implementation is often limited.

The CFD modeling work conducted in this research has been used to examine the details of auxiliary fuel combustion characteristics within the tuyere and raceway. CFD modeling techniques and methodology have been developed and implemented to simulate the phenomena within an active industry-scale blast furnace raceway. Simulations have explored a number of novel concepts regarding blast furnace auxiliary fuel injection and their effects upon furnace operation. A new technique for conveying pulverized coal into the furnace using natural gas instead of carrier air or nitrogen was developed, with modeling predicting a 23% increase in injected fuel burnout and a potential increase in productivity of 2.5% from application to an industry-scale blast furnace.

Additionally, research explored the influence of high natural gas injection rates on gas species and temperature distribution within the furnace raceway, with an eye towards improving understanding of the limitations preventing higher levels of natural gas injection. The replacement ratio of natural gas typically starts around 1 kg of gas per 1.05 kg of coke and decreases as the injection rate of gas increases. Better understanding of raceway conditions under high rates of natural gas injection are necessary to maintain or even increase this replacement ratio. For a typical North American blast furnace operating at 5,500 MTHM/day (metric tons of hot metal per day), with a coke rate of 390 kg/MTHM, a PC rate of 90 kg/MTHM, and a NG injection rate of 60 kg/MTHM, a shift in replacement ratio from 1-1.05 to 1-1.3 would result in 15 kg/nthm in coke savings. At a coke price of $225/metric ton, this equates to roughly $8.2 million in annual savings for a single blast furnace.

Additionally, visualization of the blast furnace raceway in this research led to the development of a new method for examining raceway flame temperature through the use of a topographical distribution as opposed to a single value as represented by standard industrial Raceway Adiabatic

Flame Temperature (RAFT) calculations. These newly proposed techniques can provide the industry with tools for operator training and further furnace analysis, including the development of clear pathways toward stable and efficient fuel injection. Additionally, improved understanding of combustion within the raceway highlights future avenues for potential furnace operational optimization.

CHAPTER 2. CFD MODELS

Modeling of the blast furnace raceway is conducted using two sub-models. One focuses on phenomena near the blowpipe, tuyere, and injection lances, while another models the formation of the blast furnace raceway and combustion inside the raceway envelope. Many CFD studies assume a pre-defined size and shape for the raceway geometry before proceeding to calculate combustion reactions, gas flow patterns, temperature distributions and other parameters within the envelope. Instead, the raceway sub-model and methodology developed and utilized in this research calculates the raceway size and shape to better represent the influence of changing operating conditions on flow and combustion phenomena. A robust methodology is utilized to integrate the CFD sub-models into a single simulation technique.

2.1 CFD Model for Blowpipe, Injection Lances, and Tuyere

2.1.1 General Description and Model Assumptions

There are a variety of complex phenomena taking place within the blast furnace blowpipe-tuyere region. Additionally, the geometry and relative positioning of the injection lances, tuyere, and blowpipe can vary significantly between blast furnaces. With this in mind, the comprehensive CFD model must be capable of accurately representing 3-D turbulent multi-phase flow, heat transfer between high temperature gases, lance walls, injected gases, and solid coal particles, and the initialization and continuation of coal and natural gas combustion inside the tuyere.

The following general assumptions were made in the development of this model:

1. As conditions within this zone are typically held constant for long periods of time during standard operation, a steady-state simulation approach was used for the flow inside the blowpipe and tuyere.
2. Conditions are typically identical between tuyeres inside the blast furnace, and a simulation of a single tuyere can be used to represent conditions throughout the furnace.
3. Solid particles of pulverized coal are treated as a Lagrangian discrete phase.
4. A pre-defined size distribution is adopted for coal particles based on industrial coal sizing data, and all coal particles are assumed to be spherical.

5. Radiative heat flux from the inside the raceway is represented through a specified radiative boundary condition at the tuyere exit.

2.1.2 Governing Equations and Phenomenological Models

As the average Reynolds number for flow within the blast furnace tuyere and raceway is quite high, the entirety of the flow domain is in the turbulent regime. Therefore, gas flow conditions in this research are calculated based on the Reynolds-averaged Navier-Stokes (RANS) equations. The RANS equations account for the randomized variations of flow properties due to turbulence via the Reynolds stresses term introduced by decomposing flow properties into mean and fluctuating components. The generalized form of this equation is as follows:

$$\nabla \cdot (\rho \phi u) = \nabla \cdot \left(\Gamma_{\phi} \nabla \phi\right) - \nabla \cdot (\rho u^{t} \phi^{t}) + S_{\phi} \quad (1)$$

where ϕ is the general property modeled. When $\phi = 1.0$, the generalized equation represents mass conservation for the gas phase, also known as continuity. When $\phi =$ velocity, the generalized equation represents conservation of momentum. When $\phi =$ enthalpy, the equation represents conservation of energy. Γ is diffusivity, representing mass diffusion in the conservation of momentum equation, the viscous term in the conservation of mass equation, and heat conduction in the conservation of energy equation. The second term on the right-hand side of the equation represents the influence of Reynolds stresses in the fluid momentum equations. Within this term, u^{t} represents the fluctuating components of velocity due to turbulence. Similarly, ϕ^{t} is the fluctuating component of the transported property, whether that be velocity or a scalar property. Additionally, S_{ϕ} is a source term.

2.1.2.1 Turbulence Modeling

The existence of Reynolds stresses in the RANS equations, however, mean that the equations are not closed. One of the most common resolutions to this problem is the application of the Boussinesq hypothesis relating the values of Reynolds stresses to the gradients observed in mean velocity.

In suffix notation the hypothesis can be written as:

$$\tau_{ij} = -\rho u_i^t u_j^t = \mu_t \left(\frac{\partial u_i}{\partial x_j} + \frac{\partial u_j}{\partial x_i} \right) - \frac{2}{3} \rho k \delta_{ij} \quad (2)$$

where μ_t is the turbulent or eddy viscosity (representing the turbulent transfer of momentum by eddies and the corresponding internal friction) and δ_{ij} is the Kronecker delta ($\delta_{ij} = 1 \; if \; i = j$ and $\delta_{ij} = 0 \; if \; i \neq j$). *k* is the turbulent kinetic energy per unit mass of eddies in turbulent flow, which can be represented by:

$$k = \frac{1}{2} \left(\overline{u^{t2}} + \overline{v^{t2}} + \overline{w^{t2}} \right) \quad (3)$$

This energy is generated by fluid shear, friction, or buoyancy, or via external forces occurring at larger eddy scales. It is then transferred down through turbulent length scales through the turbulence energy cascade until it is dissipated into internal thermal energy via viscous resistance. This dissipation occurs overwhelmingly at the finest scale of turbulent flow structures, the Kolmogorov microscale. For typical operating conditions observed in this research, the Kolmogorov length scale (calculated based upon the turbulent kinetic energy and turbulence dissipation rates) ranges from 28.45 μm down to 9.00 μm. The corresponding time scales range from 0.047 milliseconds to 0.00467 milliseconds.

In a similar vein, turbulent transport of other scalar properties are taken to be proportional to the gradient of the mean value of that property. In suffix notation once more, we have:

$$-\rho u_i^t \phi_j^t = \Gamma_t \frac{\partial \phi}{\partial x_i} \quad (4)$$

where Γ_t is the turbulent or eddy diffusivity. As turbulent transport of both momentum and scalar properties is due to the same mechanism (that of eddy mixing) it is often assumed that the value of turbulent diffusivity is close to that of turbulent viscosity. Experiments in various flows have put forth that this ratio is almost always a constant. This relationship is often known as the

Reynolds analogy. With this in mind, unity is most often selected as the ratio between turbulent viscosity and diffusivity (turbulent Prandtl number) [46].

Gas phase turbulence is then described through the use of the standard k-ε turbulence model, a semi-empirical model based on transport equations for turbulent energy (*k*) and the turbulence dissipation rate (*ε*) [47]. In this model, the velocity and length scales of large-scale turbulence are defined as:

$$v = k^{1/2} \tag{5}$$

$$l = \frac{k^{3/2}}{\varepsilon} \tag{6}$$

For a generic case under blast furnace operating conditions representative of those found in this research, the large-scale turbulent length scales in the *k-ε* model are near 0.013 m in the blowpipe. These length scales are far smaller than the size of the simulation domain, and are on the same order of scale as the computational grids. Grids of this size do not come close to approaching the Kolmogorov microscales, which are on the order of micrometers.

The transport equations for k and ε are as follows:

Turbulent kinetic energy (k):

$$\nabla \cdot (\rho k \boldsymbol{U}) = \nabla \cdot \left(\frac{\mu_t}{\sigma_k} \nabla \mathrm{k}\right) + 2\mu_t S_{ij}.S_{ij} - \rho\varepsilon \tag{7}$$

Turbulence dissipation rate (*ε*):

$$\nabla \cdot (\rho \varepsilon \boldsymbol{U}) = \nabla \cdot \left(\frac{\mu_t}{\sigma_\varepsilon} \nabla \varepsilon\right) + C_{1\varepsilon} \frac{\varepsilon}{k} 2\mu_t S_{ij}.S_{ij} - C_{2\varepsilon} \rho \frac{\varepsilon^2}{k} \tag{8}$$

where μ_t, the turbulent viscosity, is defined as:

$$\mu_t = C\rho vl = \rho C_\mu \frac{k^2}{\varepsilon} \qquad (9)$$

and the production term can be expanded in the manner of:

$$\mu_t S_{ij}.S_{ij} = \mu_t \left\{ 2\left[\left(\frac{\partial u}{\partial x}\right)^2 + \left(\frac{\partial v}{\partial y}\right)^2 + \left(\frac{\partial w}{\partial z}\right)^2 \right] + \left(\frac{\partial u}{\partial y} + \frac{\partial v}{\partial x}\right)^2 + \left(\frac{\partial u}{\partial z} + \frac{\partial w}{\partial x}\right)^2 + \left(\frac{\partial v}{\partial z} + \frac{\partial w}{\partial y}\right)^2 \right\} \qquad (10)$$

The five constants in these equations, $C_\mu = 0.09$, $\sigma_k = 1.00$, $\sigma_\varepsilon = 1.30$, $C_{1\varepsilon} = 1.44$, and $C_{2\varepsilon} = 1.92$, are defined based on wide-ranging data fitting for a broad spectrum of turbulent flows.

This methodology is widely utilized in CFD modeling for its robust, flexible nature when it comes to confined flows where Reynolds shear stresses are crucial [46]. While this model has some limitations in accuracy when attempting to resolve unconfined flows and boundary layer separation (delayed and reduced separation when compared to experiments), it has been widely utilized in internal industrial flow applications and also presents a significant advantage in computational efficiency when compared to more complex methods such as the Reynolds stress equation model (RSM). The Semi-Implicit Method for Pressure Linked Equations (SIMPLE) scheme is utilized to solve the discretized form of the RANS equations, with second order upwind discretization for momentum, turbulent kinetic energy, turbulence dissipation rate, species, and energy.

2.1.2.2 Coal particle motion

The Lagrangian discrete phase model is utilized to model the motion of pulverized coal particles within the continuous fluid phase. This dispersed phase is solved by tracking injected coal particles that can exchange momentum, mass, and energy with the gas phase as they travel through the calculated gas flow field. The trajectory of a discrete phase particle is predicted by integrating the force balance upon that particle. This force balance can be written as:

$$\frac{d\vec{u}_p}{dt} = F_D\left(\vec{u} - \vec{u}_p\right) + \frac{\vec{g}(\rho_p - \rho)}{\rho_p} + \vec{F} \qquad (11)$$

where $\vec{F}$ is an additional acceleration term (virtual mass force, pressure gradient forces, thermophoretic forces, and lift due to shear), $F_D(\vec{u} - \overrightarrow{u_p})$ is the drag force per unit particle mass, and where F_D is calculated via the spherical drag law:

$$F_D = \frac{18\mu}{\rho_p d_p^2}\frac{C_D Re}{24} \tag{12}$$

Additionally, $\vec{u}$ is the gas phase velocity, $\overrightarrow{u_p}$ is the velocity of the particle phase, μ is the molecular viscosity of the gas, ρ is the gas density, ρ_p is the effective particle density, and d_p is the diameter of the particles. *Re* is the relative Reynolds number, defined here as:

$$Re \equiv \frac{\rho d_p |\vec{u}_p - \vec{u}|}{\mu} \tag{13}$$

The turbulent dispersion of particles is accounted for via the inclusion of turbulent fluid velocity fluctuations in the calculation of trajectory. This fluctuation is determined with the discrete random walk (DRW) model. Here, the fluctuations are divided into piecewise constant functions of time, over a length of time corresponding to the lifetime of turbulent eddies.

2.1.2.3 Particle heat and mass exchange

Heat and mass exchange is handled through several laws including inert heating and cooling, devolatilization, surface combustion, and a multicomponent particle definition. An inert heating and cooling law governs particle heat transfer until it exceeds the vaporization temperature, utilizing a heat balance to account for the influences of convective and radiative heat transfer to and from the particle.

$$m_p C_p \frac{dT_p}{dt} = hA_p(T_\infty - T_p) + \varepsilon_p A_p \sigma(\Theta_R^4 - T_p^4) \tag{14}$$

where m_p is the particle mass, C_p is the particle heat capacity, A_p is the particle surface area, T_∞ is the continuous phase temperature near the particle surface, h is the convective heat transfer

coefficient (W/m^{2}K), ε_p is the emissivity of the particle, σ is the Stefan-Boltzmann constant, and Θ_R is the radiation temperature.

Once beyond the vaporization temperature, volatiles are released into the gas phase as additional species (a combination of a low molecular weight hydrocarbon species and CO), decreasing the particle mass. This devolatilization process continues for as long as the particle mass is greater than the mass of non-volatile material. Coal devolatilization is modeled through the use of two competing first-order irreversible reactions, dependent upon the mass of dry ash-free (*daf*) coal, and with the following form [48].

$$daf\ coal \overset{k_1}{\rightarrow} (1-\alpha_1)Char_1 + \alpha_1 Volatiles_1 \qquad \textit{(Reaction 1)} \quad (15)$$

$$daf\ coal \overset{k_2}{\rightarrow} (1-\alpha_2)Char_2 + \alpha_2 Volatiles_2 \qquad \textit{(Reaction 2)} \quad (16)$$

The rates of these reactions, k_1 and k_2, defining the speed of volatile release over different temperature ranges, are of the form:

$$k_1 = B_1 e^{-(E_1/RT_p)} \quad (17)$$

$$k_2 = B_2 e^{-(E_2/RT_p)} \quad (18)$$

The first reaction is dominant at lower coal temperatures, while the second becomes dominant at temperatures over 1,220 K. The second reaction also generates much higher devolatilization rates from the coal than the first. Kinetics for these two reactions are sourced from published literature on curve fitting with experimental data [49], where E_1 = 17.6 kcal/mole, B_1 = 3.7 x 10^5 s^{-1}, E_2 = 60 kcal/mole, and B_2 = 1.46 x 10^{13} s^{-1}.

The production of volatiles from these two reactions is given by the sum of two release rates of the form:

$$\dot{m}_n = \alpha_n m_{cu} k_n, n = 1, 2 \tag{19}$$

where α_n is a mass stoichiometry coefficient (in this research, α_1 is equivalent to the fraction of volatile in the coal, and α_2 is equal to $1.5 * \alpha_1$) and m_{cu} is the mass of the unreacted part of the coal particle.

After all volatile material contained within a given coal particle has been released, surface combustion begins to consume the combustible fraction (carbon or char) of the particle. The kinetic/diffusion surface reaction rate model of Baum and Street [50] and Field [51] is used to represent surface combustion. In this, a diffusion rate coefficient and a kinetic rate are weighted to develop a combustion rate for char as follows:

$$\dot{m}_p = -A_p \frac{\rho R T_\infty Y_{ox}}{M_{w,ox}} \frac{D_0 \boldsymbol{R}}{D_0 + \boldsymbol{R}}, D_0 = C_1 \frac{\left(\frac{T_p + T_\infty}{2}\right)^{0.75}}{d_p}, \boldsymbol{R} = C_2 e^{-(E/RT_p)} \tag{20}$$

where A_p is the particle surface area, R is the universal gas constant, Y_{ox} is the mass fraction of oxidant species, $M_{w,ox}$ is the molecular weight of the oxidant species, $\boldsymbol{R}$ is the kinetic rate, and D_0 is the diffusion rate coefficient. Rate constants are defined depending upon the coal blend. Heat and mass transfer are incorporated into gas phase source terms within the governing equations. It should be noted that the particle absorbs a fraction of the heat generated by combustion (0.3 when the product is CO_2) and as such, the only the remainder of this heat is added to the gas phase as a part of the source term.

To simplify particle drag and motion calculations, the size of particles is held constant in this model, with decreasing density accounting for the reduction in mass. The surface reaction provides a source term for the particle transport equation, and it serves as a gas phase species source. The reaction also produces or consumes energy with a magnitude dependent on the heat of reaction. As previously mentioned, the inert heating or cooling laws are applied once more, after all char has combusted or reacted with gas. Heat is transferred to or from the coal particle as it traverses each computational cell, serving as a source in the gas phase energy equation. Once this

combustible material has been consumed, any remaining ash reverts to the inert heating law governing heat transfer.

2.1.2.4 Gas Phase Chemical Reactions

Gas phase chemical reactions occur whenever reactants are mixed on a molecular level at temperatures high enough to initialize the reaction. In this research, reactions are simulated using species transport conservation equations, similar to the generic scalar transport equation. A generic form of the species conservation equation is detailed below.

$$\nabla \cdot (\rho u Y_i) = \nabla \cdot (\rho \Gamma_i \nabla Y_i) + R_i + S_i \tag{21}$$

where Y_i is the local mass fraction of a given species, i, R_i is the net production rate of that species via chemical reactions, Γ_i is the species diffusion coefficient (viscosity in m^2/s) and S_i is the rate of creation of that species from other sources. In the case of the blast furnace, S_i primarily stems from the release of volatiles from pulverized coal particles.

As turbulence time scales are often quite low under flow conditions in the blast furnace, the Eddy-Dissipation Concept (EDC) model was utilized to simulate detailed chemical kinetics [52]. The standard Eddy-Dissipation model was considered, however, as kinetics for multi-step reactions based on Arrhenius rates are available for natural gas, the EDC model was selected to model this multi-stage process. The EDC model includes more complex chemical reaction mechanisms in turbulent flows. Combustion reactions are assumed to take place within turbulent flow structures at the same scale as or smaller than the Kolmogorov length scale. Assuming that turbulence is essentially isotropic at this small scale (a far smaller scale than the scale of a single computational grid cell required in the k-ε model), the length fraction of the fine structure regions can be defined based on turbulent kinetic energy and turbulence dissipation rate.

$$\xi^* = 2.1377 \left(\frac{\nu\varepsilon}{k^2}\right)^{1/4} \tag{22}$$

where ν is the kinematic viscosity.

For typical conditions within this research, this fraction ranges from 0.042 to 0.136. The corresponding time scale of reactions in this model can also be given in terms of the turbulent kinetic energy and dissipation rate, and range from 0.002 milliseconds to 0.019 milliseconds.

$$\tau^* = 0.4082 \left(\frac{\nu}{\varepsilon}\right)^{1/2} \tag{23}$$

For these rapid times, the fine scale regions can be treated as well-stirred, constant pressure reactors, with initial conditions defined based upon the current species fractions and temperature within the computational cell. Reactions within the fine scales occurring over the given time scale are then governed by the direct use of Finite-Rate kinetics, through a 28-step mechanism detailed by M. Jazbek et al [53]. The molar consumption or production of a given species for a given reaction can be written as:

$$R_{i,r} = \left(\alpha_{react} - \alpha_{prod}\right)\left(k_f \prod_{j=1}^{N} C_{j,r}^{\eta'_{j,r}} - k_b \prod_{j=1}^{N} C_{j,r}^{\eta''_{j,r}}\right) \tag{24}$$

where α_{react} and α_{prod} are the stoichiometric coefficients for the species reactant or product in the reaction, k_f and k_b are the forward and backward rate constants for the reaction, $C_{j,r}$ is the molar concentration of species j in reaction r, and $\eta'_{j,r}$ and $\eta''_{j,r}$ are the rate exponents for reactant and product species j in reaction r.

This mechanism utilizes 15 species in the reactions of natural gas, including O_2, H_2, H_2O, H, O, OH, HO_2, H_2O_2, CO_2, CO, CH_4, CH_3, CH_3O, CH_2O, and HCO. The species that enter the combustion process and those that are stable products of reaction are CH_4, H_2O, O_2, H_2, CO, and CO_2. The corresponding source term in the species conservation equation for a given species i is represented by Equation (25).

$$R_i = \frac{\rho \xi^{*2}}{\tau^*(1-\xi^{*3})}(Y_i^* - Y_i) \tag{25}$$

where Y_i^* is the fine-scale species mass fraction after reacting over time τ^*.

Due to the complexity and variety of computational geometries encountered in the blast furnace blowpipe and tuyere region, including custom lance tips and varying auxiliary fuel injection positions, the commercially available CFD package ANSYS Fluent® is used to solve the governing equations for the gas and particle phases.

2.2 CFD Model for Raceway Formation

2.2.1 General Description and Model Assumptions

The blast furnace raceway deals with a slightly less complex physical geometry than the tuyere and blowpipe region, given that the raceway region is set entirely in slice of the cylindrical blast furnace. However, the introduction of a packed bed of coke particles directly outside the tuyere adds a new layer of complexity to the simulation model. As previously mentioned, the CFD models in this study aim to calculate the raceway size and shape, as opposed to using a fixed raceway cavity inside a coke bed. This requires the selection of a method for tracking the movement of not only the gas phase and injected coal particles, but also the solid coke particles already in the furnace.

The methodology for conducting CFD modeling of the raceway includes two major components, both developed using a comprehensive Eulerian approach. First, the formation of the raceway is simulated using a transient approach. Gas flow matching the mass flow rate exiting the tuyere enters a packed bed of coke, simulated using a continuous granular phase. This simulation is used to generate a static porosity distribution file which is then transferred to the second portion of the raceway simulation model to calculate heat transfer, combustion, and other chemical reactions in a steady state solver. The changes in gaseous temperature affect fluid density, which is then transferred back to the raceway formation simulation. Additionally, a source term in the continuity governing equation serves to represent the additional mass generated via combustion reactions of oxygen with coke. An iterative procedure is then adopted, running each simulation based on data from the previous step until the raceway shape converges.

The following assumptions were made in the development of the raceway formation model:

1. The coke bed is treated as a continuous granular phase with a constant particle size.

2. Momentum interaction between the granular and gas phases is handled through source terms estimating gas-solids drag.
3. Combustion, chemical reactions, and heat transfer are not included, and there is no mass exchange between continuous phases. However, source terms are introduced to take into account the influence of gas generation and density changes calculated in the combustion model.

Most modern blast furnaces utilize anywhere from 20 to 40 tuyeres, depending on the furnace size, volume, and production rate. Figure 4 illustrates a sample horizontal cross-section diagram of a 20 tuyere blast furnace at the tuyere level. As previously mentioned, the conditions in each tuyere are often uniformly consistent around the annulus of the furnace. While this can vary in practice, the optimal operating conditions of a given blast furnace are typically aimed at annular uniformity. Because of this, the CFD models utilized in this study simplify the blast furnace annulus to a single, periodic domain focused on the gas flow conditions, raceway shape, and combustion generated by the corresponding tuyere.

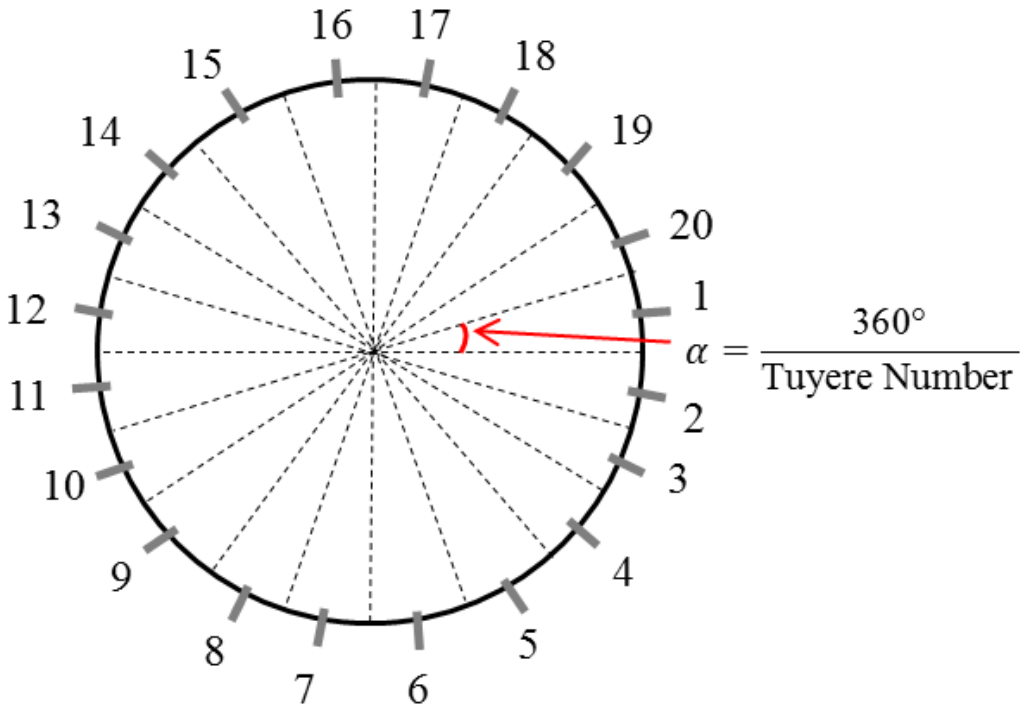

Figure 4. Simplified cross-section of the blast furnace at tuyere level.

In the initial implementations of this methodology, the commercially available CFD package ANSYS Fluent® was used to simulate raceway formation. However, while commercial codes provide a straightforward platform for the design of various furnace geometries, the transfer of information between Fluent and the in-house code requires additional manual data modification and processing between each step of the iteration process, resulting in extended total runtimes.

In an effort to address this limitation, a new FOTRAN CFD solver has been developed. This new solver is capable of functioning in concert with the raceway combustion solver detailed in section 2.3, increasing computational speed and removing the requirement for manual intervention in the simulation process. Additionally, the new solver utilizes the aforementioned primary governing equations and assumptions in conjunction with an enhanced treatment for interphase momentum exchange to remove some assumptions regarding momentum transfer between the gas and solid phases at high velocities.

2.2.2 Governing Equations and Phenomenological Models

This section details the governing equations and phenomenological models utilized by both the commercial and in-house modeling approaches to simulating the raceway shape. As previously mentioned, raceway formation is modeled through the use of a comprehensive 3-D Eulerian continuum approach. Each phase is treated as interpenetrating continua in the mathematical formulation of the model. In order to account for the effects of multiple phases upon the governing equations, α, a variable tracking phasic volume fraction, is introduced, corresponding with the use of density. Within any given cell, the volume fractions of all phases, gas and coke in this case, must sum up to one. This model was developed based on a large body of published correlations and previous work from a wide range of sources [54-60], incorporating specific enhancements to allow for shifting definitions of both particle drag coefficient and terminal velocity ratio.

2.2.2.1 Conservation equations and inter-phase momentum exchange

The general form of the governing equations is:

$$\nabla(\alpha_i \rho_i \phi) + \nabla \cdot (\alpha_i \rho_i \phi \vec{u}_i) = \nabla \cdot \left(\Gamma_\phi \nabla \phi\right) + S_\phi \tag{26}$$

where α_i is the volume fraction of the *ith* phase, ρ_i is the material density of the *ith* phase, and $\vec{u}_i$ is the gas phase velocity vector.

For gas phase momentum:

$$\frac{\partial}{\partial t}\left(\alpha_{gas}\rho_{gas}\vec{u}_{gas}\right) + \nabla\cdot\left(\alpha_{gas}\rho_{gas}\vec{u}_{gas}\vec{u}_{gas}\right) = -\alpha_{gas}\nabla P_{gas} + \nabla\cdot\bar{\bar{\tau}}_{gas} + \alpha_{gas}\rho_{gas}\vec{g} + K_{gs}\left(\vec{u}_p - \vec{u}_{gas}\right) + \left(\vec{F}_{gas} + \vec{F}_{vm,gas} + \vec{F}_{td,gas}\right) \quad (27)$$

where α_{gas} is the volume fraction of the gas phase, alternatively known as the void fraction, ρ_{gas} is the material density of the gas phase, and $\vec{u}_{gas}$ is the gas phase velocity vector.

Additionally, $\bar{\bar{\tau}}_{gas}$ is the gas phase stress tensor, expressed by:

$$\bar{\bar{\tau}}_{gas} = \alpha_{gas}\mu_{gas}\left(\nabla\vec{u}_{gas} + \nabla\vec{u}_{gas}^{T}\right) + \alpha_{gas}\left(\lambda_{gas} - \frac{2}{3}\mu_{gas}\right)\nabla\cdot\vec{u}_{gas}\bar{\bar{I}} \quad (28)$$

where μ_{gas} and λ_{gas} are the shear and bulk viscosity of the gas phase, and the Boussinesq hypothesis is once again utilized to relate the Reynolds stresses to gradients in mean velocity.

Additionally, P_{gas} is the pressure in the fluid phase, $\vec{g}$ is the acceleration due to gravity, $\vec{F}_{gas}$ is an external body force, $\vec{F}_{vm,gas}$ is a virtual mass force, and $\vec{F}_{td,gas}$ is a turbulent dispersion force.

K_{gs} is the gas-solid momentum exchange coefficient, defined as:

$$K_{gs} = \frac{\alpha_p\rho_p f}{\tau_p} \quad (29)$$

where τ_p is the particulate relaxation time defined as:

$$\tau_p = \frac{\rho_p d_p^2}{18\mu_{gas}} \quad (30)$$

where d_p is the coke particle diameter.

f is defined according to the equations proposed in the Syamlal-O'Brien drag model [54] as follows:

$$f = \frac{C_D Re_p \alpha_{gas}}{24 V_{rs}^2} \tag{31}$$

where the drag coefficient is calculated using a modified equation based on work by Wadell [61], assuming spherical particles. Additionally included in the in-house FORTRAN solver is a new modification to the definition of drag coefficient within this factor, based on the well-accepted assumption that C_D drops suddenly due to the onset of turbulence to the rear of the sphere at Re_s greater than 3×10^5:

$$C_D = \begin{cases} \left(0.63 + 4.8\sqrt{\frac{V_{rs}}{Re_s}}\right)^2 & if\ Re_s \leq 3 \times 10^5 \\ 0.1 & if\ Re_s > 3 \times 10^5 \end{cases} \tag{32}$$

and Re_s is the granular phase particle Reynolds number.

$$Re_s = \frac{d_{coke} |\vec{u}_{coke} - \vec{u}_{gas}| \rho_{gas}}{\mu_{gas}} \tag{33}$$

This granular phase Reynolds number can vary significantly based on the tuyere jet velocity and diameter of the coke being utilized in the furnace, and as such, the piecewise formulation of the drag coefficient provides additional flexibility for various conditions.

Additionally, V_{rs} is the ratio of the terminal velocity of a group of particles to that of an isolated particle, defined by:

$$V_{rs} = 0.5\left(A - 0.06Re_s + \sqrt{(0.06Re_s)^2 + 0.12Re_s(2B - A) + A^2}\right) \tag{34}$$

Here, $A = \alpha_{gas}^{4.14}$ (35)

$$\text{and } B = \begin{cases} 0.8\,\alpha_{gas}^{1.28} \;\; if\; \alpha_{gas} \leq 0.85 \\ \alpha_{gas}^{2.65} \;\; if\; \alpha_{gas} > 0.85 \end{cases} \tag{36}$$

The piecewise functions listed above contribute to model convergence and assist in providing a more detailed profile for particle drag forces throughout the raceway region. When using the commercial CFD solver, the movement of the coke phase is defined by singular versions of each equation, with no changes dependent on gas phase volume fraction or granular particle Reynolds number.

Similar to the gas phase momentum governing equation, the solid phase momentum governing equation is:

$$\frac{\partial}{\partial t}\left(\alpha_p \rho_p \vec{u}_p\right) + \nabla \cdot \left(\alpha_p \rho_p \vec{u}_p \vec{u}_p\right) = -\alpha_p \nabla P_{gas} + \nabla \cdot \bar{\bar{\tau}}_{coal} + \alpha_p \rho_p \vec{g} + K_{sg}\left(\vec{u}_{gas} - \vec{u}_p\right) + \left(\vec{F}_p + \vec{F}_{vm,p} + \vec{F}_{td,p}\right) \tag{37}$$

where α_p is the volume fraction of the granular phase (coke), ρ_p is the granular phase material density, and $\vec{u}_p$ is the granular phase velocity vector.

Additionally, $K_{sg} = K_{gs}$, and $\bar{\bar{\tau}}_{coal}$, $\vec{F}_p$, $\vec{F}_{vm,p}$, and $\vec{F}_{td,p}$ are analogous to their corresponding terms in the gas phase equation.

2.2.2.2 Turbulence Modeling

In this multi-phase flow, turbulence is simulated via the *k-ε* mixture turbulence model, with the same constraints as the standard *k-ε* turbulence model. This model is applied here as the phases are almost entirely stratified for the time period in which the raceway formation simulation occurs. The governing equations for *k* and *ε* respectively are:

$$\frac{\partial}{\partial t}(\rho_m k) + \nabla \cdot (\rho_m \vec{u}_m k) = \nabla \cdot (\Gamma_k \nabla k) + G_{k,m} - \rho_m \varepsilon \tag{38}$$

$$\frac{\partial}{\partial t}(\rho_m \varepsilon) + \nabla \cdot (\rho_m \vec{u}_m \varepsilon) = \nabla \cdot (\Gamma_\varepsilon \nabla \varepsilon) + \frac{\varepsilon}{k}\left(C_{1\varepsilon} G_{k,m} - C_{2\varepsilon} \rho_m \varepsilon\right) \quad (39)$$

where $\Gamma_k = \mu_m + \frac{\mu_{t,m}}{\sigma_k}$ and $\Gamma_\varepsilon = \mu_m + \frac{\mu_{t,m}}{\sigma_\varepsilon}$

Additionally, ρ_m is the mixture density, computed by:

$$\rho_m = \alpha_{gas}\rho_{gas} + \alpha_p \rho_p \quad (40)$$

μ_m is the mixture viscosity computed by:

$$\mu_m = \alpha_{gas}\mu_{gas} + \alpha_p \mu_p \quad (41)$$

$\vec{u}_m$ is the velocity computed by:

$$\vec{u}_m = \frac{\alpha_{gas}\rho_{gas}\vec{u}_{gas} + \alpha_p \rho_p \vec{u}_p}{\alpha_{gas}\rho_{gas} + \alpha_p \rho_p} \quad (42)$$

and $\mu_{t,m}$ is the turbulent viscosity for the mixture, computed by:

$$\mu_{t,m} = \rho_m C_\mu \frac{k^2}{\varepsilon} \quad (43)$$

$G_{k,m}$ is the production of turbulence, defined by:

$$G_{k,m} = \mu_{t,m}(\nabla \vec{u}_m + (\nabla \vec{u}_m)^t) \quad (44)$$

The constants in these equations, $\sigma_k = 1.00$, $\sigma_\varepsilon = 1.30$, $C_{1\varepsilon} = 1.44$, and $C_{2\varepsilon} = 1.92$, are defined based on the same wide-ranging data fitting as in the standard *k*-*ε* turbulence model.

As previously mentioned, two methods exist to solve the governing equations in this model. This research has utilized both the commercial CFD software ANSYS Fluent® and the in-house CFD

solver to simulate raceway shapes. Both methods produce essentially identical raceway coke distributions under the conditions examined, however, use of the newly developed in-house CFD solver allows for more rapid computation. The use of commercial code requires significant user intervention to transfer data between the commercial and in-house CFD solvers. With the development of the new solver method, the simulation model can be integrated directly with the raceway combustion model, removing the necessity for user intervention. The combustion model determines the rate of gas generation due to combustion and the changes in gas density due to temperature, and that information can be fed directly into the formation solver as source terms. Both the raceway formation and raceway combustion in-house CFD codes are written in FORTRAN, and use identical linear solve algorithms. These two solvers also use an identical computational grid, further simplifying the problem setup.

2.3 CFD Model for Raceway Combustion

2.3.1 General Description and Model Assumptions

The second major component in the CFD raceway model handles chemical reactions, heat transfer, turbulence, and gas flow patterns within the raceway using a steady-state solver. An Eulerian multi-phase model is also used to simulate gas-coal particle motion and combustion within the raceway region, with the pulverized coal plume treated as a secondary continuous phase. As previously mentioned, the raceway formation model provides a porosity map that serves as porous geometry for the combustion model. The raceway envelope is then represented as a steady region of high void fraction within the coke bed, and gas flow is impacted by the geometry of the denser porous media. Coke can react within incoming oxygen to produce heat and gas, and injected fuels react within the raceway. Changes in gaseous temperature influence fluid density, and the reaction of carbon solids with oxygen produces additional gas mass. Both of these influences are in turn fed back into the raceway formation simulation as source terms to update the raceway shape. The methodology of information exchange between steps is detailed in section 2.4.

The following assumptions were made in the development of the raceway combustion model:

1. Coke is treated as a non-moving bed of porous media which can react with the gas phase.

2. The gas and dispersed pulverized coal phases are solved using an Eulerian continuum approach.
3. Momentum interaction between the particle and gas phases is handled through source terms estimating gas-solids drag.
4. A steady-state solver is used to simulate gas flow, turbulence, combustion, multi-species reactions, coal devolatilization, and heat transfer, as conditions within the raceway region are often held constant for long periods of time relative to the residence times of gases and particles within the raceway envelope.

2.3.2 Governing Equations and Phenomenological Models

In the combustion model, continuity, momentum, heat transfer, and species transport are described by the standard conservation equations, modified by a phasic volume fraction in a similar form to that of Equation (26). The primary difference between the governing equations for the formation and combustion models comes from the assumption of steady-state flow conditions within the raceway under standard operation. Additionally, the interphase momentum exchange coefficient is defined in a different manner, as the coal particle phase is more dilute and is comprised of much finer particles than the coke bed.

2.3.2.1 Gas – Solid Momentum Exchange

Interphase momentum exchange between the coal particle phase and the gas phase is handled by an exchange coefficient when the particle phase makes up less than 20% of the fluid volume, as follows:

$$\beta_{gc} = \frac{3}{4} C_D \rho_{gas} \frac{|u_{gas} - u_p|(1-\alpha_p)^2}{d_p} f(\alpha_p) \tag{45}$$

where α_p is the coal particle volume fraction, d_p is the coal particle diameter, and $f(\alpha_p)$ is a correction to Stoke's law for a particle in free fall that accounts for the influence of the presence of other particles, calculated by:

$$f(\alpha_p) = (1-\alpha_p)^{-3.8} \tag{46}$$

The drag coefficient, C_D for this coefficient is calculated by:

$$C_D = \begin{cases} \frac{24}{Re_p}\left(1 + \frac{Re_p^{0.667}}{6}\right) & for \quad Re_p < 1000 \\ 0.44 & for \quad Re_p \geq 1000 \end{cases} \tag{47}$$

where Re_p is calculated by:

$$Re_p = \frac{d_p|\vec{u}_p - \vec{u}_{gas}|\rho_{gas}}{\mu_{gas}} \tag{48}$$

This Reynolds number is typically quite low compared to the particle Reynolds number observed in the formation model (10-100 vs. 250,000+), as the particle sizes are far smaller (sample average of 0.05 mm vs. roughly 3 cm), and the relative velocities between particle and gas are lower (5 – 50 m/s vs. 150+ m/s).

2.3.2.2 Turbulence Modeling

Turbulence modeling is handled via the *k-ε* turbulence model in which predictions of kinetic energy and dissipation rate are calculated for both continuous phases using the standard *k-ε* model with additional terms to include the effects of interphase turbulent momentum transfer. The conservation equations for turbulent kinetic energy and turbulence dissipation rate are as follows:

$$\frac{\partial}{\partial t}\left(\rho_{gas}k_{gas}\right) + \nabla \cdot \left(\rho_{gas}\vec{u}_{gas}k_{gas}\right) = \nabla \cdot \left(\frac{\mu_{t,g}}{\sigma_k}\nabla k_{gas}\right) + G_{k,gas} - \rho_{gas}\varepsilon + G_p + G_R \tag{49}$$

$$\frac{\partial}{\partial t}\left(\rho_{gas}\varepsilon\right) + \nabla \cdot \left(\rho_{gas}\vec{u}_{gas}\varepsilon\right) = \nabla \cdot \left(\frac{\mu_{t,g}}{\sigma_k}\nabla\varepsilon\right) + G_{k,gas} + \frac{\varepsilon}{k_{gas}}\left(C_{1\varepsilon}G_{k,gas} - C_{2\varepsilon}\rho_{gas}\varepsilon_{gas} + C_{1\varepsilon}G_p + C_{2\varepsilon}G_R\right) \tag{50}$$

where $\mu_{t,g}$ is the gas phase turbulent viscosity, which can be written in terms of the gas turbulent kinetic energy and turbulence dissipation rate:

$$\mu_{t,g} = \rho_{gas} C_\mu \frac{k_{gas}^2}{\varepsilon} \tag{51}$$

where G_p and G_R are source terms used to represent the turbulent interaction between the dispersed phase and the continuous phase. They can be written as:

$$G_p = \frac{2\rho_p}{\tau_{rp}} \left(C_{p,p} \sqrt{k_{gas} k_p} - k_{gas} \right) \tag{52}$$

$$G_R = -k_{gas} \dot{m}_p \tag{53}$$

where $\dot{m}_p$ is the change in mass per unit time of the coal particle phase.

When the gas phase turbulent kinetic energy is larger than the particle phase, G_p serves as a destruction term for gas phase turbulent kinetic energy. When the opposite is true, it is a production term. G_R accounts for turbulent energy generation due to the mass change of the particle (via combustion or other reactions). As the particle loses mass in these reactions, this is also a production term. Additionally, $G_{k,gas}$ is the gas phase production of turbulent kinetic energy, defined similarly to Equation (10). As before, the constants in these equations, σ_k, σ_ε, $C_{1\varepsilon}$, $C_{2\varepsilon}$, and C_μ, are defined based on the same data fitting as in the standard *k*-ε turbulence model.

The transport equation for turbulent kinetic energy of the coal phase is also solved, and the turbulence dissipation rate is shared between phases. The source terms for the coal phase equation are $G_{k,coal}$, defined identically to $G_{k,gas}$ except using coal phase velocities, and G_{gk}, a single source term representing the interaction between gas and particle phase turbulent kinetic energy [46,62].

$$G_{gk} = \frac{2\rho_p}{\tau_{rp}} \left(C_{p,p} \sqrt{k_{gas} k_p} - k_{gas} \right) + \left(C_{p,p} \sqrt{k_{gas} k_p} - k_{gas} \right) \dot{m}_p \tag{54}$$

where k_p is the coal phase turbulent kinetic energy. Additionally, the turbulent viscosity for the coal phase is given by:

$$\mu_{t,p} = \rho_p C_\mu \frac{k_{gas}^{3/2} k_p^{1/2}}{\varepsilon} \tag{55}$$

2.3.2.3 Interphase Heat Transfer

The interphase heat transfer model utilizes the assumption of a stagnant film, and heat transfer between a coal particle and the continuous gas phase is determined by [28,63]:

$$Q_{coal} = \pi d_p Nu_p \lambda \frac{B_p}{\exp(B_p)-1}\left(T - T_p\right) \tag{56}$$

where, d_p is the coal particle diameter, T is the temperature of the gas phase, T_p is the temperature of the particle, and λ_p is thermal conductivity of the gas mixture, given by:

$$\lambda = 5.526 \times 10^{-5} * T + 0.01155 \tag{57}$$

Additionally, B_p is the transfer number, which is given by:

$$B_p = -\frac{\dot{m}_p C_{ps}}{\pi d_p Nu_p \lambda_p} \tag{58}$$

where C_{ps} is the specific heat capacity around the coal particle:

$$C_{ps} = 0.106 * T + 1173 \tag{59}$$

and

$$Nu_p = 2 + 0.5 Re_p^{0.5} \tag{60}$$

2.3.2.4 Moisture Evaporation

The rate of moisture evaporation is defined via a diffusion model [64]. It is assumed that all moisture inside the coal particle diffuses to the coal particle surface and forms a liquid film. This film is treated as the surface layer of a droplet with a diameter equal to the coal particle diameter. Given these assumptions, the moisture evaporation rate is defined by:

$$\dot{m}_{wc} = \begin{cases} \pi d_p Nu_p \rho_p \ln\left(1 + \frac{Y_{H2O,p} - Y_{H2O,g}}{1 - Y_{H2O,c}}\right) & T_p < T_b \\ -\pi d_p Nu_p \frac{\lambda_p}{C_{ps}} \ln\left(1 + \frac{C_{ps}(T - T_p)}{1 - Q_{vap}}\right) & T_p \geq T_b \end{cases} \quad (61)$$

where T_b is the boiling temperature, Q_{vap} is the heat of vaporization for H_2O, and $Y_{H2O,p}$ is the mass fraction of water vapor at the surface of the coal particle, defined by:

$$Y_{H2O,p} = A \exp\left(\frac{-E_w}{RT_p}\right) \quad (62)$$

The Nusselt number of heat convection is defined as in Equation (60).

2.3.2.5 Devolatilization

As in the tuyere/blowpipe portion of the model, thermal decomposition of the carbon molecules of coal particles occurs once their temperatures are high enough, releasing volatile matter into the gas phase. The devolatilization rate is represented by two simultaneous competing first order irreversible reactions [48,49].

Released volatile matter quickly begins to undergo homogeneous combustion. As previously noted, this research assumes that volatile material consists purely of hydrocarbons and carbon monoxide, allowing for the reactions:

$$C_d H_b + \frac{d}{2} O_2 \rightarrow d\ CO + \frac{b}{2} H_2 \quad (63)$$

$$2\ CO + O_2 \rightarrow 2\ CO_2 \quad (64)$$

$$2\ H_2 + O_2 \rightarrow 2\ H_2O \quad (65)$$

The reaction rates of volatiles in the gas phase are defined in the same manner as other gas phase chemical reactions, detailed in the following section.

2.3.2.6 Gas Phase Chemical Reactions

Within the raceway region, the reactants and products are reduced compared to within the tuyere. The gas species tracked within the raceway are N_2, CH_4, coal volatiles, H_2O, O_2, H_2, CO, and CO_2. The Eddy Breakup (EBU) model accounts for the impacts of turbulence on calculate gas species reactions within the raceway, as it makes reasonably good predications and allows for faster convergence in the CFD solver. This method defines the rate of consumption of a fuel based on local flow properties in each computational cell. The primary limiting factor of this model is the accuracy of the turbulence model, as the fuel dissipation rate is dependent on the turbulence time scale (k/ε). As it has been established that the standard k-ε turbulence model appears accurate for the current scenario, the EBU model should provide reasonable results [46]. The reaction rates of fuel, products, and oxygen in the EBU model are equal to the turbulent dissipation rate for each. The actual reaction rate of fuel in this model is then defined as the slowest of the three dissipation rates, which can be defined as:

$$w_{EBU} = -\rho \frac{k}{\varepsilon} \min\left(C_R Y_{Fuel}, C_R \frac{Y_{O2}}{s}, C_R' \frac{Y_{product}}{1+s}\right) \tag{66}$$

The standard EBU model has been modified to include the influence of the Arrhenius chemical kinetics upon the reaction rates of species [65,66]. The Arrhenius reaction rate is given as:

$$w_{Arr} = A_s \rho^2 Y_{Fuel} Y_{O2} exp(-\frac{E_s}{RT}) \tag{67}$$

where C_R and $C_R{}'$ are constants with literature based values of 1.0 and 0.5 respectively, and Y_{Fuel}, Y_{O2}, and $Y_{product}$ are the mass fractions of fuel, oxygen, and products. Additionally, A_S is a pre-exponential factor, E_s is the activation energy of a given gas species reaction, and R is the universal gas constant.

w_{final} then uses the smaller (limiting) value between the Eddy Breakup and Arrhenius rates as the overall reaction rate.

$$w_{final} = \min(w_{EBU}, w_{Arr}) \tag{68}$$

2.3.2.7 Char Combustion/Gasification

The reaction rate of char in the raceway is calculated using reaction kinetics. This model assumes a first-order reaction with respect to O_2, CO_2, and H_2O concentrations. The reactions taken into account in this model are as follows:

$$C + O_2 \rightarrow CO_2 \tag{69}$$

$$2\,C + O_2 \rightarrow 2\,CO \tag{70}$$

$$C + CO_2 \rightarrow 2\,CO \tag{71}$$

$$C + H_2O \rightarrow CO + H_2 \tag{72}$$

Equations (64) and (65) represent combustion of char, while Equations (66) and (67) represent gasification reactions. In the presence of oxygen, gasification reactions are much smaller than combustion. However, in the regions above the raceway, after oxygen has been converted to CO_2 and H_2O, gasification reactions are far more significant. The rates for these reactions can be defined as follows:

$$\dot{m}_{c,A} = -\pi d_p^2 \rho Y_{O2,p} B_A exp\left(-\frac{E_A}{RT_p}\right) \tag{73}$$

$$\dot{m}_{c,B} = -\pi d_p^2 \rho Y_{O2,p} B_B exp\left(-\frac{E_B}{RT_p}\right) \tag{74}$$

$$\dot{m}_{c,C} = -\pi d_p^2 \rho Y_{CO2,p} B_C exp\left(-\frac{E_C}{RT_p}\right) \tag{75}$$

$$\dot{m}_{c,D} = -\pi d_p^2 \rho Y_{H2O,p} B_D exp\left(-\frac{E_D}{RT_p}\right) \tag{76}$$

where d_p is the coal particle diameter and Y_{O2}, Y_{H2O}, and Y_{CO2} are the concentrations of gas species at the particle surface. B_A – B_D are rate constants and E_A – E_D are activation energies, listed in Table 1 in section 2.3.2.9.

2.3.2.8 Coke Combustion/Gasification

The reaction of gases with coke in the porous media is also taken into account in this model, using the reactions listed below [67]:

$$C + O_2 \rightarrow CO_2 \tag{77}$$

$$C + CO_2 \rightarrow 2CO \tag{78}$$

$$C + H_2O \rightarrow CO + H_2 \tag{79}$$

These reactions serve to generate and consume heat via exothermic and endothermic reactions, as well as generate mass sources via the conversion of solids into the gaseous phase. The reactions rates are given by:

$$R_i = k_i C_i \tag{80}$$

where C_i is the instantaneous concentration of coke, and k_i is defined as follows:

$$k_i = \left(\frac{1}{k_{fi}a} + \frac{1}{\eta_i k_{mi} \rho_{bc}}\right)^{-1} \tag{81}$$

Here, k_{fi} is the mass transfer coefficient, a is specific surface area of the coke in (m^2/kg), η_i is the effectiveness factor of the catalytic reaction, k_{mi} is the chemical rate constant, and ρ_{bc} is the bulk density of coke. The mass transfer coefficient is defined as:

$$k_{fi} = \frac{D_i}{\phi d_p} Sh \tag{82}$$

Sh is the Sherwood number, defined as:

$$Sh = 1.5Re_p^{0.55} \tag{83}$$

The chemical rate constant for the C – O reaction (Equation (77)) can be defined as:

$$k_{m1} = 6.53x10^5 \frac{a}{\rho_{bc}} \sqrt{T_m} exp\left(-\frac{22140}{T_m}\right) \tag{84}$$

where T_m is the average temperature of the gas/coke mixture in the cell.
Likewise, the constant for the C – CO_2 reaction (Equation (78)) is:

$$k_{m2} = 8.31x10^9 exp\left(-\frac{30190}{T_m}\right) \tag{85}$$

And the constant for the C – H_2O reaction (Equation (79)) is:

$$k_{m3} = 13.7T_m exp\left(-\frac{17310}{T_m}\right) \tag{86}$$

2.3.2.9 Reaction Constants

Kinetic constants for the reaction equations of gaseous CO, H_2, CH_4, and the constants for moisture evaporation, devolatilization, and char reactions are detailed in Table 1. Constants for CH_4, H_2, and CO combustion, as well as moisture evaporation and char reactions are obtained from published literature [68]. It should be noted that the constants for coal devolatilization utilized are intended for high-volatile coals, such as lignite and bituminous coals. Kinetic constants for char reactions are obtained from other sources [69,20]. It should be noted that the reaction kinetics for char may vary with coal types, however, the kinetics selected for use in this study are representative of a semi-standard bituminous coal that is representative of many industry blends.

Table 1. Summarized reaction kinetics for the raceway combustion model [20,68,69].

Reaction	B [1/s]	A [m^3/(kg*s)]	Activation Energy E [J/mol]
$CH_4 + 2O_2 \rightarrow CO_2 + 2H_2O$	N/A	1.6×10^{10}	1.081×10^5
$2CO + O_2 \rightarrow 2CO_2$	N/A	7.0×10^4	6.651×10^4
$2H_2 + O_2 \rightarrow 2H_2O$	N/A	5.4×10^2	1.255×10^5
Moisture Evaporation	8.32×10^5	N/A	4.228×10^4
Devol. Reaction 2	1.46×10^{13}	N/A	2.511×10^5
Char reaction A	1.225×10^3	N/A	9.977×10^4
Char reaction B	1.813×10^3	N/A	1.089×10^5
Char reaction C	7.351×10^3	N/A	1.380×10^5
Char reaction D	1.650×10^5	N/A	1.420×10^5

2.3.2.10 Radiative Heat Transfer

As radiative heat transfer accounts for a signification portion of the heat transfer between surfaces in industrial-scale combustion systems, accurate radiation modeling is needed to fully represent heat flux within the raceway. Radiative properties of particulates, such as the coke bed, depend on a number of factors. Additionally, radiation fluxes are highly dependent on surface temperature, emissivity, and temperature of the participating medium.

Various radiative heat transfer models have been developed utilizing zone and flux methods and empirical correlations for flow phenomena, temperatures, heat flux rates, and gas composition [70,71]. Flux methods such as the discrete-ordinates (DO) model appear to provide an optimized combination of computational efficiency and solution accuracy, and as such, the DO model was used in the raceway combustion model.

The DO method solves the integro-differential radiative transfer equation (RTE) in several discrete angular directions spanning the total of 4π solid angle. The assumption of non-variance of radiative intensities in prescribed solid angles allows the angular integral to be discretized. From this discretization, a set of coupled PDEs are obtained for intensity transport. These equations can then be further discretized with the application of finite-difference methods. The number of equations

obtained stems from the number of discrete directions, which in turn depends on the order of the DO approximation. For a given S_N approximation, N(N+2) discrete angular directions are utilized.

The DO version of the RTE is written below in terms of instantaneous spectrally-averaged intensities and properties and expanded in Cartesian coordinates, as:

$$\mu_m \frac{\partial I_m}{\partial x} + \eta_m \frac{\partial I_m}{\partial y} + \xi_m \frac{\partial I_m}{\partial z} = e_{bgp} - k_{ext} I_m + \frac{k_s}{4\pi} \sum_{i=1}^{M} \Phi(i,m) I_i w_i \quad (87)$$

where μ_m, η_m, and ξ_m are direction cosines for the discrete angular direction Ω_m, I_m is the radiation intensity in the direction Ω_m, e_{bgp} is the sum of emitted intensities for gas and particles, and k_{ext} is the extinction coefficient (the sum of the gas absorption coefficient, k_{ag}, the particle absorption coefficient, k_{ap}, and the particle scattering coefficient, k_s). w_i is the angular quadrature weight, and the sum is taken over the total number of discrete directions, M = N(N+2), used in this approximation. In order for important integrals in the RTE and boundary conditions to be accurately solved, the selection of proper discrete directions and angular quadrature weights is necessary. Published literature details the Level Symmetric (LSH) quadrature values and weights that can satisfy the zeroth, first, and second-order moments corresponding to incident energy, heat flux, and the diffusion condition [72]. These values are listed in Table 2, for a single octant of the sphere. Other octants use similar values, with varying signs depending on directions.

Table 2. LSH quadrature sets for the S_4 DO model.

Designation	μ_m	η_m	ξ_m	w_m
S_4	0.295876	0.908248	0.295876	0.523599
	0.908248	0.295876	0.295876	0.523599
	0.295876	0.295876	0.908248	0.523599

The intensity in any given direction at the center of a computational cell in Cartesian coordinates can be defined as:

$$I_m = \frac{\mu_m A I_i + \eta_m B I_j + \xi_m C I_k + (e_{bg} + e_{bp} + k_s I_s) V}{\mu_m A + \eta_m B + \xi_m C + k_{ext} V} \quad (88)$$

where *A*, *B*, and *C* are the cell surface areas, defined as:

$$A = A_i + f A_{i+1} \quad (89)$$

$$B = B_j + f B_{j+1} \quad (90)$$

$$C = C_k + f C_{k+1} \quad (91)$$

and I_s is the in-scattering source term, defined as:

$$I_s = \frac{1}{4\pi} \sum_{i=1}^{M} \Phi(i, m) I_i w_i \quad (92)$$

where the summation takes into consideration in-scattered intensities from every incoming direction. The intensity values at the inlet and outlet faces of each cell are defined based on the intensity at the cell center, and linked to one another by interpolation.

2.4 Raceway Simulation Methodology

As previously mentioned, the CFD models used to simulate conditions within the tuyere, raceway formation, and combustion within the raceway region are coupled to provide a complete picture of the blast furnace raceway process. A methodology for this simulation process was developed in conjunction with research on several industrial blast furnaces. Initial versions of this simulation technique have been utilized to couple the major CFD models, as illustrated in Figure 5 [27,31,32,45,73,74]. This methodology has undergone continuous improvement throughout its use in applied research, with the most recent developmental modifications completed as a component of this research.

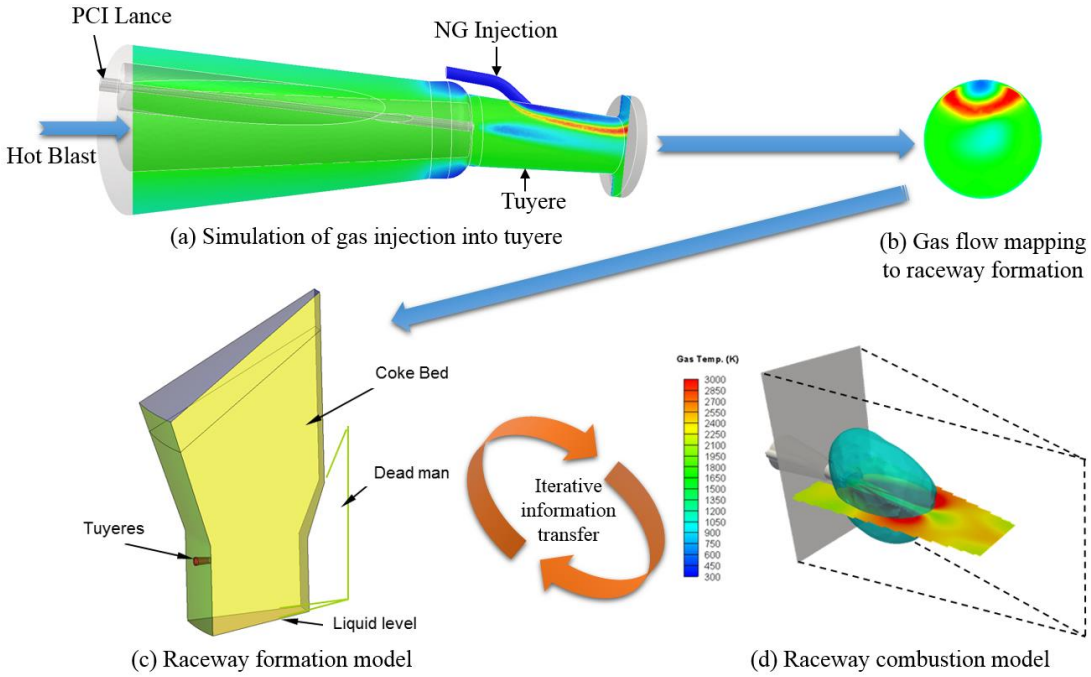

Figure 5. CFD model integration methodology.

Calculations of gas flow, turbulence, chemical reactions, heat transfer, and other phenomena are completed in the following procedure.

Step 1. Simulate steady-state flow conditions inside the blowpipe and tuyere, including the effects of auxiliary fuel combustion, with a focus on obtaining the distribution of flow properties (temperature, species concentration, etc.) at the outlet of the domain.

Step 2. Take a snapshot of flow conditions at the exit cross-section of the tuyere from the simulation conducted in Step 1. Use the properties as input conditions for the raceway formation CFD model, and simulate raceway formation. Generate a static porosity map for the raceway combustion model.

Step 3. Using the flow conditions developed in Step 1, set input conditions for the raceway combustion CFD model from the tuyere. Using these conditions and the porosity map generated in Step 2, simulate gas flow, reactions, and heat transfer inside the raceway.

Step 4. Account for the effects of combustion on raceway shape by adding additional gases and changes in volume generated by combustion in Step 3 to the raceway formation model.

Step 5. Use the mapping conditions from Step 1 and the data from Step 4 to re-simulate raceway formation.

Step 6. Repeat Steps 3, 4, and 5 until there is no observable change in raceway size and shape between steps. After this, the solution is converged.

2.5 CFD Model Validation

The multi-phase flow models have been widely validated in previous publications and in observations by industrial partners collaborating with current research. Some qualitative validation relating to individual industrial plant operations will be presented in Chapter 4, but confidentiality prevents the disclosure of exact comparisons to measurements obtained at specific industrial sites except where otherwise mentioned. The models used in this research have been calibrated and developed against published literature and industrial measurements, a summary of which data is included here for reference.

Validation of any model of the blast furnace raceway relies heavily on comparisons with practice and theory, as direct measurement of conditions within industrial scale blast furnaces is practically impossible. With this in mind, a comparison of raceway formation phenomena was conducted between the Eulerian multi-phase model used in this research and work by Nogami et al. examining discrete element modeling and experimental raceway shapes, with parameters defined based on conditions in an experimental test setup [73].

Additional verification utilizing theoretical correlations was also conducted for the new in-house raceway formation solver using the improved interphase momentum exchange terms. As raceway size is difficult to measure in practice, Rajneesh et al developed a correlation for theoretical calculation of raceway depth, as defined by Equation (93) [40].

$$D_r = 164\left(\frac{\rho_g v_b^2 D_T^2}{\rho_{eff} g d_p HW}\right)^{0.8} \mu_w^{-0.25} D_T \tag{93}$$

where D_r is the depth of the raceway from the tuyere tip, D_T is the diameter of the tuyere nose, H is the height of the fluidized bed of coke, W is the bed width, g is the acceleration due to gravity, v_b is the velocity of gas leaving the tuyere, and μ_w is the wall friction coefficient.

Comparisons of CFD results to this theoretical correlation under conditions based on industrial blast furnace operation at AK Steel Dearborn Works yielded a variation of 5.6%, with CFD data predicting a raceway 1.27 m in depth, and the correlation predicting a depth of 1.34 m. The coal and gas combustion models have been validated through a variety of previous studies, including comparisons with experimental data [74], and calibration of liftoff and blowout phenomena [75].

In addition, an analysis of numerical uncertainty was undertaken as part of this research to determine the impacts, if any, of error on the accuracy of modeling results within the blast furnace raceway region. A case utilizing a generic blast furnace raceway geometry at typical operating conditions (hot blast temperature of 1420 K, oxygen enrichment of 10%, NG injection rate of 40 kg/MTHM and PCI rate of 120 kg/MTHM) was simulated using three different mesh resolutions. Uniform element sizes of 0.03 m, 0.025 m, and 0.02 m were used in these three meshes, with total grid sizes of 220,000, 375,000, 720,000 elements respectively.

For these three cases, the mass-weighted averages of gas temperature, CO mass fraction, and gas y-velocity at the outlet of the raceway model was selected for comparison. The Grid Convergence Index (GCI) methodology outlined by the Journal of Fluids Engineering is utilized to provide a basis for uncertainty in this research [76]. The results of this examination of discretization error are detailed in Table 3 below.

Table 3. Discretization error.

	Temperature (K)	**CO Mass Fraction**	**Gas Y-Velocity (m/s)**
220,000 Cells	2350	48.72 %	4.37
375,000 Cells	2400	49.58 %	4.48
720,000 Cells	2375	51.05 %	4.57
Approx. Relative Error	0.80 %	2.88 %	1.97 %
Extrap. Relative Error	3.30 %	10.32 %	7.3 %
GCI	4.00 %	14.40 %	9.85 %

Hence, the numerical uncertainty in the finest grid solution (not including any modeling errors), the numerical uncertainty is 4% for temperature, 14.4% for CO mass fraction, and 9.85% for gas y-velocity. Given these values, as well as the industrial comparisons and previous model validation, the uncertainty of numerical results in this research appear to be within a reasonable range.

CHAPTER 3. RACEWAY MODEL NUMERICAL SCHEME

3.1 Computational Grid

The grid utilized in the development of three-dimensional simulations of raceway formation and combustion consists entirely of rectangular computational cell zones. When defined in standard Cartesian coordinates, these computational cells zones have a center point, P, and six cell faces, two in each cardinal direction. The faces are labeled simply as north (n), south (s), east (e), west (w), top (t), and bottom (b). A representation of a computational grid cell in Cartesian coordinates is shown in Figure 4.

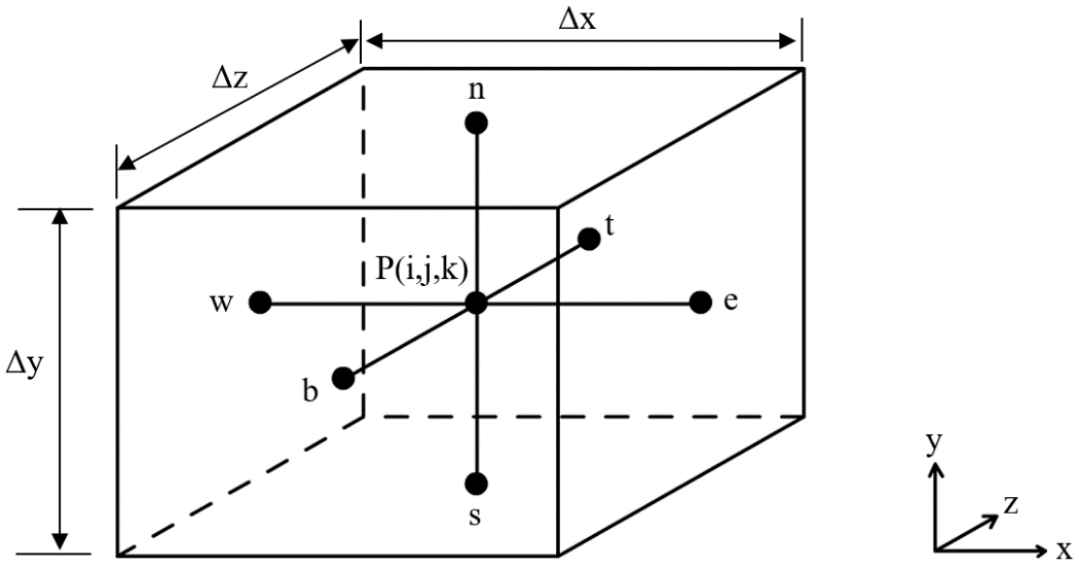

Figure 6. Typical cell in a Cartesian computational grid.

The center points of each neighboring cell are named similarly, with capital letters defining the north, south, east, west, top, and bottom adjacent cells (N, S, E, W, T, and B). Non-uniform cell sizes are possible, with varying cell widths, lengths, and heights. The operative variable of the general governing equation is solved using iterative methods at point P, and the physical properties of fluid phases are determined by interpolation of cell-centered values. Figure 5 illustrates the arrangement of adjacent cells and the nodal indices of those cells' data points.

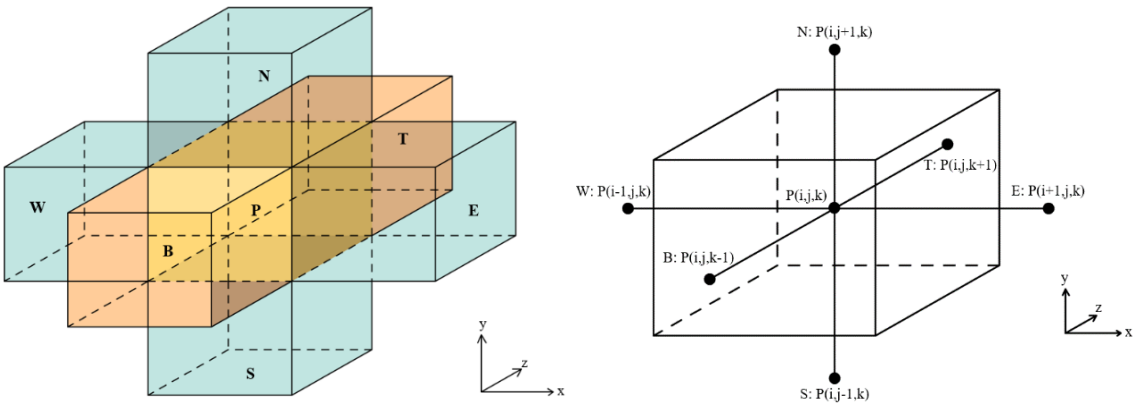

Figure 7. Cells centered on point P (left) and nodal indices of neighboring cells (right).

Patankar detailed the pitfalls present in a solution where the components of velocity and pressure values are stored at identical grid locations [77]. This type of discretization can result in a checkerboard pressure field as a solution to the numerical scheme, a physically impossible result. In order to prevent the formation of non-physical flow fields such as this, staggered control volumes are used to discretize the momentum equation. Figure 8 illustrates the concept behind the staggered grid locations for discretizing the components of the momentum equation. Scalar variables are stored at the cell nodes (P, E, W, N, S, T, and B), while velocities are calculated at cell faces between those nodes. The various components of velocity are stored at their corresponding faces (u-velocities are stored at faces *e* and *w*, v-velocities are stored at *n* and *s*, and w-velocities are stored at *t* and *b*). The velocity control volumes are staggered from the standard cell control volumes, and are centered on the cell faces.

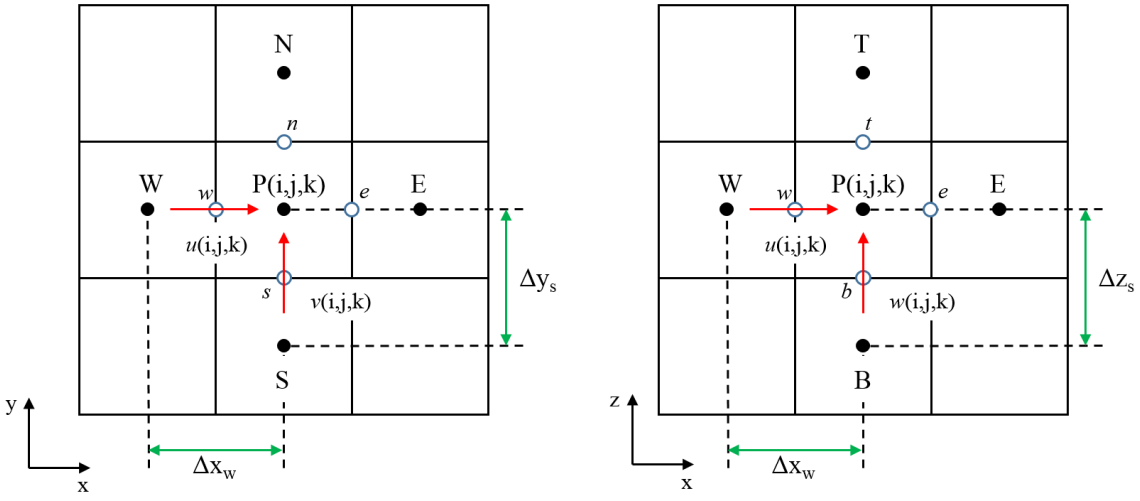

Figure 8. Staggered grid in both the x-y and x-z planes.

The three-dimensional grid system is generated by dividing the domain (a rectangular box large enough to encompass the entirety of the raceway region) into a set of extremely small rectangular cells. Cell faces are set up parallel to the box faces, and the geometry of the periodic raceway region is defined by blocking all cells outside the simulation region boundaries. Physically, this means that all cells located outside the geometry of the furnace or outside the periodic zone are locked out of the calculation. The grid used to model the raceway region in this research consists of roughly 700,000 computational cells. Figure 9 shows a sample grid, with the simulation domain highlighted by making all of the blocked cells within the rectangle invisible. Figure 10 shows a similar representation, but with an added cross-section through the center plane of the domain to showcase the tuyere and domain inlet.

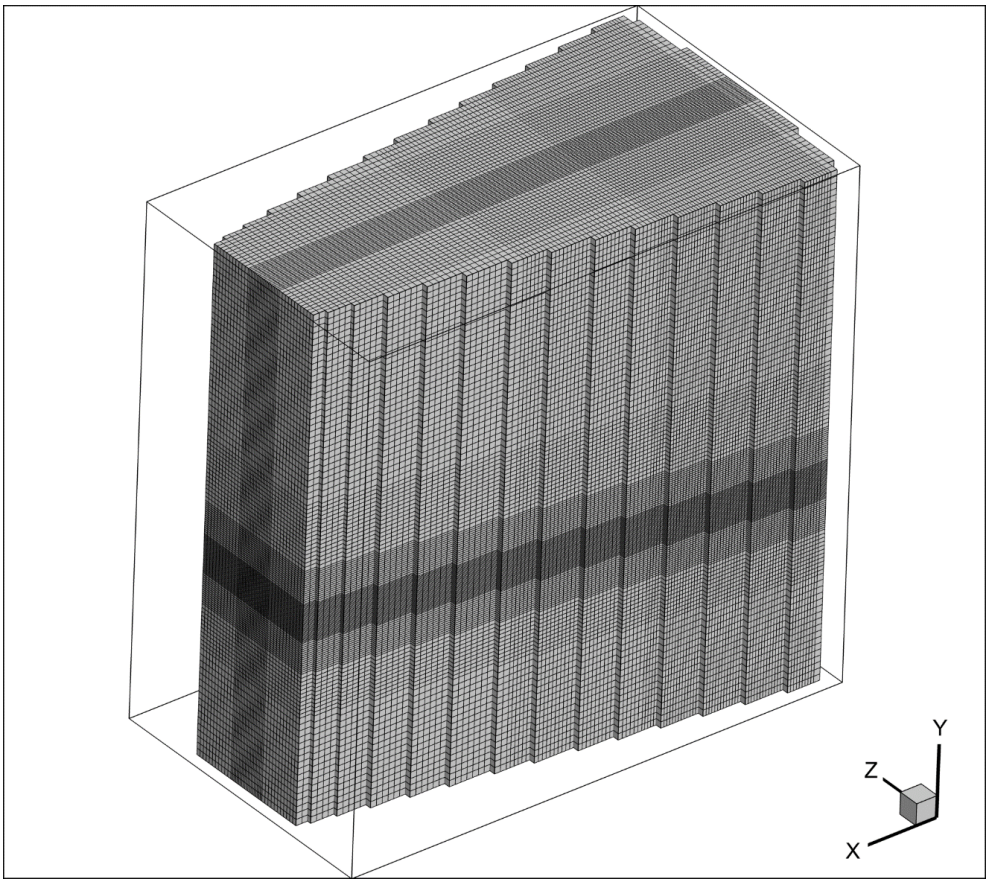

Figure 9. 3-D representation of the numerical grid used by the raceway model.

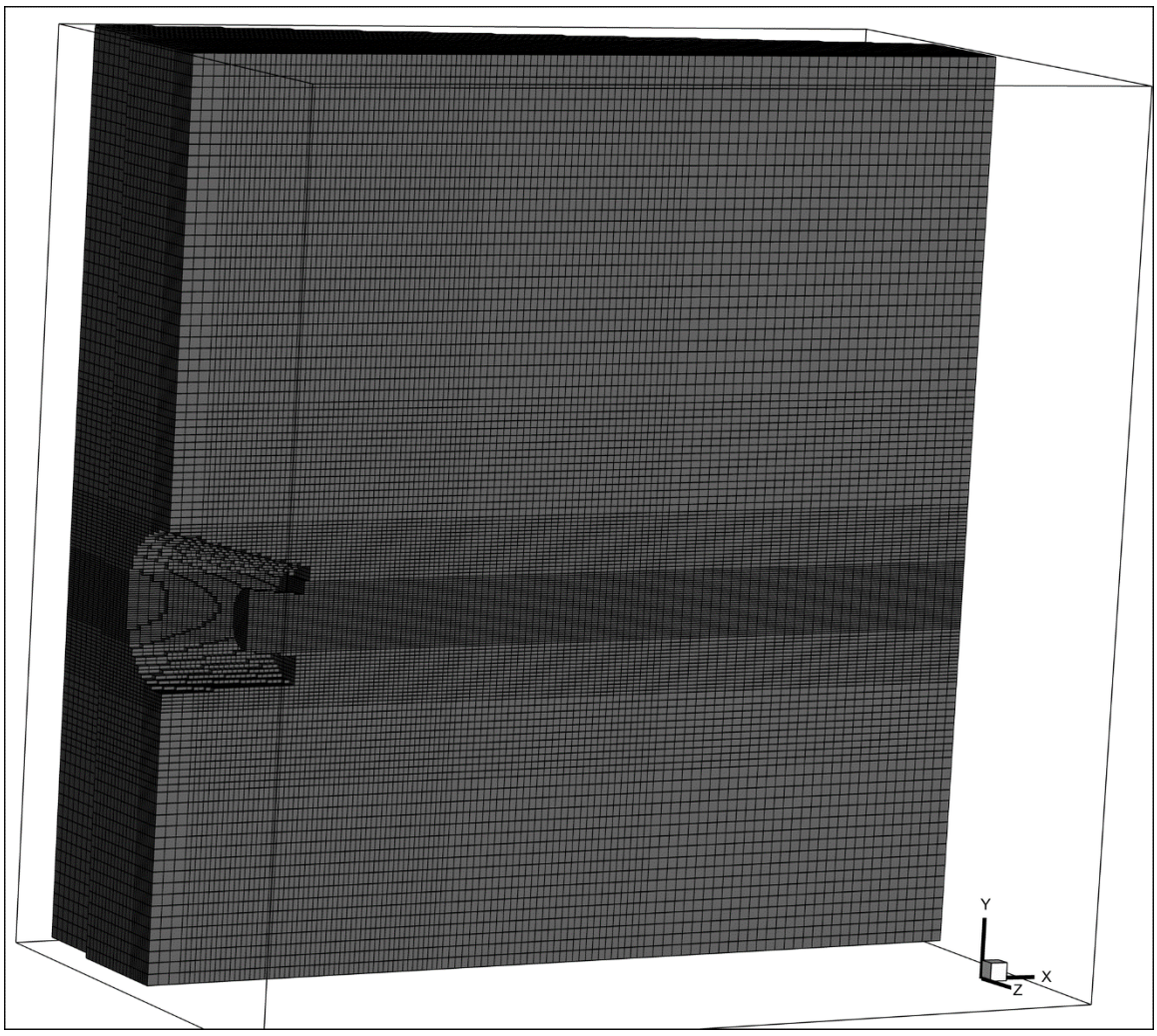

Figure 10. Cross-section of the numerical grid used by the raceway model.

The governing equations are solved within the non-blocked flow cells, and they are skipped when the solver encounters blocked grids. The major defining boundaries of the raceway region are reasonably simple: a cylindrical outer wall, a tuyere, periodic boundary conditions in both annular directions, and the furnace deadman at the center. The primary variations in geometry inside the furnace come from the raceway itself, the shape of which is a feature of the flow in the formation model and is defined by fixed porosity values at each cell in the combustion solver. This allows for the implementation of a simple, computationally efficient numerical algorithm, with high numerical accuracy.

The computational grid for the tuyere-blowpipe region of the blast furnace is generated using the mesh generation software package available with the commercial CFD software ANSYS 17.1®.

This grid is an unstructured grid of roughly 940,000 cells, defined with variable cell sizing dependent on the curvature of the geometry and proximity of boundaries. Figure 11 shows a cross-section along the centerline of the tuyere-blowpipe region grid utilized by the commercial CFD solver.

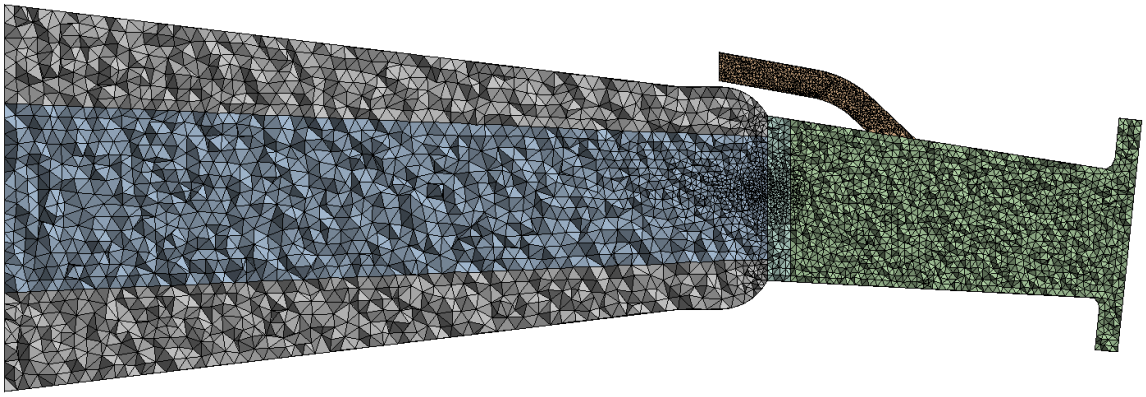

Figure 11. Cross-section of the numerical grid for the tuyere-blowpipe region.

These grids are fine enough to resolve flow features generated due to geometry variations in the tuyere and blowpipe region, however, they do not aim to capture turbulent phenomena directly. The turbulence and combustion modeling techniques selected in this study rely upon use of a grid coarse enough such that the effects of turbulent eddies at the Kolmogorov scale can be averaged over the cell control volumes. The Kolmogorov length scale for an arbitrary cell in end of the tuyere is approximately 10 μm, far smaller than the computational grid size minimums of 0.01-0.02 m. The cell selected can be seen in Figure 12. Gas temperatures within the cell reach 2,900 K (±4%) and coal temperatures reach 1,400 K (±4%). The reaction rate of natural gas in this cell is 5.57 kg $CH_4/(m^3s)$ and the consumption rate of coal is 0.1 kg $C/(m^3s)$.

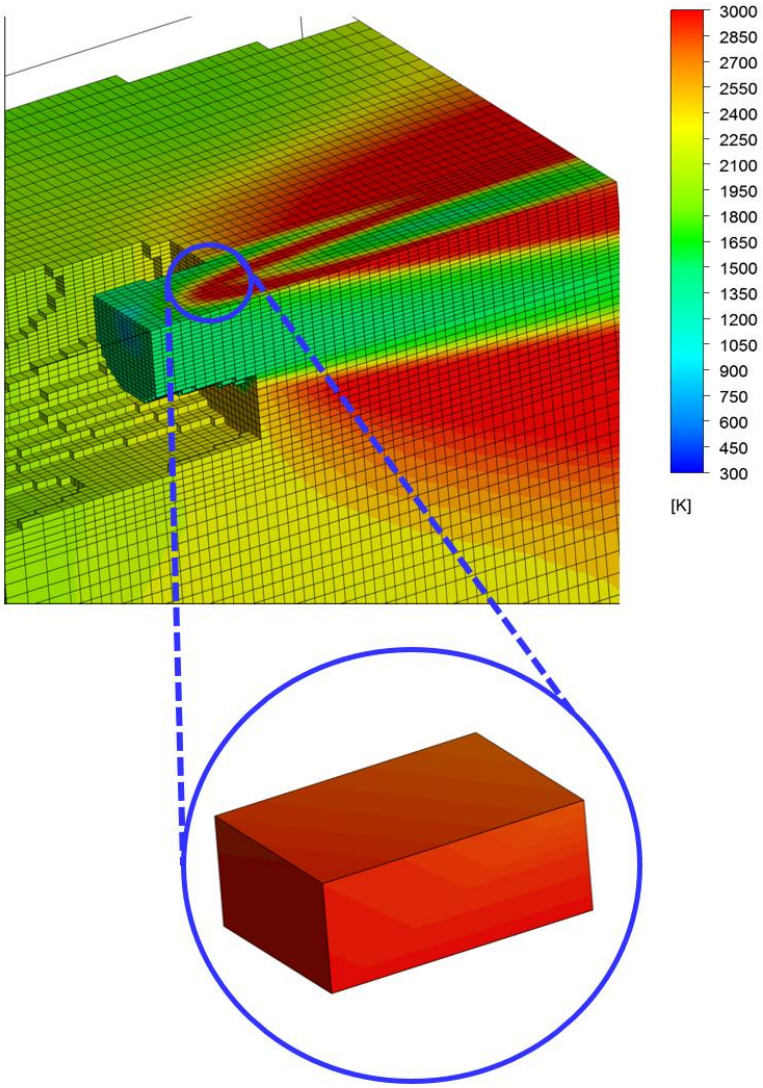

Figure 12. Gas temperature distributions on a cross-section of the structured grid.

3.2 Discretization of General Transport Equation

3.2.1 Steady-State Governing Equations

The conservation equations used in the steady state combustion CFD model are represented by the generalized scalar transport equation, sans the transient term:

$$\nabla \cdot \left(\rho_{eff}\vec{u}\phi - \Gamma\nabla\phi\right) = S \tag{94}$$

where ϕ is the general flow property being transported, Γ is the effective diffusivity, and $\vec{u}$ is the gas or pulverized coal velocity. ρ_{eff} is the effective density, defined as:

$$\rho_{eff} = \alpha_{phase}\rho_{phase} \tag{95}$$

where α_{phase} is the volume fraction of the gas or particle phase and ρ_{phase} is the density of the corresponding gas or particle phase. The convective and diffusive fluxes can be combined into a single term J as follows:

$$J = \rho_{eff}\vec{u}\phi - \Gamma\nabla\phi \tag{96}$$

Expanding the divergence operator in Cartesian coordinates and expressing the source term in terms of a linear relationship with the general variable gives:

$$\frac{\partial J_x}{\partial x} + \frac{\partial J_y}{\partial y} + \frac{\partial J_z}{\partial z} = S_c + S_p\phi \tag{97}$$

where the combined flux component terms are defined as:

$$J_x = \rho_{eff}u\phi - \Gamma\frac{\partial\phi}{\partial x} \tag{98}$$

$$J_y = \rho_{eff}v\phi - \Gamma\frac{\partial\phi}{\partial x} \tag{99}$$

$$J_z = \rho_{eff}w\phi - \Gamma\frac{\partial\phi}{\partial x} \tag{100}$$

Integrating the partial differential equation obtained in Equation (97) over the control volume detailed in Figure 6 produces:

$$(J_e - J_w)\Delta y\Delta z + (J_n - J_s)\Delta x\Delta z + (J_t - J_b)\Delta x\Delta y = \left(S_c + S_p\phi\right)\Delta x\Delta y\Delta z \tag{101}$$

Here, the combined flux terms represent the flux through each face of the control volume. J_e corresponds to the east face, J_w to the west face, J_n to the north face, J_s to the south face, J_t to the top face, and J_b to the bottom face. Δx, Δy, and Δz are also defined in Figure 6.

These combined flux terms can then be approximated using the first order upwind scheme, yielding [73]:

$$J_e \approx max[0, F_e]\phi_P - max[0, -F_e]\phi_E + \Gamma_e \frac{\phi_P - \phi_E}{(\partial x)_e} \quad (102)$$

$$J_w \approx max[0, F_w]\phi_W - max[0, -F_w]\phi_P + \Gamma_w \frac{\phi_W - \phi_P}{(\partial x)_e} \quad (103)$$

$$J_n \approx max[0, F_n]\phi_P - max[0, -F_n]\phi_N + \Gamma_n \frac{\phi_P - \phi_N}{(\partial y)_n} \quad (104)$$

$$J_s \approx max[0, F_s]\phi_S - max[0, -F_s]\phi_P + \Gamma_s \frac{\phi_S - \phi_P}{(\partial y)_s} \quad (105)$$

$$J_t \approx max[0, F_t]\phi_P - max[0, -F_t]\phi_T + \Gamma_t \frac{\phi_P - \phi_T}{(\partial z)_t} \quad (106)$$

$$J_b \approx max[0, F_b]\phi_B - max[0, -F_b]\phi_P + \Gamma_b \frac{\phi_B - \phi_E}{(\partial z)_b} \quad (107)$$

where:

$$F_e = \rho_{eff,e} u_e \quad (108)$$

$$F_w = \rho_{eff,w} u_w \quad (109)$$

$$F_n = \rho_{eff,n} u_n \quad (110)$$

$$F_s = \rho_{eff,s} u_s \quad (111)$$

$$F_t = \rho_{eff,t} u_t \quad (112)$$

$$F_b = \rho_{eff,b} u_b \quad (113)$$

$(\partial x)_e$, $(\partial x)_w$, $(\partial y)_n$, $(\partial y)_s$, $(\partial z)_t$, and $(\partial z)_b$ are the distances between cells, as seen in Figure 13. With the possibility for non-uniform cell sizes in the domain, these distances may vary with direction throughout the domain.

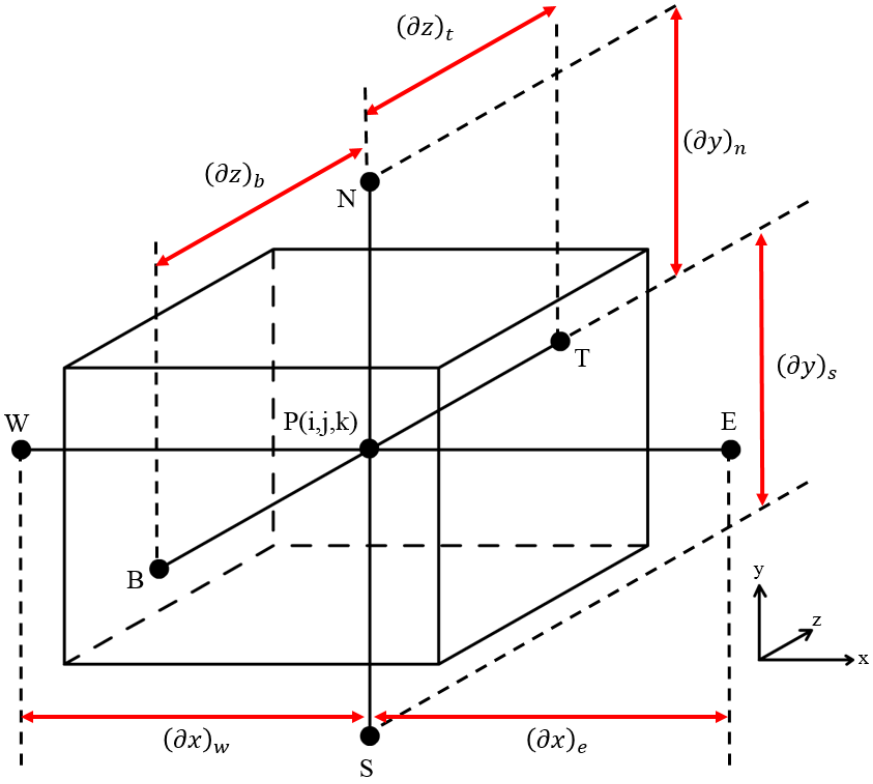

Figure 13. Distances between cells in Cartesian coordinates.

The final form of the discretized algebraic equation solved by the technique given in section 3.3 is determined through substitution of Equations (102)-(107) into Equation (101).

$$a_p\phi_p = a_E\phi_E + a_W\phi_W + a_N\phi_N + a_S\phi_S + a_T\phi_T + a_B\phi_B + b \tag{114}$$

where:

$$a_E = \left(\max[0, -F_e] + \frac{\Gamma_e}{(\partial x)_e}\right)\Delta y \Delta z \tag{115}$$

$$a_W = \left(\max[0, F_w] + \frac{\Gamma_e}{(\partial x)_w}\right)\Delta y \Delta z \tag{116}$$

$$a_N = \left(\max[0, -F_n] + \frac{\Gamma_n}{(\partial y)_n}\right)\Delta x \Delta z \tag{117}$$

$$a_S = \left(\max[0, F_s] + \frac{\Gamma_s}{(\partial y)_s}\right)\Delta x \Delta z \tag{118}$$

$$a_T = \left(\max[0, -F_e] + \frac{\Gamma_t}{(\partial z)_t}\right)\Delta x \Delta y \tag{119}$$

$$a_B = \left(\max[0, F_b] + \frac{\Gamma_b}{(\partial z)_b}\right)\Delta x \Delta y \tag{120}$$

$$a_P = a_E + a_W + a_N + a_S + a_T + a_B - S_p \Delta x \Delta y \Delta z \tag{121}$$

$$b = S_c \Delta x \Delta y \Delta z \tag{122}$$

3.2.2 Transient Governing Equations

A similar procedure is followed for the discretization of the governing equations with the addition of a transient term in the raceway formation model. The conservation equations are represented by the full generalized scalar transport equation:

$$\frac{\partial}{\partial t}\left(\rho_{eff}\phi\right) + \nabla \cdot \left(\rho_{eff}\vec{u}\phi - \Gamma \nabla \phi\right) = S \tag{123}$$

Following the same procedure for discretization as laid out in section 3.2.1 and taking the additional transient term into account, we have the coefficients for Equation (114):

$$a_E = \left(\max[0, -F_e] + \frac{\Gamma_e}{(\partial x)_e}\right)\Delta y \Delta z \tag{124}$$

$$a_W = \left(\max[0, F_w] + \frac{\Gamma_e}{(\partial x)_w}\right)\Delta y \Delta z \tag{125}$$

$$a_N = \left(\max[0, -F_n] + \frac{\Gamma_n}{(\partial y)_n}\right)\Delta x \Delta z \tag{126}$$

$$a_S = \left(\max[0, F_s] + \frac{\Gamma_s}{(\partial y)_s}\right)\Delta x \Delta z \tag{127}$$

$$a_T = \left(\max[0, -F_e] + \frac{\Gamma_t}{(\partial z)_t}\right)\Delta x \Delta y \tag{128}$$

$$a_B = \left(\max[0, F_b] + \frac{\Gamma_b}{(\partial z)_b}\right)\Delta x \Delta y \tag{129}$$

$$a_P = a_E + a_W + a_N + a_S + a_T + a_B + a_p^0 - S_p \Delta x \Delta y \Delta z \tag{130}$$

$$b = a_p^0 \phi_p^0 + S_c \Delta x \Delta y \Delta z \tag{131}$$

$$a_p^0 = \frac{\rho_{eff}^0}{\Delta t}\Delta x \Delta y \Delta z \tag{132}$$

3.3 Solution Technique

Through the application of neighbor cell indexing, Equation (114) can be written in a general form for a cell located at point P with coordinates *(i,j,k)*:

$$\mathrm{a_p}\phi(i,j,k) = \mathrm{a_E}\phi(i+1,j,k) + \mathrm{a_W}\phi(i-1,j,k) + \mathrm{a_N}\phi(i,j+1,k) + \mathrm{a_S}\phi(i,j-1,k) + \mathrm{a}_T\phi(i,j,k+1) + \mathrm{a_b}\phi(i,j,k-1) + \mathrm{b} \tag{133}$$

The discretized governing equations for the gas and particle phases are solved over the computational domain using a tri-diagonal matrix algorithm (TDMA) with under-relaxation factors and using the alternating direction implicit (ADI) method. Coupling of gas phase pressure and velocity is handled through the SIMPLEC algorithm with a TDMA line-by-line solver [77]. The combustion solver utilizes a similar procedure for the particle phase, omitting the pressure-velocity corrections. In order to converge the two phase solution, the solver iterates between the gas and particle phases. The raceway formation solver can also utilize the PC-SIMPLE algorithm [78].

3.4 Iterative Procedure

Flow charts of the solution procedure for the raceway formation and raceway combustion solvers are shown in Figures 14 and 15 respectively. Both solvers require input information from the CFD simulation of the blowpipe/tuyere region, including gas flow rates, species concentrations, temperatures, and other values.

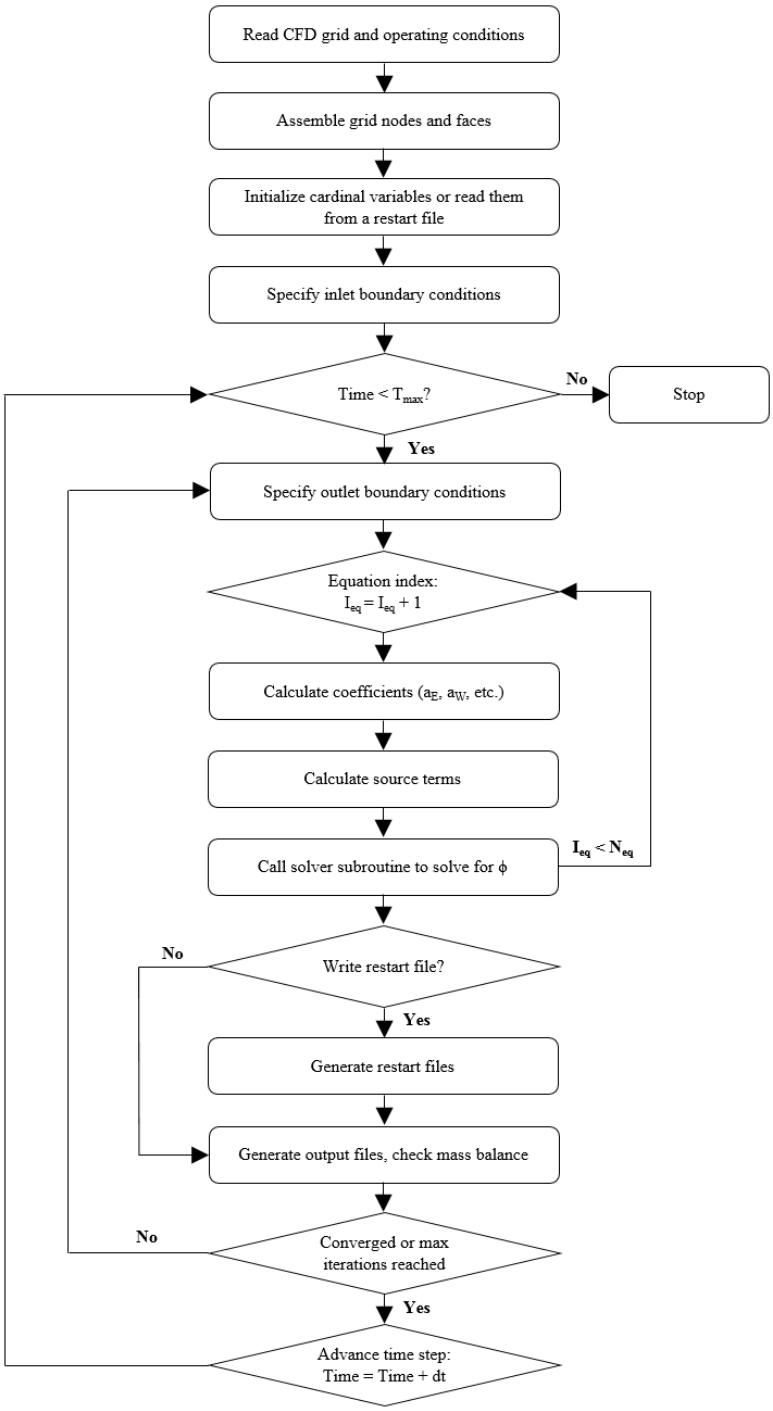

Figure 14. Flowchart of raceway formation CFD model.

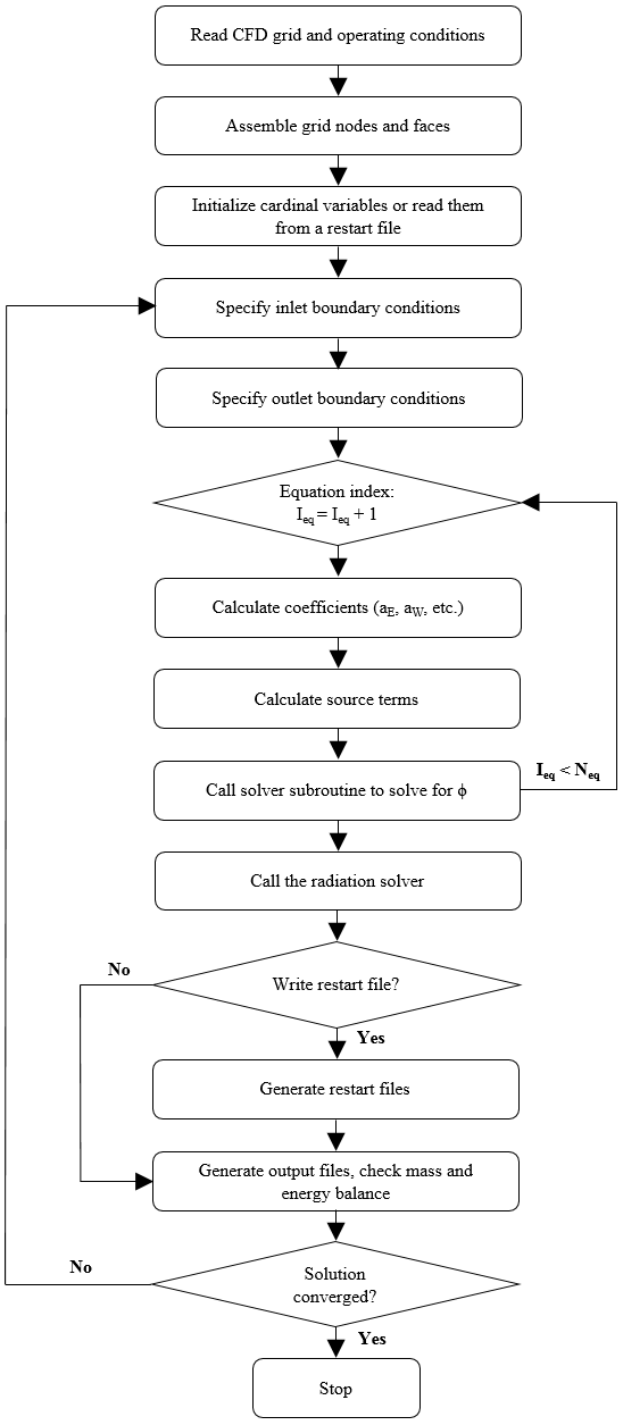

Figure 15. Flowchart of raceway combustion CFD model.

CHAPTER 4. COMPUTATIONAL MODELING RESEARCH

Applied research utilizing the CFD models detailed above has been conducted to develop new knowledge regarding furnace operation and the effects of unique and previously unexplored operating conditions. Simulations were conducted for various industrial blast furnaces under a variety of conditions of interest in furnace operation. This chapter is divided into several major sections, one for each of the industrial furnaces modeled using the previously detailed CFD techniques. These simulations provide crucial insights into the phenomena inside industrial scale blast furnaces, the influence of various novel auxiliary fuel injection techniques upon combustion characteristics, and possible benefits to blast furnace operation.

4.1 Investigation of Natural Gas and Pulverized Coal Co-injection

AK Steel's Dearborn Works facility, located in Dearborn, MI, produces a variety of high-quality hot and cold rolled steels for many applications. The Dearborn Works blast furnace was rebuilt and modernized in 2007, and numbers among the most efficient and productive blast furnaces in the world for its size. The furnace has a total working volume of 1,797 m^3 and is supplied hot blast by 20 tuyeres around the bosh annulus. As is common practice in the operation of many modern blast furnaces, the Dearborn Works facility utilizes tuyere level natural gas and pulverized coal injection to reduce total coke consumption. The existing design of the Dearborn Works injection facilities injects natural gas through a tuyere port in the upper inner surface of the tuyere. Additionally, PCI is performed through a lance that is inserted through the side of the blowpipe [79]. The pneumatic carrier gas for PCI is nitrogen, as is the case in many reported PCI systems. As an inert gas with similar properties to air, nitrogen is often the pneumatic conveyance method of choice for PCI. However, the use of nitrogen also presents certain disadvantages. When injected at standard temperature, the nitrogen serves to cool pulverized coal particles, delaying the process of coal devolatilization. In addition, a fraction of the combustion energy generated in the raceway is lost in the process of heating the inert carrier gas.

In the past, operators and engineers at the Dearborn Works facility began to explore the concept of using natural gas as the carrier gas for PCI. Prior to this research, there has been very little

detailed reporting of this concept in the public domain. A publication in the late 1990s focusing on co-injection of pulverized coal and natural gas mentions a method for utilizing natural gas as the carrier for PCI, however, little detail was discussed, and the concept was not adopted [15]. This portion of the research will present the industrial drivers for the research before examining computational simulations of combustion phenomena in the tuyere and raceway of the Dearborn Works blast furnace under a wide variety of operating conditions.

Based on best practice correlations and industrial experience, it was posited that this novel injection technique could enhance combustion performance, increase furnace productivity, and reduce operational expenses. Additionally, one of the aims of this new injection technique was to develop a method of overcoming some existing complications with high rate PCI, including increased total fuel rates for a given production rate and a reduction of permeability in the coke bed [80]. Limiting excess nitrogen injection into the furnace also presents the possibility to increase furnace productivity, as combustion energy will not be lost to the heating of an inert gas. AK Steel Dearborn Works performed estimations of potential productivity increase in scenarios with reduced nitrogen injection. These estimations are presented in Table 4.

Table 4. Potential production benefits of reducing nitrogen injection.

Variable	**Baseline**	**Potential 1 (Wind for N_2)**	**Potential 2 (O_2 for N_2)**	**Potential 3 (Wind for N_2, BGV constant)**	**Potential 4 (O_2 for N_2, BGV constant)**
Wind (Nm^3/hr)	199,020	200,700	199,020	200,625	199,020
O_2 enrich. (% of wind)	13.5	13.5	14.3	13.5	14.0
NG/PCI (kg/MTHM)	65/85	65/85	65/85	65/85	65/85
Bosh Gas Vol. (Nm^3/hr)	353,100	353,100	353,100	353,100	353,100
Production rate (mtpd)	5,670	5,720	5,810	5,710	5,750
Impact on annual production (metric tons)	N/A	16,980	49,500	16,180	29,330

As a whole, these potential benefits could yield significant reductions in operational and production expenses in the Dearborn Works ironmaking unit. However, there exist significant risks and expenses related to a drastic shift to natural gas as the PCI conveyance method. Due to this, CFD modeling is an ideal choice to develop a detailed informational basis prior to capital investment. Additionally, parametric studies using the model can provide insight into combustion characteristics under both the existing and proposed injection designs and operating conditions at Dearborn Works.

4.1.1 Simulation Geometry

This study is concerned with the effects of injection parameters, designs, and operating conditions on the combustion of natural gas and pulverized coal in the raceway of the Dearborn Works furnace. The simulation domain modeled includes the blowpipe, pulverized coal and natural gas injection locations, and the raceway. Two major designs were modeled in the current research: the injection apparatus currently in use at Dearborn Works which utilizes a tuyere port to inject natural gas, shown in Figure 16, and a second proposed design using dual symmetric lances for natural gas and pulverized coal injection, shown in Figure 17.

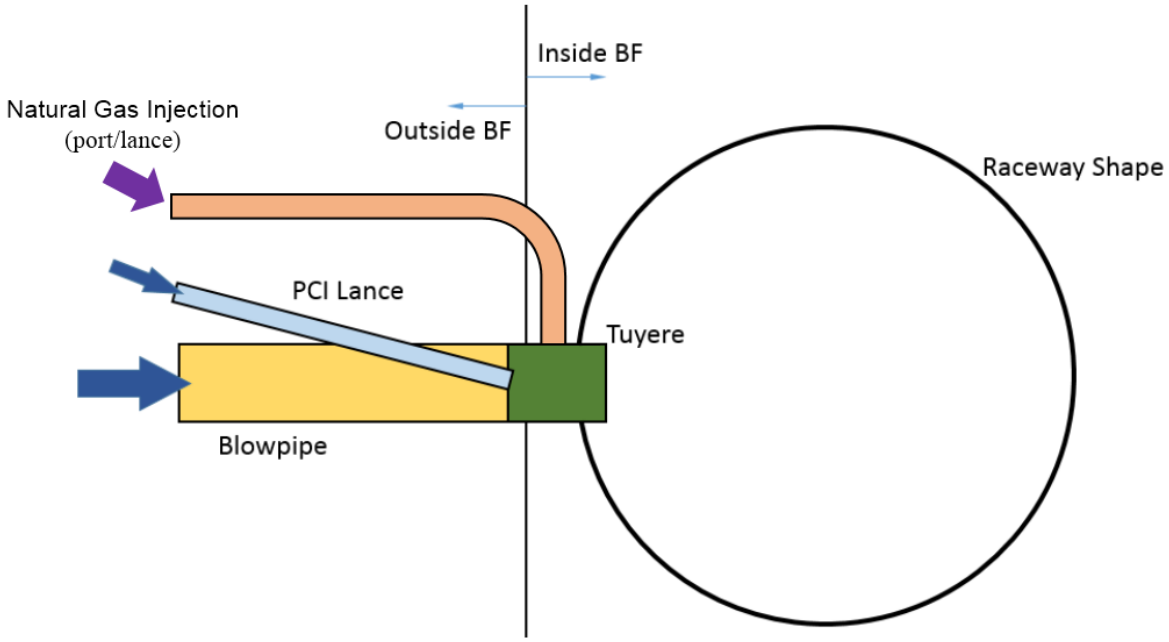

Figure 16. Simplified schematic of current injection apparatus at Dearborn Works.

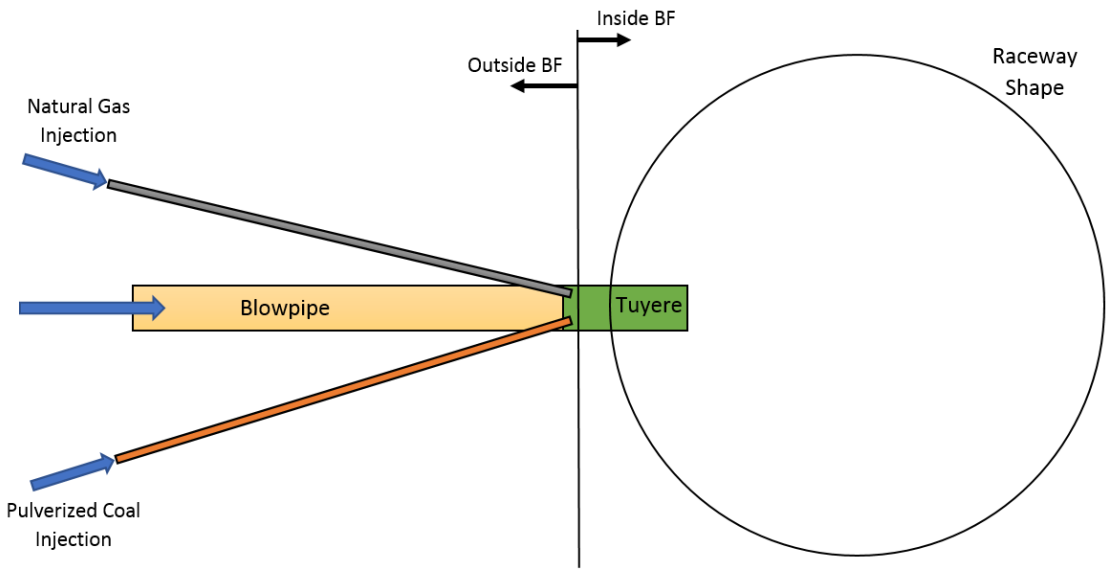

Figure 17. Simplified schematic of proposed dual lance injection apparatus.

The outlet of the tuyere is defined as an outflow boundary condition. The walls of the domain include heat flux boundary conditions to represent cooling water flow through the tuyere and ambient air passing over the outside the blowpipe. Material thermal properties and surrounding ambient temperatures are based on plant data. A baseline case was developed using operating conditions representative of standard operation at the Dearborn Works furnace, including total wind rate, hot blast temperature, oxygen enrichment, and fuel injection rates, and the geometry of the current injection apparatus. This case serves as a reference point to which all further parametric study cases, regardless of operating conditions, injection parameters, or designs, can be compared. The geometry simulated in the baseline case is shown in Figures 18 and 19. The size and position of the deadman in the Dearborn Works furnace was based on best practice data from previous simulation studies and industrial experience from Dearborn Works plant personnel.

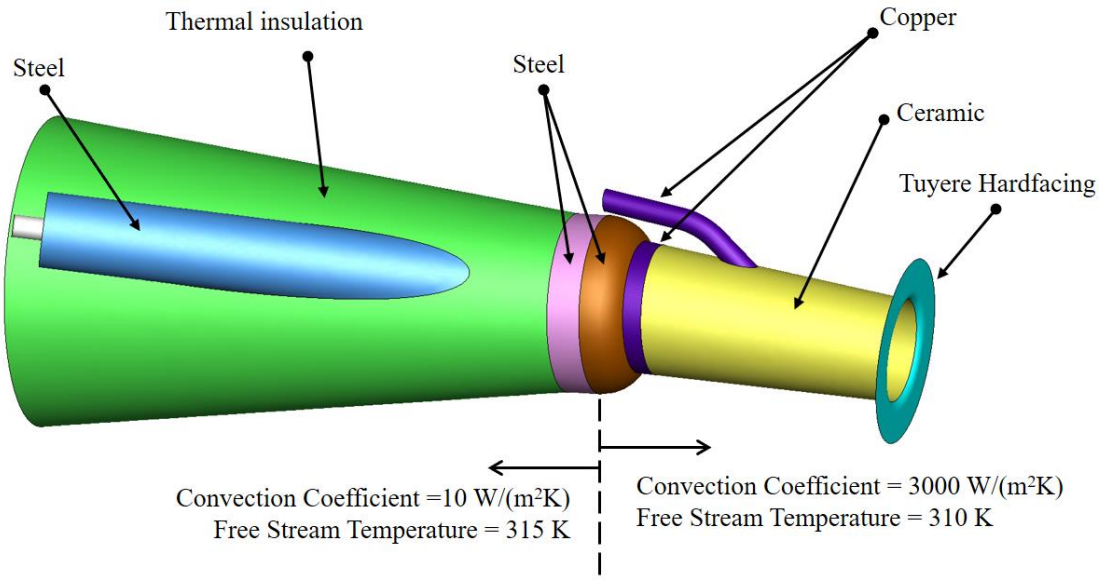

Figure 18. Geometry of blowpipe and tuyere simulation for the Dearborn Works furnace.

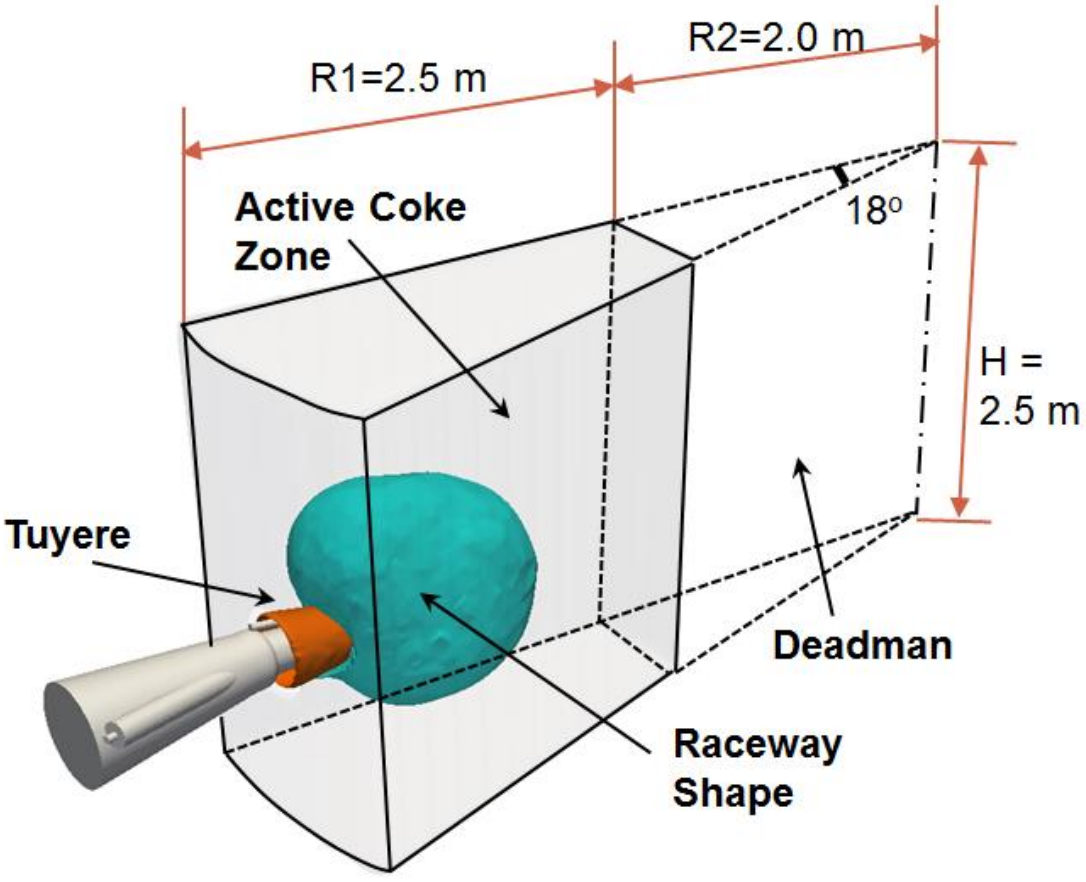

Figure 19. 3-D geometry of raceway domain for the Dearborn Works baseline design.

The parametric studies conducted in this project examined a wide variety of modified operating conditions including the use of natural gas vs. nitrogen as the carrier gas for PCI, uncommon operating conditions, such as reduced hot blast temperatures and wind rates, and more. Simulation results were examined to provide a detailed analysis of phenomena in the tuyere and raceway such as combustion location, gas temperatures, lance temperatures, species distributions, and fuel burnout rates.

Additionally, studies were conducted on the effects of shifting the natural gas injection location on combustion within the raceway using the proposed dual lance injection apparatus. These design alterations were obtained by shifting the natural gas injection lance axially in and out of the blowpipe by 5.08 cm (two inches) with respect to the proposed design. Though computational modeling allows for a theoretically infinite number of possible lance designs and positions in the blowpipe, spatial restrictions on the Dearborn Works furnace tuyere deck limit the implementation of certain lance designs. Given this, the designs simulated in this study were focused only on feasible injection locations that could be implemented at the Dearborn Works furnace. In addition, the PCI lance position was not adjusted from the existing Dearborn Works design due in large part to concerns regarding possible abrasion and/or thermal damage to the refractory inside the blowpipe. Combustion phenomena in both the proposed dual lance design and the injection apparatus currently in use at the Dearborn Works furnace were compared to further examine the effects of natural gas injection location on auxiliary fuel combustion performance.

4.1.2 Baseline Case

Co-injection of pulverized coal and natural gas in the standard configuration and at typical operating conditions at the AK Steel Dearborn Works blast furnace was modeled using CFD. As previously mentioned, the baseline case simulated in this research project provides a reference point for comparisons of combustion and flow phenomena within the tuyere and raceway, as well as to perform validation of the simulation model against industrial observations. Pulverized coal is carried by nitrogen gas through a single lance, and natural gas is injected through a tuyere port. Operating conditions are typical for standard operation at the Dearborn Works furnace, a blast furnace wind rate of 199,020 Nm^3/hr, hot blast temperature of 1,408 K, 13.5% oxygen enrichment in the hot blast, 85 kg/MTHM of PCI, and 65 kg/MTHM of NG. Coal particle size was defined by

a Rosin-Rammler distribution centered on an average of 66 μm, based on data provided by Dearborn Works coal analysis [81-83].

The injection of natural gas through a tuyere port on the upper surface of the inside of the tuyere leads to a unique combusting gas plume inside the tuyere. Natural gas combustion takes place in the region of gas mixing between injected natural gas and oxygen in the hot blast, near the upper tuyere wall. The high temperatures generated by combustion in this area remain in the upper portion of the tuyere jet, with very little mixing occurring between the combustion plume and the pulverized coal injected through the lance. This phenomenon can be observed in Figure 20, detailing temperature distributions throughout the blowpipe and tuyere. Figure 21 shows gas velocity distributions within the blowpipe and tuyere on the same cross-section. Aside from a reduced velocity zone where pulverized coal is injected into the hot blast, gas velocity accelerates as the blast travels down the tuyere due to both thermal expansion and the narrowing of the tuyere nozzle.

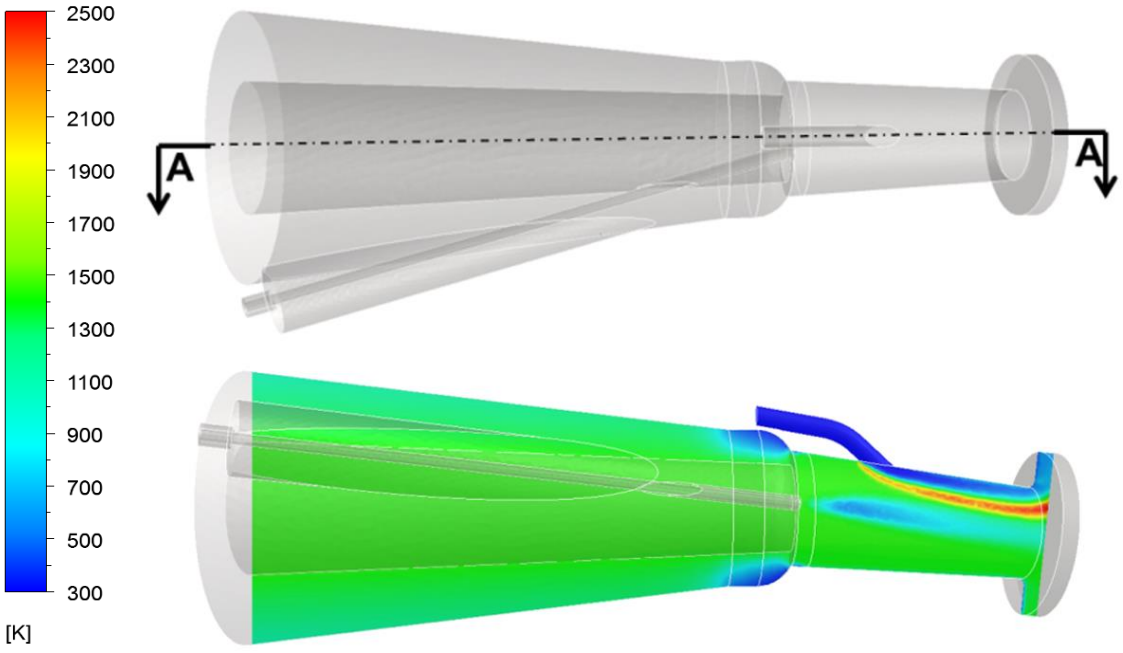

Figure 20. Blowpipe/tuyere geometry (top) and gas temperature on section A-A (bottom).

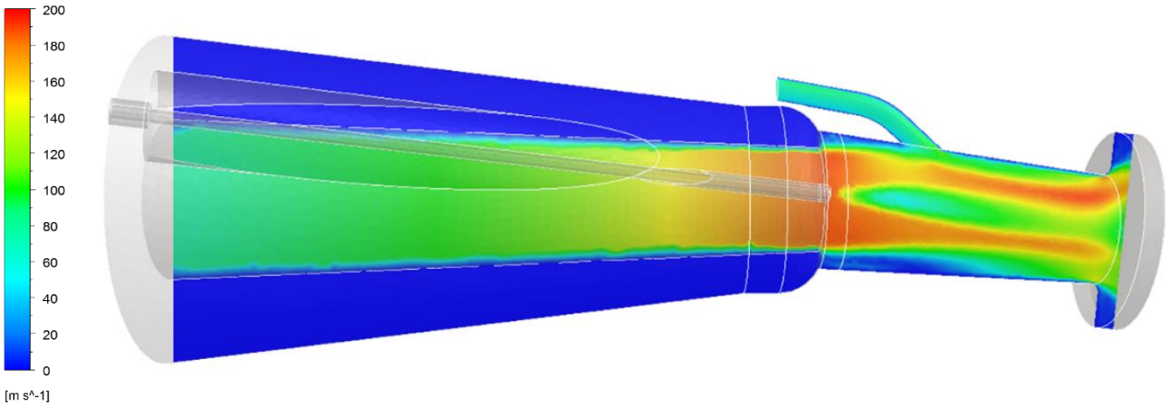

Figure 21. Gas velocity inside the tuyere and blowpipe on section A-A.

Unfortunately, these mixing conditions represent a significant failure of the current injection apparatus at the Dearborn Works furnace, as one of the primary benefits of natural gas injection is to supply additional heat for rapid devolatilization of pulverized coal. Since the combustion of natural gas occurs almost entirely in the upper portion of the tuyere, downstream of the pulverized coal injection lance tip, the high temperature combustion gases generated contribute very little to the heating of pulverized coal. The coal particles are primarily heated by the hot blast itself, which is at a significantly lower temperature than the natural gas combustion byproducts. This leads to slower pulverized coal heating and less rapid devolatilization. Pulverized coal temperature increases steadily as the particles travel down the tuyere, corresponding to the amount of time they have spent in contact with the hot blast and minor heat transfer from the natural gas combustion byproducts. Figure 22 details the flow paths of coal particles as they travel from the injection lance through the tuyere. The path lines are colored by particle temperature, serving to highlight the very minor influence of natural gas combustion on pulverized coal heating.

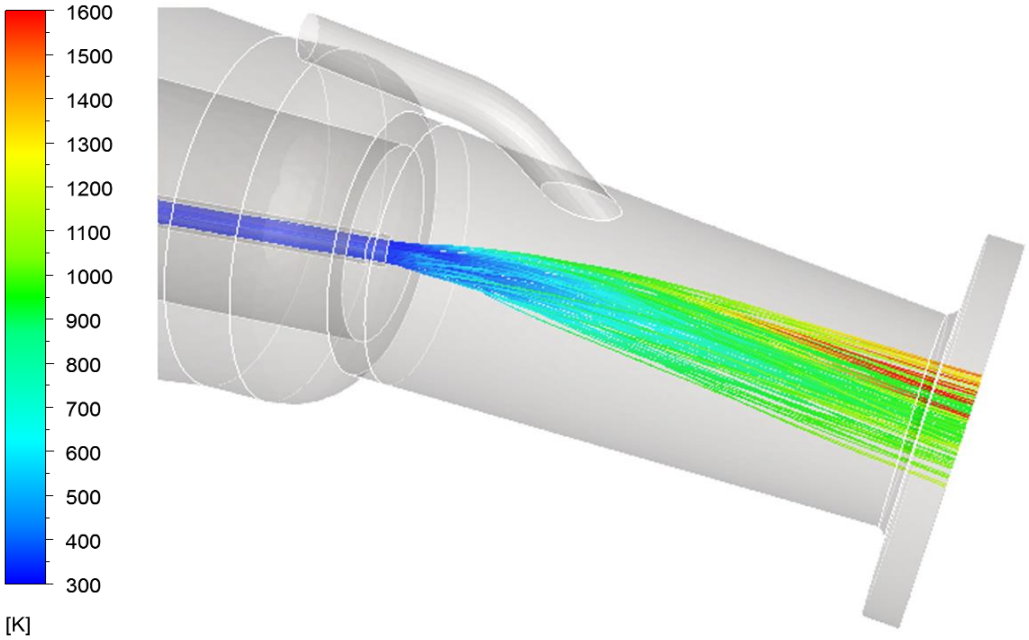

Figure 22. Coal particle path lines drawn in the tuyere, colored by particle temperature.

Figure 23 illustrates the gas temperature and along the tuyere centerline, and three parallel lines located 2, 4, and 6 cm above the centerline.

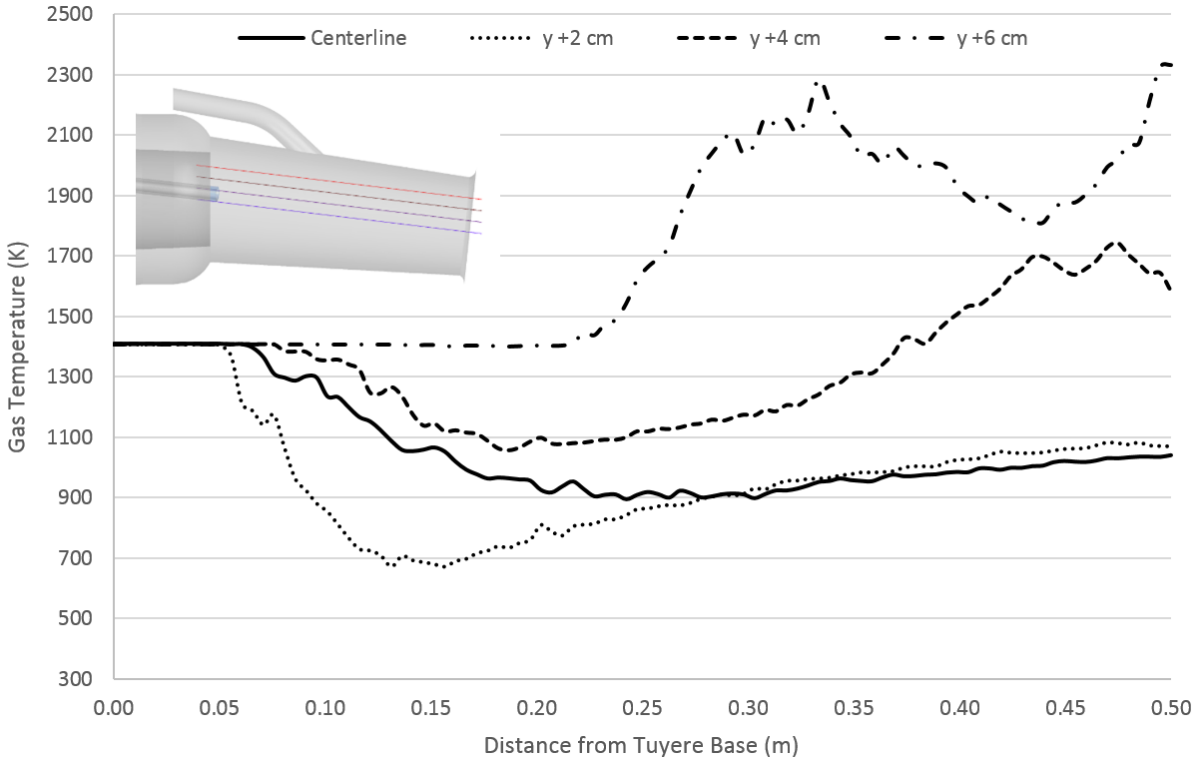

Figure 23. Coal particle temperature and average gas temperature plotted along the tuyere.

An examination of devolatilization as pulverized coal particles pass through the tuyere yields the expected results. Devolatilization is intense in the regions of the tuyere where coal particles come into contact with the high temperature gases generated by natural gas combustion, while the remainder of the injected coal releases little to none of its volatile matter. Figure 24 shows contours of the volatile mass fraction in the gas phase on section A-A and several perpendicular cross sections through the tuyere, parallel to the tuyere outlet. These results show direct correlation with Figure 22, highlighting the link between enhanced coal particle heating from the natural gas combustion plume and rapid volatile matter release.

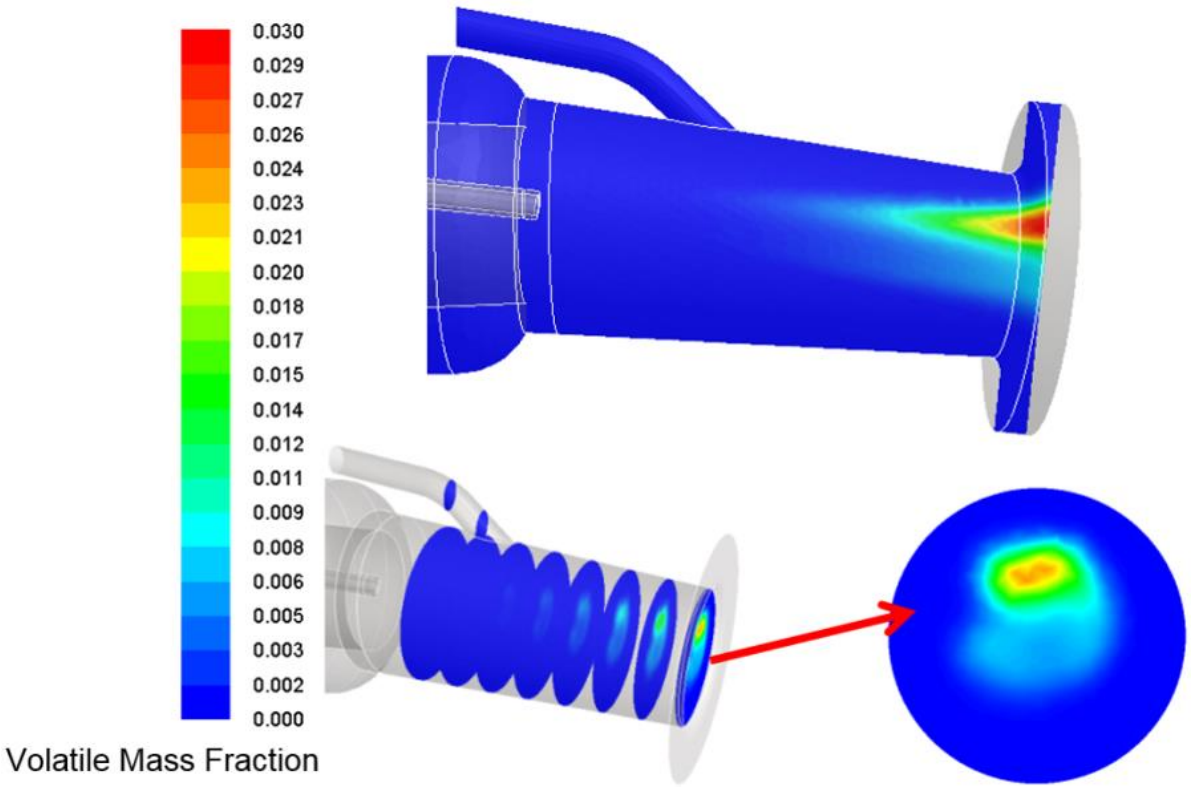

Figure 24. Volatile mass fraction distribution throughout the tuyere (bottom).

It is also worth noting the mass fractions of free radicals generated by natural gas combustion within the tuyere region. Figure 25 shows the distribution of free radicals included in the simulation model along a line parallel to and 6 cm above the tuyere centerline, passing directly through the plume of natural gas combustion from the tuyere port.

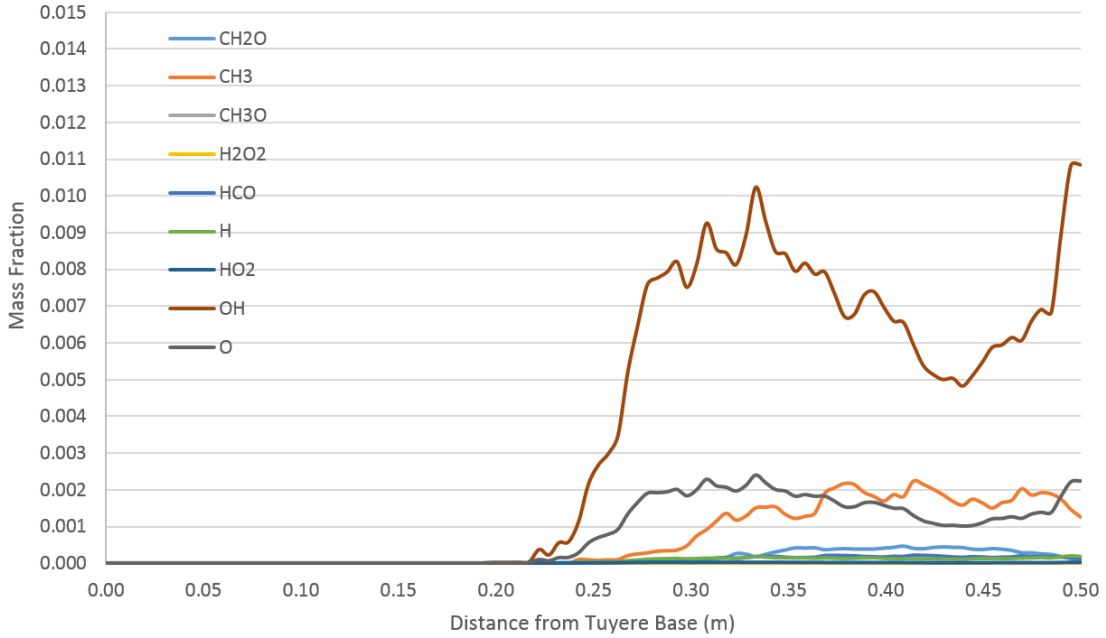

Figure 25. Distribution of radical species through the natural gas plume in the tuyere.

All radicals observed are below 1% mass fraction, with most radicals peaking below 0.05%. With this in mind, there should be no observable inconsistency between the species distributions calculated using the EDC model in the tuyere and the corresponding eight species (primary stable species) considered in the raceway region using the EBU model.

The results of the tuyere and blowpipe region model are supplied as inlet conditions for the raceway simulation procedure. As the void fraction of the coke bed inside the furnace decreases in a gradual fashion as one moves farther away from the tuyere, the raceway itself has no strictly defined outer boundary in this simulation model. However, for purposes of illustration, a specific boundary between ‘inside’ and ‘outside’ the raceway envelope must be defined. A void fraction of 0.7 is selected to represent the boundary in the research presented herein. Figure 26 details the shape and size of the raceway envelope for the simulation conducted at baseline operating conditions. Overall the raceway size under these operating conditions measures approximately 1.2 meters in depth, 0.7 meters in width, and 1.1 meters in height.

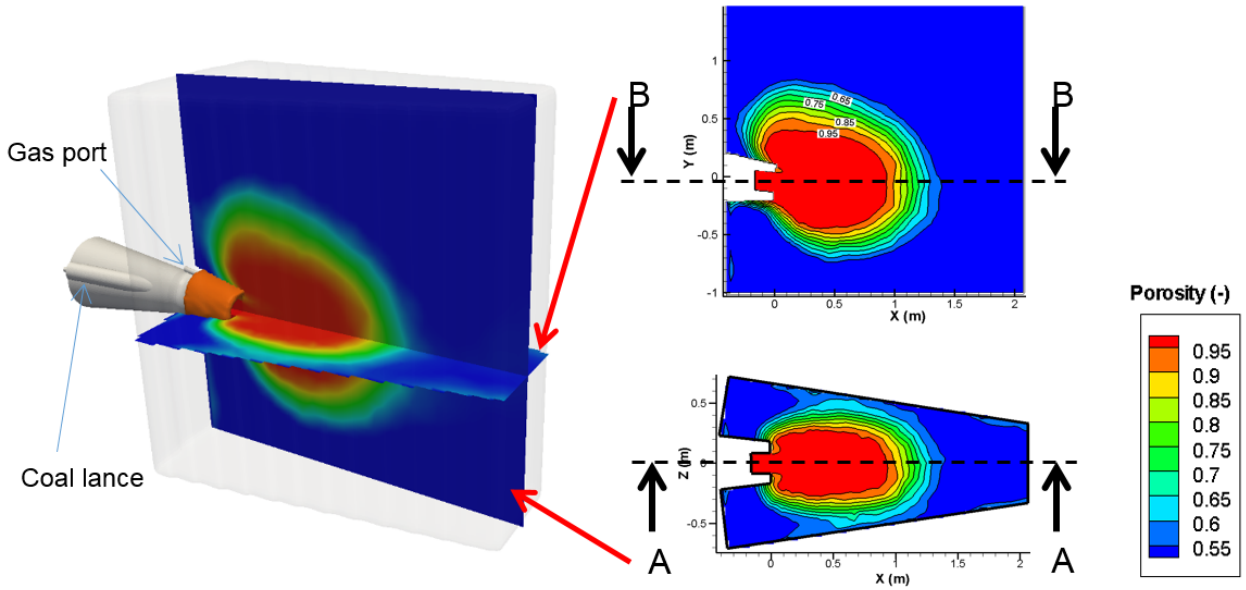

Figure 26. Contours of coke bed porosity (void fraction) for the baseline case.

As mentioned in section 1.1, the primary purpose of the tuyere blast assembly is to supply a jet of hot blast gas into the lower regions of the furnace to facilitate combustion and generate the necessary reducing gas for furnace operation. The momentum of the tuyere gas jet begins to dissipate as the gas encounters lower void fraction regions of the raceway, and the jet disappears entirely by the edge of the raceway envelope. Additional momentum is required to accelerate pulverized coal and the corresponding carrier gas injected into the blowpipe, slightly reducing the jet velocity near the tuyere centerline. Figure 27 details temperature and gas velocity distributions and gas flow streamlines throughout the raceway region. Recirculation zones can be identified in which pulverized coal and natural gas combustion produces significant amounts of heat. The upper set of contours are located on section A-A and the lower set are located on section B-B, as defined in Figure 26.

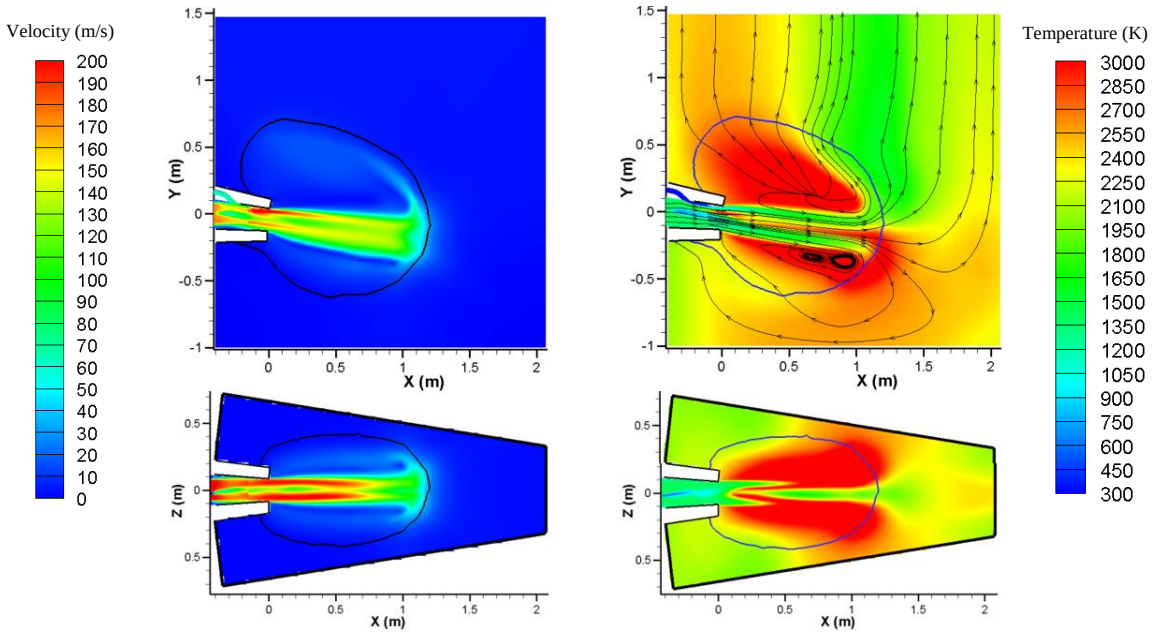

Figure 27. Gas velocity (left) and temperature (right) in the raceway region.

The CFD model can also be used to predict an average value of raceway gas temperature after all carbon, oxygen, and water vapor has been converted to CO and H_2. This value is a numerically calculated analogue to the Raceway Adiabatic Flame Temperature (RAFT). The RAFT is widely utilized in industrial practice, and is a theoretical value based on furnace operating conditions that can be used to calculate the temperature of raceway gas when all carbon, oxygen, and water vapor have been converted into carbon monoxide and hydrogen gas. Under these conditions, the predicted RAFT analogue is approximately 2,240 K (±4%). This compares favorably to the industry-provided value for the stated baseline conditions of 2,290 K, with a total variation of roughly 2%. Obviously, the temperature of these gases have a considerable influence on the amount of heat energy available for reduction reactions and melting inside the blast furnace, and as such they can impact the stability and performance of the process. The RAFT analogue is calculated based upon the mass-weighted average values of gas temperatures above the raceway, limited to gas containing less than one percent of O_2, H_2O, or CO_2. However, it is also useful to examine the distribution of gas temperature within the raceway region.

Examination of conditions within the raceway and surrounding coke bed under these conditions indicates that significant stratification in gas temperatures is present throughout both the raceway and coke bed above it due to the distribution of injected fuels in the tuyere. The rate of oxygen

consumption is significantly higher in the upper part of the tuyere jet, in large part due to the combustion of natural gas injected from the tuyere port. All remaining oxygen in the hot blast jet is consumed by reactions with pulverized coal and coke inside the raceway envelope, producing carbon monoxide, carbon dioxide, water vapor, and hydrogen. The carbon dioxide and water vapor are further reduced to carbon monoxide (CO) and hydrogen gas (H_2) through endothermic, non-combustion reactions. Figure 28 details the distribution of gas species in the raceway region on section A-A, while Figure 28 details the distributions on section B-B.

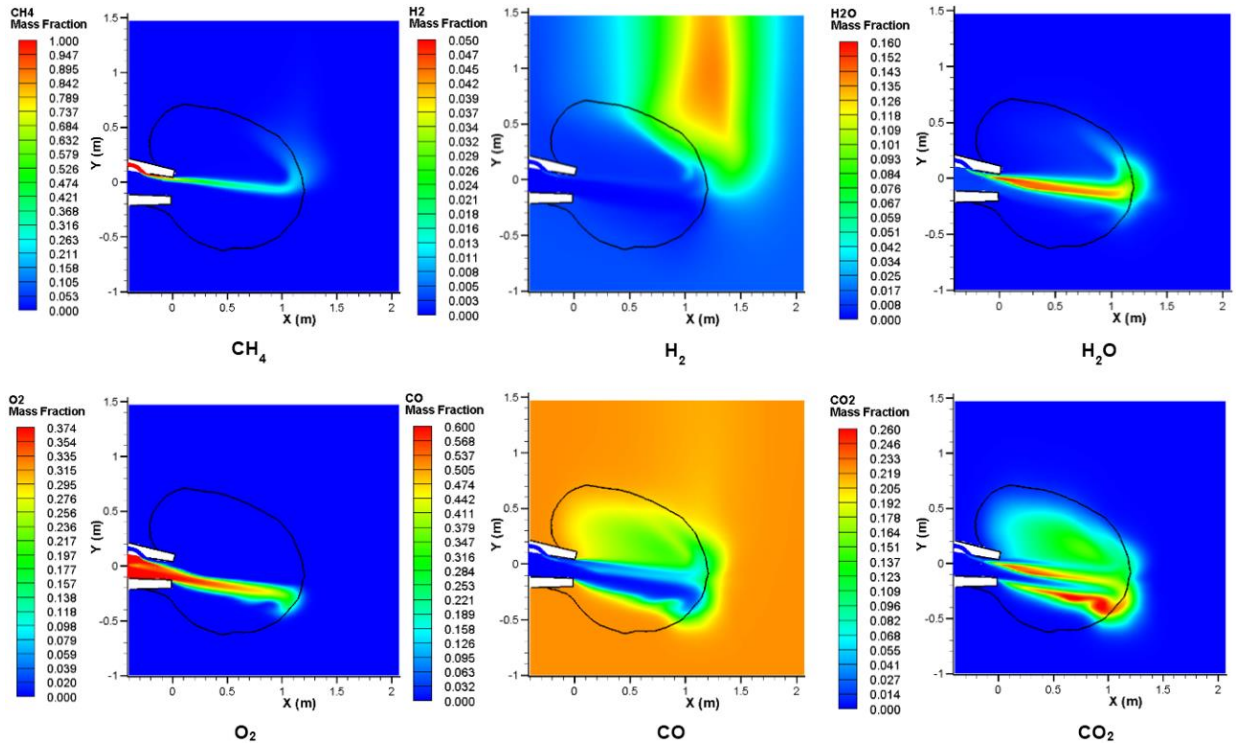

Figure 28. Predicted gas species distributions on section A-A for the baseline simulation.

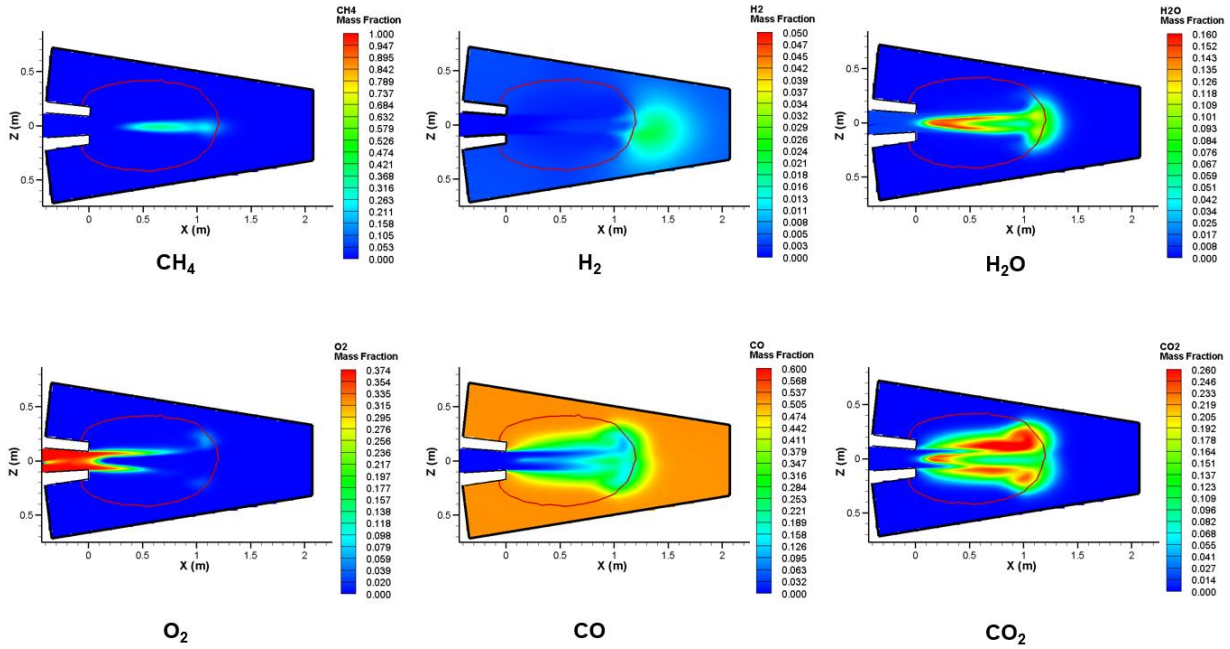

Figure 29. Predicted gas species distributions on section B-B for the baseline simulation.

The lower temperature zone visible above the tip of the raceway region in Figure 27 corresponds to a region of high hydrogen gas concentration in Figures 28 and 28, indicating that the temperature drop is caused by endothermic reaction of water vapor with carbon. Additionally, gas species distributions in the raceway are somewhat symmetric, as the injection apparatus has a large degree of left-right symmetry. However, it can be observed that there exist some variations in CO_2, CO, O_2, and H_2 distribution. These asymmetries exist primarily due to the injection angle of the PCI lance. Looking at the raceway from the outside of the furnace, the PC plume enters from the lance on the upper right and drifts to the left of the raceway, producing the corresponding distributions observed in Figure 29. In terms of a lengthwise distribution, Figure 30 details the species mass fractions of combustion byproducts along the axis of the tuyere through the raceway and coke bed beyond.

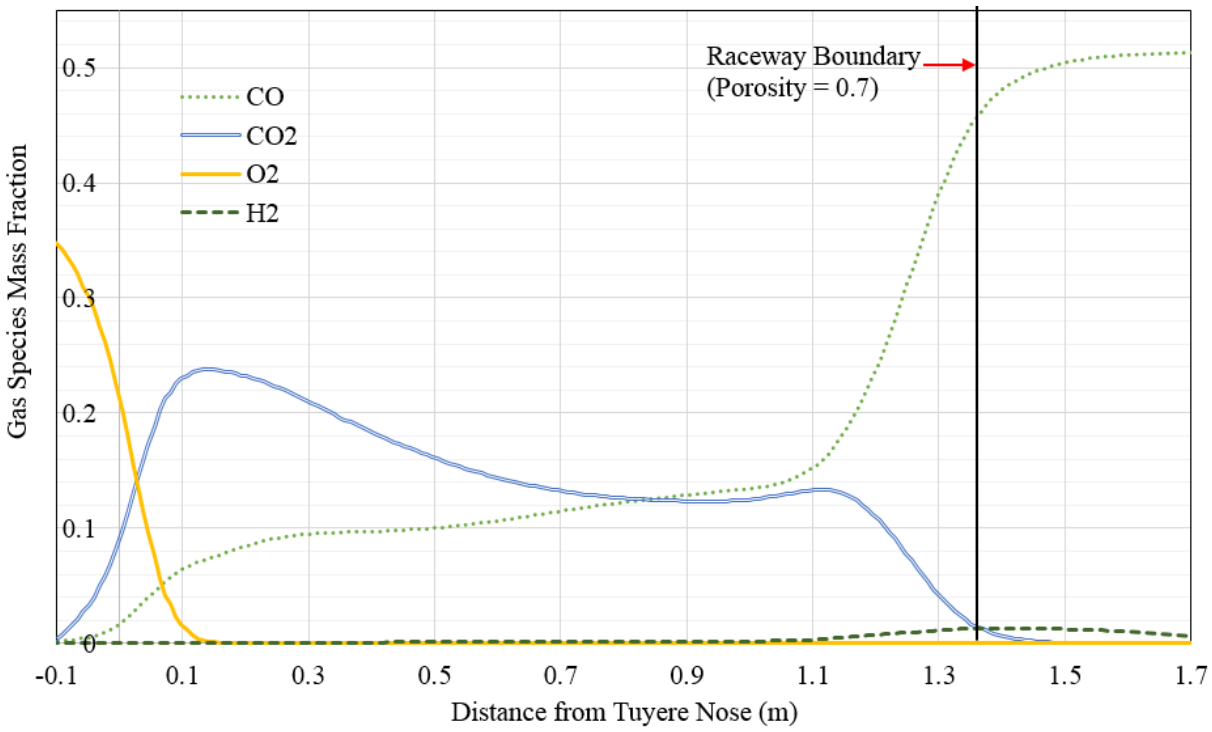

Figure 30. Species mass fractions of CO, CO_2, O_2, and H_2, plotted along the center of the tuyere jet.

Oxygen is consumed quickly within and just beyond the tuyere as pulverized coal and natural gas combustion occurs, and little oxygen remains at the center of the tuyere jet by the time the flow reaches the raceway boundary. The Boudouard reaction begins to consume CO_2 and convert it to CO throughout the tuyere, with a sharp increase in the production of CO occurring as the gases reach the coke bed near the raceway boundary. Production of H_2 via the water-gas shift reactions is also observable near the raceway boundary.

These results clearly indicate that gas temperatures within the raceway region vary significantly. Gas temperatures at or near the raceway boundary range from a predicted low of 1,760 K to a predicted high of 2,700 K, a large variation from the predicted RAFT analogue of 2,240 K (±4%). As previously mentioned, furnace operators traditionally present RAFT as a single value representing the gas temperatures throughout the raceway. While different methods of calculating this value exist, no method has thus far taken into account the variations in gas temperature observed in numerical modeling. Recent work by researchers at the University of Science and Technology, Beijing proposed developing a “uniformity index” to quantify the distribution of

temperature inside the furnace via use of a digital imaging system aimed down the furnace tuyere [84]. Measurements indicate that the temperatures in the tuyere are non-uniform, and it is clear that the system provides enhanced understanding of the conditions within the raceway. However, as this system can only view portions of the raceway in line-of-sight of the tuyere nose, there are limitations.

As seen in Figure 31, simulation modeling can explore the distribution of gas temperature on the upper boundary of the raceway and beyond, providing additional insight into furnace conditions through the development of a new "Topographical Flame Temperature."

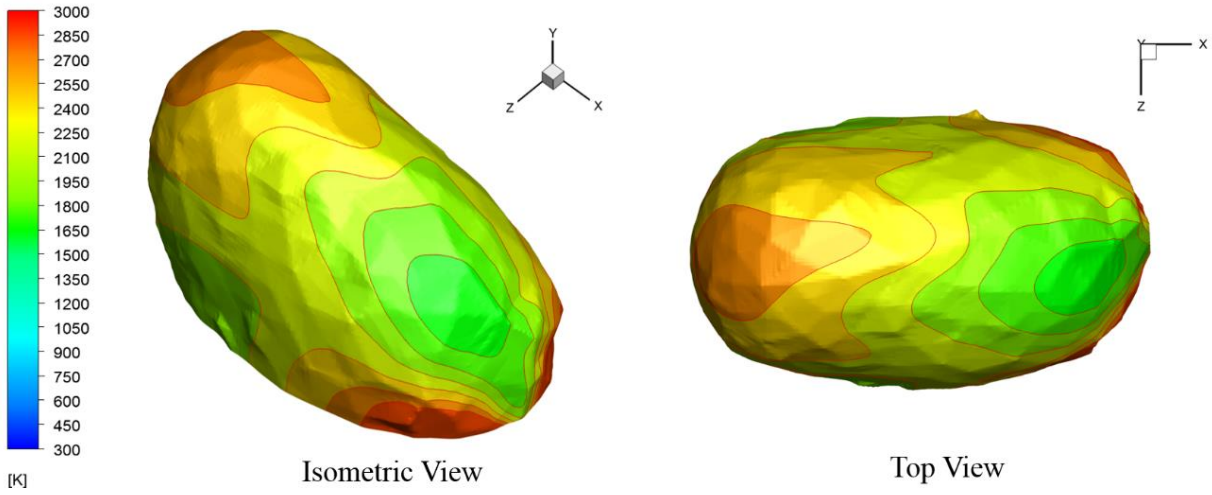

Figure 31. Representation of Topographical Flame Temperature defined at raceway upper surface.

This topographical flame temperature has proven to be a valuable tool for examining the distribution of gas temperatures and species inside the blast furnace at AK Steel. Future research could utilize this new concept to examine heat loading on the furnace bosh (with an eye towards management for campaign extension), scab formation and management, and factors contributing to localized burden slips.

Simulation of the current auxiliary fuel injection configuration at the Dearborn Works furnace led to the discovery of valuable information regarding pulverized coal combustion and burnout inside the raceway. Under the baseline conditions simulated, despite the presence of high oxygen levels throughout the hot blast tuyere jet, pulverized coal combustion remains incomplete in the raceway,

with levels in some regions reaching only 60% before passing into the denser coke bed at the raceway boundary. Poor utilization of injected fuel such as this results in economic losses, and may also cause difficulties in standard operation of the furnace due to unburned coal particles accumulating in the packed coke bed deeper in the furnace. This accumulation can result in increased furnace pressure drops and reductions in furnace production rate and stability. Contours of coal burnout in the raceway geometry are shown in Figure 32.

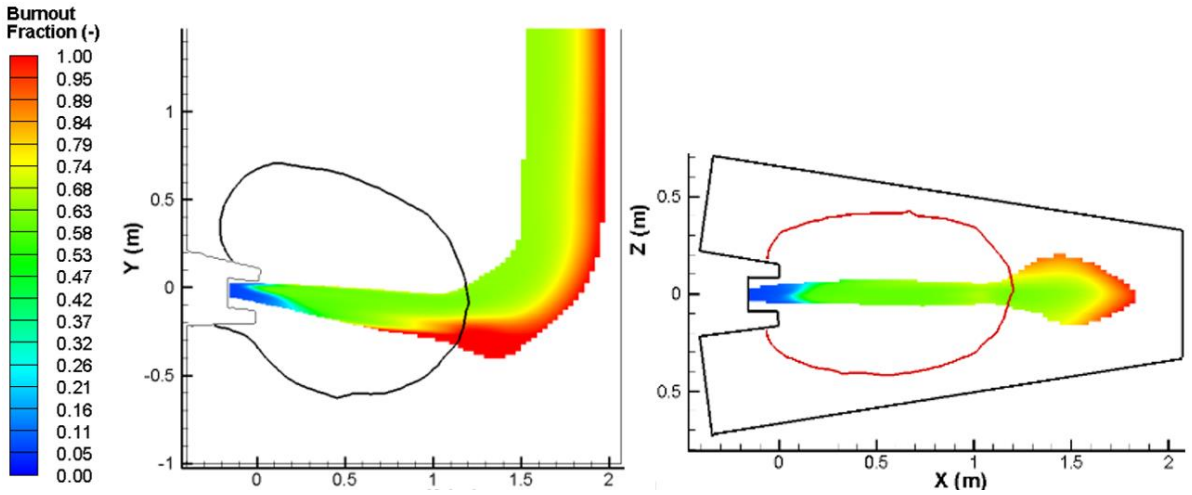

Figure 32. Contours of pulverized coal burnout fraction in the raceway region on section B-B (left) and section A-A (right).

Additional validation of the numerical modeling techniques utilized in this study was established through investigation of tuyere nose failures at the Dearborn Works blast furnace. Simulations of the current injection apparatus predicted the formation of an arc of high temperature combusting gas near the upper surface of the tuyere, leading to increased thermal wear of the tuyere nose. Contours of the high temperature gas zones are shown in Figure 33.

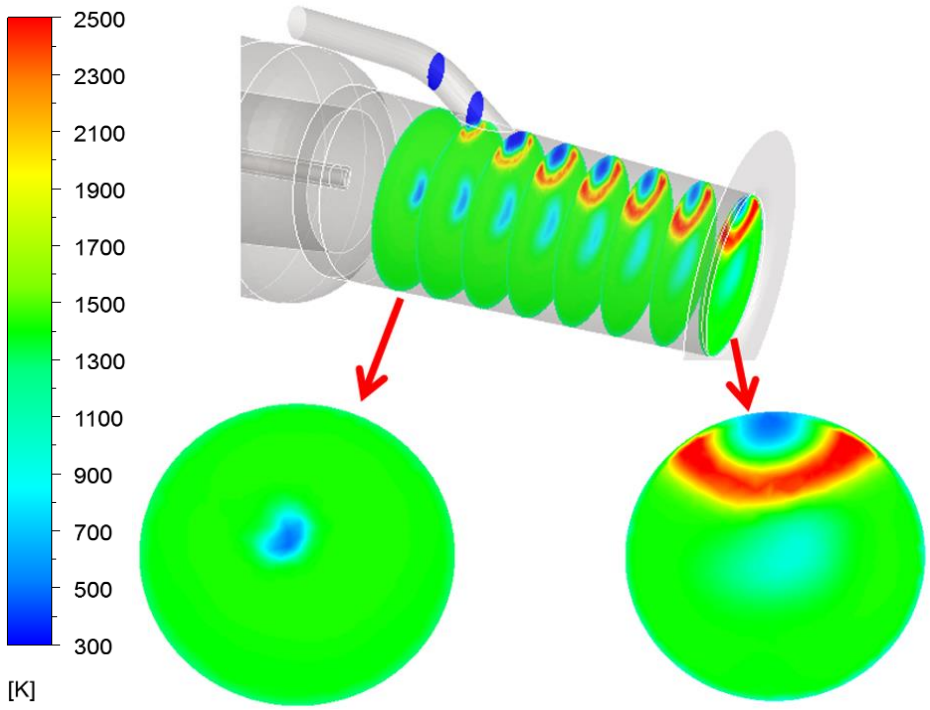

Figure 33. Gas temperature contours located on cross-sections inside the tuyere parallel to the tuyere outlet.

These regions of high gas temperature correspond to observations of thermal wear and ablation on tuyeres removed from the Dearborn Works blast furnace, as seen in Figure 34. It is clear from this analysis that the current injection apparatus of natural gas through a tuyere port results in significant thermal wear to the tuyeres, and alternative injection methods could present significant maintenance savings and shutdown avoidances in industrial operation.

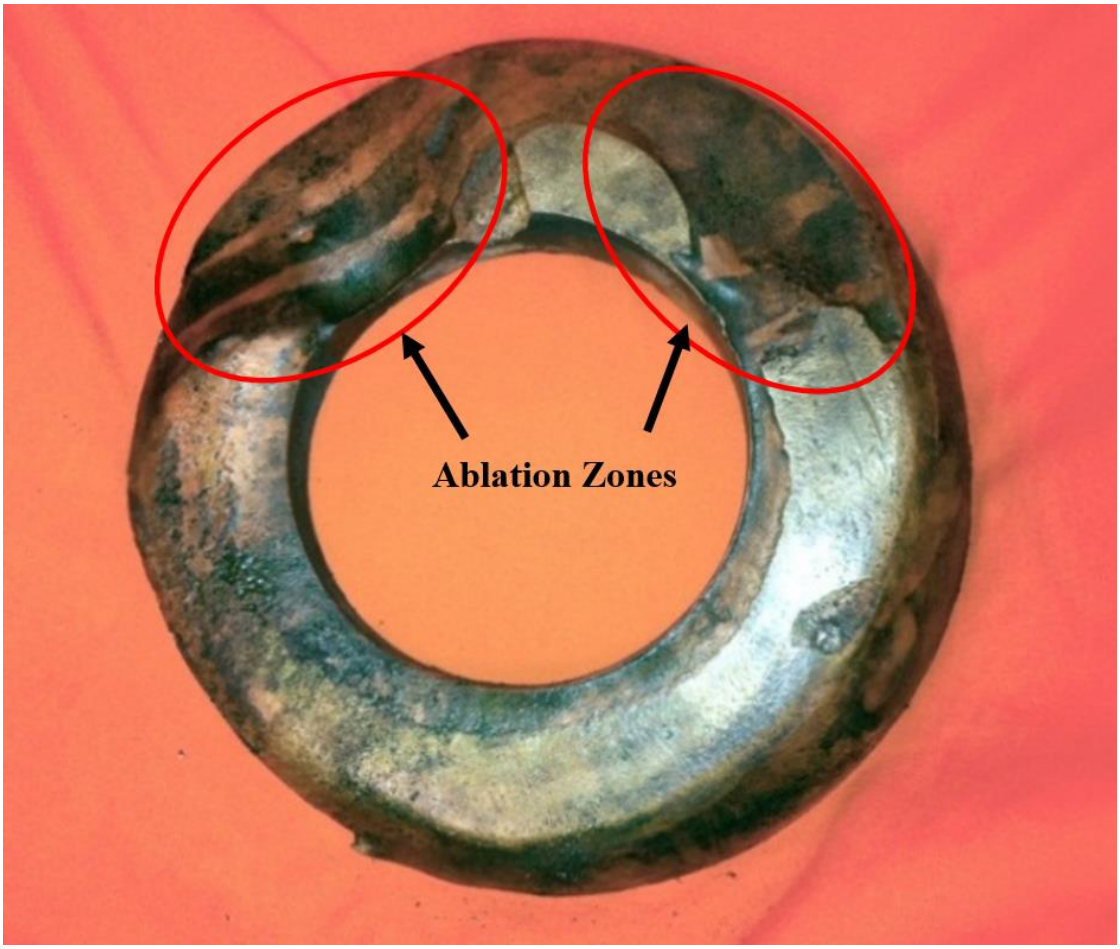

Figure 34. Sectioned nose of tuyere from AK Steel Dearborn Works with wear/ablation zones visible.

4.1.3 Parametric Study

A total of 25 different cases, including the baseline case, were examined in this research. Two different geometries for the auxiliary fuel injection apparatus were simulated: the co-injection configuration currently in use at AK Steel Dearborn Works and a proposed new design utilizing dual lance injection, with a single lance each for pulverized coal and natural gas. The parameters varied in these cases included hot blast wind rates, hot blast temperatures, PCI and natural gas injection rates, and oxygen enrichment amounts. The specific operating conditions used in each case are detailed in Table 5. Parameters that have been modified from the baseline case are highlighted in bold.

Table 5. Operating conditions for parametric study cases.

Scenario	Blast Rate (Nm^3/hr)	Hot Blast Temp. (K)	O_2 Enrich. (% of Wind)	PCI Rate (kg/thm)	NGI Rate (kg/thm)	PCI Carrier Gas	NG Injection Position
Baseline	199,020	1408	13.5	85	65	N_2	Port
Case 1	**176,550**	1408	13.5	85	65	N_2	Port
Case 2	**211,860**	1408	13.5	85	65	N_2	Port
Case 3	199,020	1408	**11.0**	85	65	N_2	Port
Case 4	199,020	1408	**15.0**	85	65	N_2	Port
Case 5	199,020	**1450**	13.5	85	65	N_2	Port
Case 6	199,020	**1310**	13.5	85	65	N_2	Port
Case 7	199,020	1408	13.5	**107.5**	**47.5**	N_2	Port
Case 8	199,020	1408	13.5	**67.5**	**77.5**	N_2	Port
Case 9	199,020	**1116**	13.5	85	65	N_2	Port
Case 10	199,020	1408	13.5	85	65	N_2	**Lance**
Case 11	**176,550**	1408	13.5	85	65	N_2	**Lance**
Case 12	199,020	1408	**15.0**	85	65	N_2	**Lance**
Case 13	199,020	1408	**11.0**	85	65	N_2	**Lance**
Case 14	199,020	1408	13.5	85	65	**CH_4**	Port
Case 15	199,020	1408	13.5	85	65	**CH_4**	**Lance**
Case 16	**176,550**	1408	13.5	85	65	**CH_4**	Port
Case 17	**176,550**	1408	13.5	85	65	**CH_4**	**Lance**
Case 18	**211,860**	1408	13.5	85	65	**CH_4**	**Lance**
Case 19	199,020	1408	**11.0**	85	65	**CH_4**	**Lance**
Case 20	199,020	1408	**15.0**	85	65	**CH_4**	**Lance**
Case 21	199,020	1408	13.5	85	65	**N_2**	**Ext. Lance**
Case 22	199,020	1408	13.5	85	65	**N_2**	**Ret. Lance**
Case 23	199,020	1408	13.5	85	65	**CH_4**	**Ext. Lance**
Case 24	199,020	1408	13.5	85	65	**CH_4**	**Ret. Lance**
Case 25	199.020	1408	13.5	**0**	**150**	N_2	**Lance**

This parametric study was performed in an effort to research the sensitivity of combustion characteristics inside the raceway to operating and design variables. Determining the influence of these varying conditions provides a baseline of information for developing best practices regarding

injected auxiliary fuels that is valuable for both the Dearborn Works furnace and other blast furnaces throughout the industry.

4.1.3.1 Comparison of Natural Gas and Nitrogen as the Pulverized Coal Carrier Gas

A significant component of this research was to examine the influence of a newly proposed method for co-injecting natural gas and pulverized coal into the blast furnace. The proposed technique utilized natural gas instead of nitrogen as the carrier gas for PCI on combustion characteristics within the raceway region. This methodology has not been previously attempted in any industrial application, and little, if any, research has been conducted upon the potential benefits of the proposed technique throughout published literature.

Application of this proposed modification to the injection configuration currently in use at the Dearborn Works blast furnace saw significant predicted changes in the combustion performance of injected fuels. Several cases were modeled to determine the influence of various other parameters on the combustion characteristics under both the natural gas carrier and nitrogen carrier PCI methods.

Three cases were simulated using the current Dearborn Works injection apparatus. Cases 14 and 16 used natural gas as the PCI carrier, with case 16 using a lower wind rate. Case 1 also used a lower wind rate, but was simulated with nitrogen as the carrier for PCI. Four cases were also simulated with an alternative injection location for natural gas, using the aforementioned proposed dual lance design as the injection apparatus. Cases 15 and 17 used natural gas as the carrier for PCI, while cases 10 and 11 retained nitrogen as the pneumatic transportation method. Cases 15 and 10 utilized the baseline wind rate, while cases 17 and 11 were simulated at a lower wind rate. The most significant results from these simulations were illuminated by examination and comparison of the baseline case with case 14, case 15, and case 10.

When comparing the alternative carrier gas to the standard injection technique, the most obvious change in phenomena inside the tuyere is the increased average gas temperature. The natural gas conveying the pulverized coal combusts almost immediately after it leaves the PCI lance. Mixing of this gas flow and oxygen in the hot blast is far greater than the natural gas injected from the

tuyere port, leading to rapid combustion and increased gas and coal temperatures throughout the tuyere. Figure 35 showcases the effects of the modified carrier gas on temperatures inside the tuyere and the extent to which combustion is altered by the new flow patterns generated.

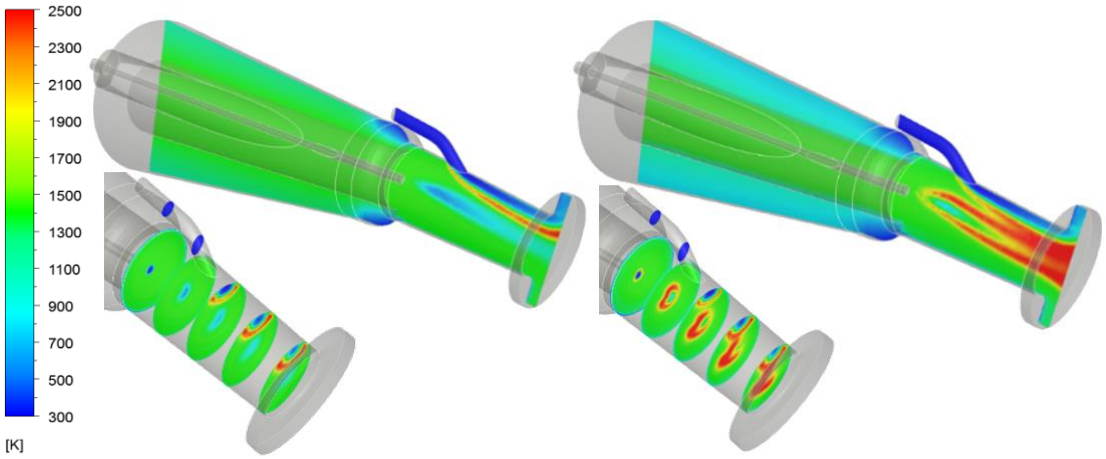

Figure 35. Gas temperature distribution inside the blowpipe and tuyere in the baseline case (left) and for case 14 (right).

The pulverized coal particle temperatures in the baseline case and in case 14 are compared in Figure 36.

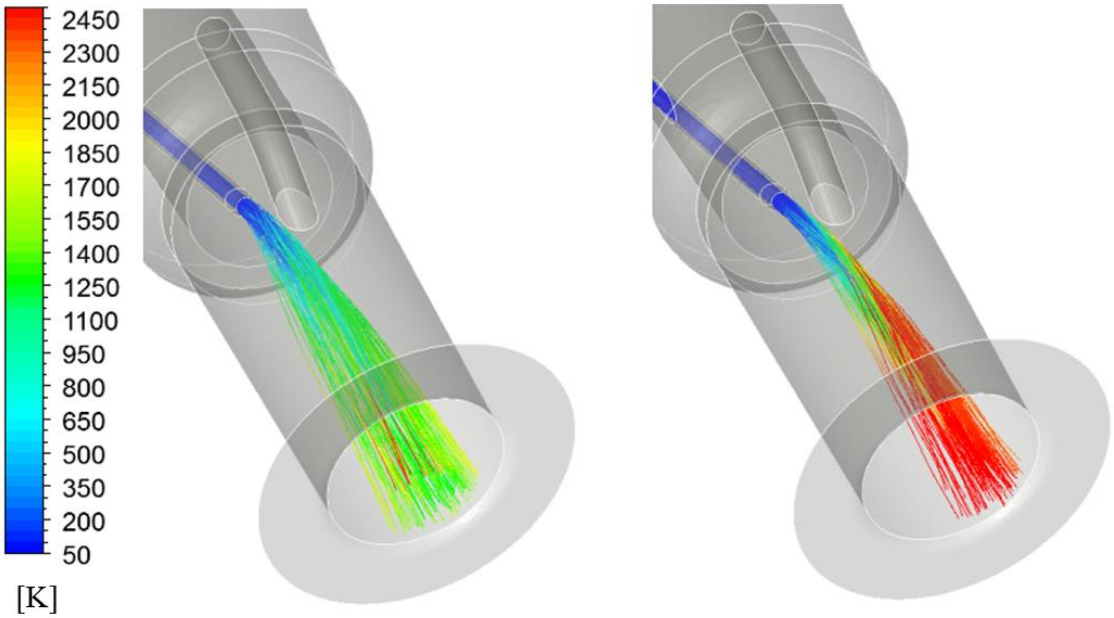

Figure 36. Coal particle path lines colored by temperature for the baseline case (left) and case 14 (right).

Pulverized coal is heated inside the tuyere much more rapidly when using natural gas as the carrier gas, due to the immediate natural gas combustion surrounding the coal particles. This in turn leads to greatly improved coal devolatilization. Overall, the percentage of volatile matter released from the coal particles inside the tuyere increased to 92.1% in case 14 compared to 13.2% in the baseline case. This rapid devolatilization and better heating of pulverized coal particles allows in turn for more rapid conversion of char into carbon monoxide and improved gas utilization throughout the furnace. The significant change in gas phase (released) volatile matter can be observed in Figure 37, and Figure 38 shows a plot of fuel burnout percentage across the raceway domain.

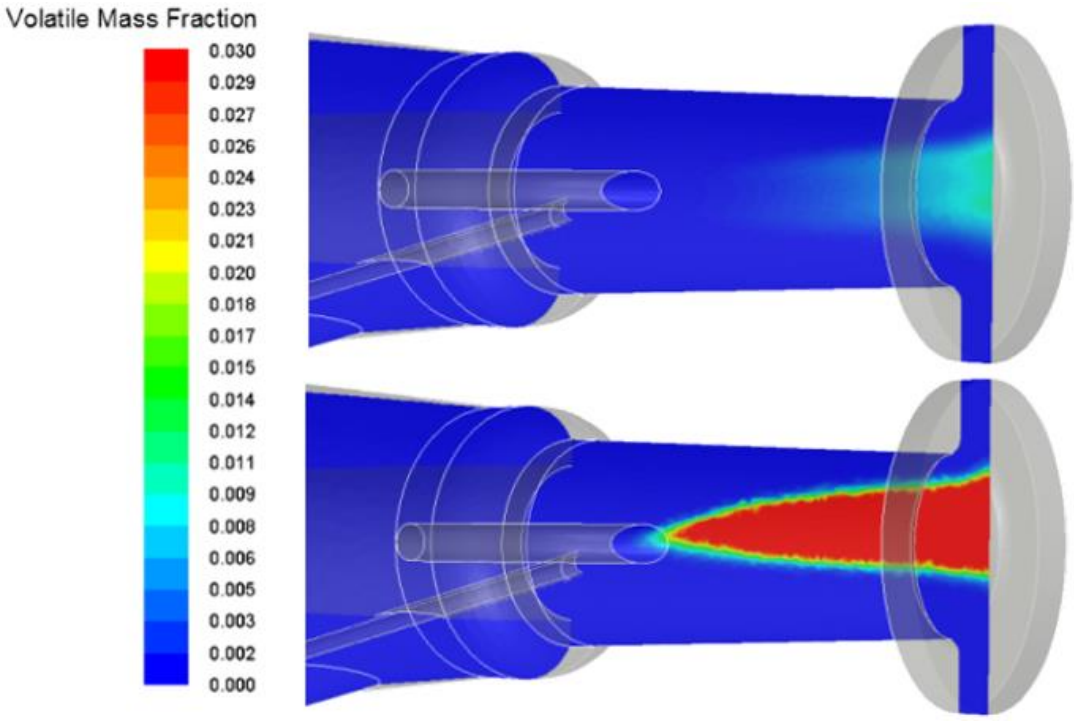

Figure 37. Contours of volatile mass fraction for the baseline case (top) and case 14 (bottom).

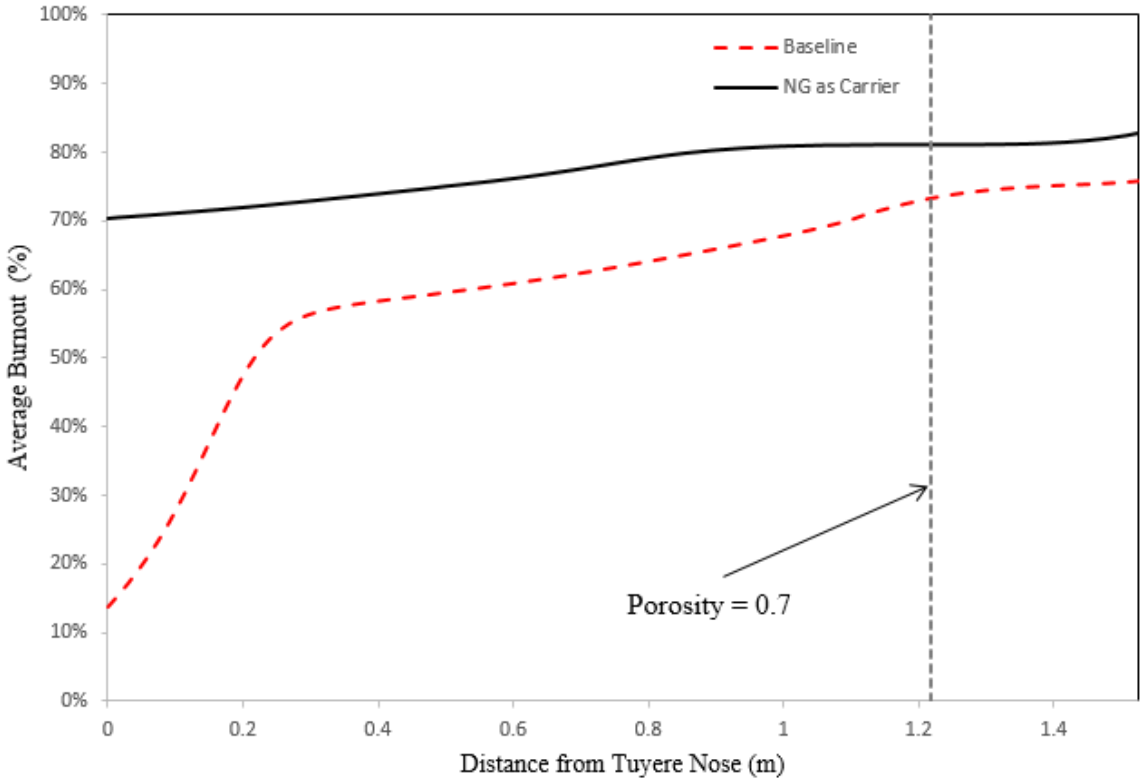

Figure 38. Burnout percentage plotted across the length of the raceway region for the baseline case and case 14.

In addition to the massive improvement in volatile release rates inside the tuyere, the total coal particle burnout ratio over the raceway increased from 70.7% to 86.8%. This enhanced combustion indicates that the switch to natural gas as the carrier for PCI could improve furnace efficiency. It also has the potential to address furnace instability issues generated by buildup of unburned pulverized coal particles in the coke bed. Despite these benefits, it is worth noting that the amount of devolatilization and combustion occurring inside the tuyere can also present concerns. High combustion rates inside the tuyere can generate high thermal loading to the tuyere walls, leading to shorter lifespans for furnace tuyeres. Additionally, it can lead to large pressure drops over the tuyere, potentially high enough to cause problems during normal plant operation.

The proposed dual lance injection configuration at the Dearborn Works furnace (case 15) was also examined with both nitrogen and natural gas as the carrier for PCI. This modified design essentially retracts the primary natural gas injection position by several inches and places it at the center of the tuyere for better mixing with the hot blast gas flow. This is a significant alteration of the

injection apparatus, and as such, it results in large changes to the combustion characteristics in the tuyere. The proposed design enhanced total fuel burnout significantly, with an injected fuel burnout ratio approaching 96%. This burnout rate represents an increase of roughly 35% over the baseline case. Devolatilization is slightly slower in the proposed design, due to the increased mass of low temperature gas in the center of the tuyere requiring additional time to fully heat the pulverized coal particles. However, this also lessens concerns over rapid combustion inside the tuyere and the corresponding pressure drops and thermal wear. These results can be observed from the gas temperature contours shown in Figure 39.

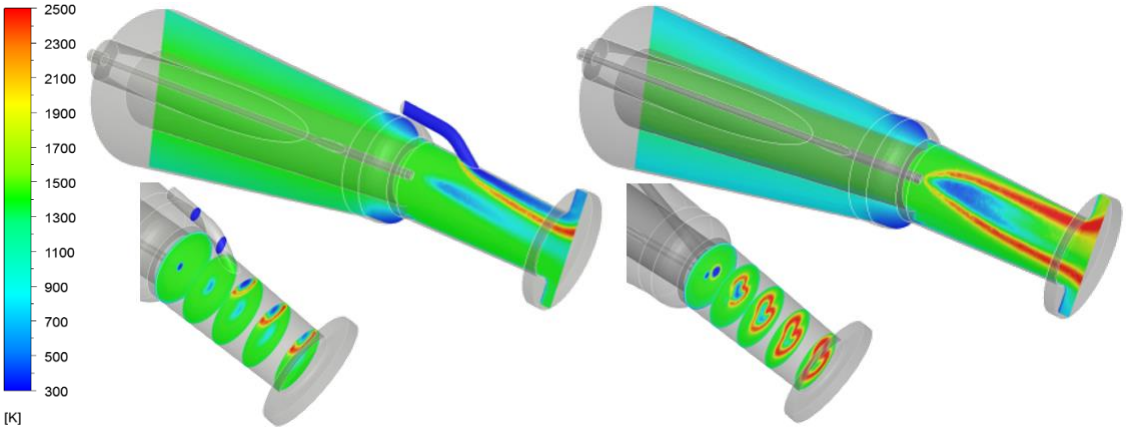

Figure 39. Gas temperature contours inside the blowpipe and tuyere for the baseline case (left) and for case 15 (right).

As was expected based on the temperature distributions inside the tuyere, the total amount of volatile matter released when using natural gas and nitrogen as the PCI carrier in the proposed design is lower than the devolatilization case 14, but higher than that of the baseline case. Inside the tuyere, devolatilization in case 15 increased to 26.4%, compared to 13.2% in the baseline case. The burnout rate in the raceway increased to 95.7%, compared to 70.7% in the baseline case. The increased devolatilization in the tuyere can be seen in Figure 40.

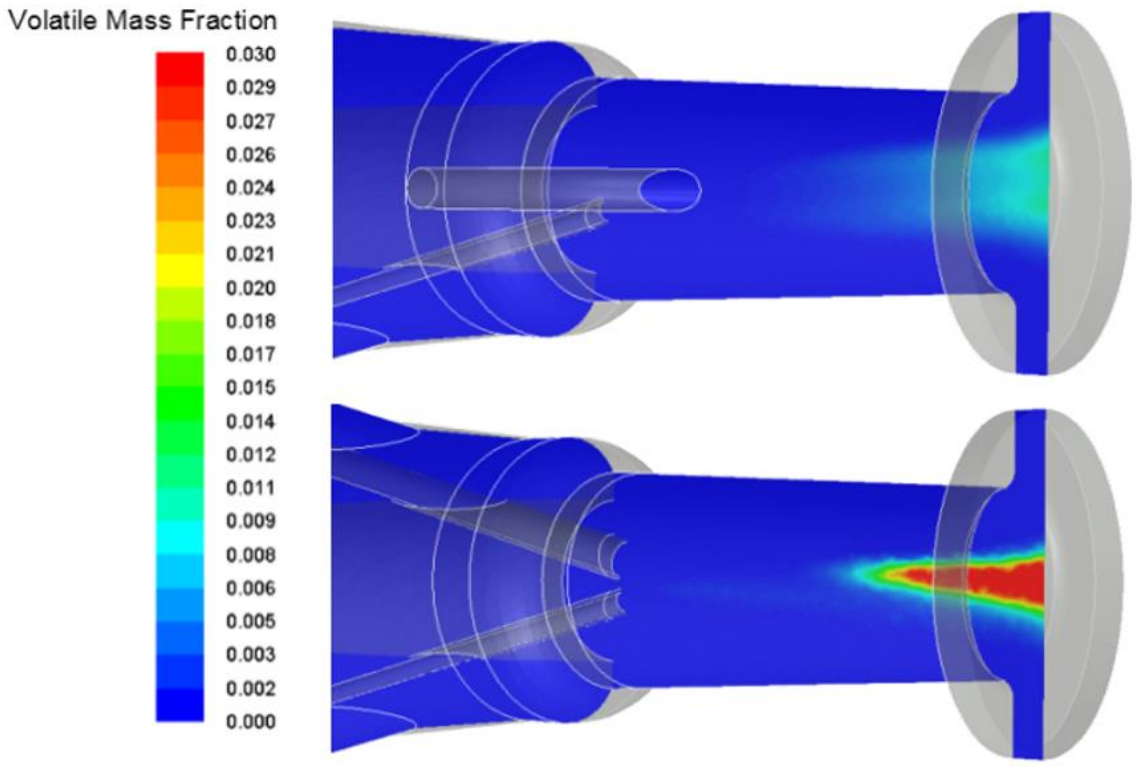

Figure 40. Contours of volatile mass fraction for the baseline case (top) and case 15 (bottom).

The proposed dual lance design also shows an improvement in combustion efficiency compared to the baseline case when utilizing the Dearborn Works blast furnace current operating conditions (case 10). Pulverized coal is injected through a blowpipe lance using nitrogen gas as the conveyance method and natural gas is injected through the secondary blowpipe lance. Although the total burnout rate showed a lesser increase (89.7% compared with 95.7%) than case 15, the predicted value remains significantly higher than that of the baseline injection apparatus (70.7%). As observed when shifting the carrier gas to natural gas, the proposed dual lance arrangement improves burnout due to enhanced mixing of pulverized coal and the high temperature natural gas plume. Devolatilization inside the tuyere was significantly higher in case 10 than in case 15, with a total of 62% volatile matter released compared to 26.4%. A comparison between the volatile mass fraction in the tuyere between case 15 and case 10 can be seen in Figure 41.

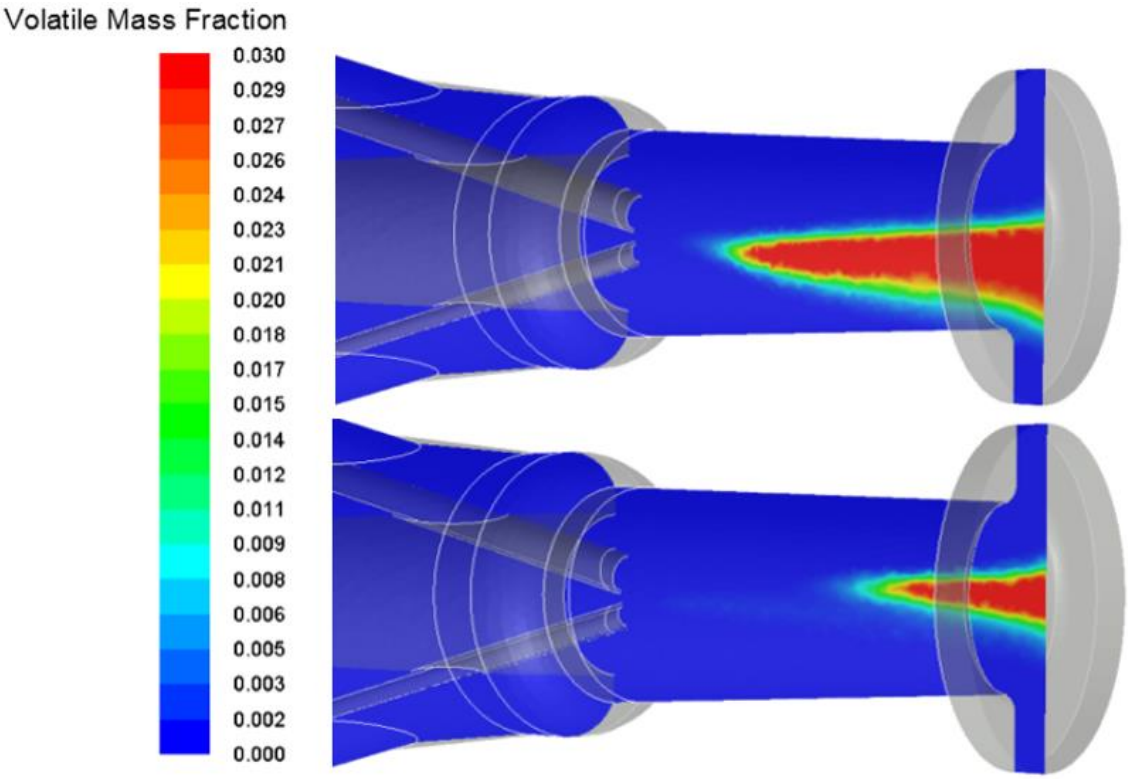

Figure 41. Contours of volatile mass fraction inside the tuyere for case 10 (top) and case 15 (bottom).

From these results, it becomes clear that the speed at which pulverized coal devolatilizes has an effect on combustion efficiency. However, it does not always directly correlate with the total burnout rate of injected fuel throughout the furnace. As injected natural gas competes with pulverized coal for available oxygen, fuel-oxygen mixing also has a significant influence on combustion characteristics. Simulations indicate that the proposed dual lance design appears to improve upon the efficiency of the current design at the Dearborn Works furnace in all cases. Further simulations will examine the effects of this design shift later on.

4.1.3.2 Effects of Blast Furnace Wind Rate

During standard furnace operation, operating parameters are often modified to meet production rates. The effects of these variations on combustion in the raceway have also been examined in this research. Holding all other operating parameters constant at baseline conditions (hot blast temperature of 1,408 K, oxygen enrichment of 13.5%, 85 kg/MTHM of PCI, and 65 kg/MTHM of NG) and using the current auxiliary fuel injection apparatus, the blast furnace wind rate was

varied between 176,550 Nm^3/hr (case 1) and 211,860 Nm^3/hr (case 2). The baseline operating condition was 199,020 Nm^3/hr. Comparisons of wind rate were also made using the proposed dual lance design with nitrogen as the PCI carrier (cases 10 and 11), the standard injection design with natural gas as the PCI carrier (cases 14 and 16), and the dual lance design with natural gas as the PCI carrier (cases 15, 17, and 18).

Comparison of the baseline case, case 1 (176,550 Nm^3/hr), and case 2 (211,860 Nm^3/hr) indicates that the primary differences result from reduced convection heat transfer from the hot blast to the blowpipe, tuyere, and lance walls in case 1. Figure 42 shows that gas temperature distributions are essentially identical between the three cases. This indicates that the combustion characteristics of natural gas and pulverized coal in the tuyere are not significantly affected by the hot blast flow rate.

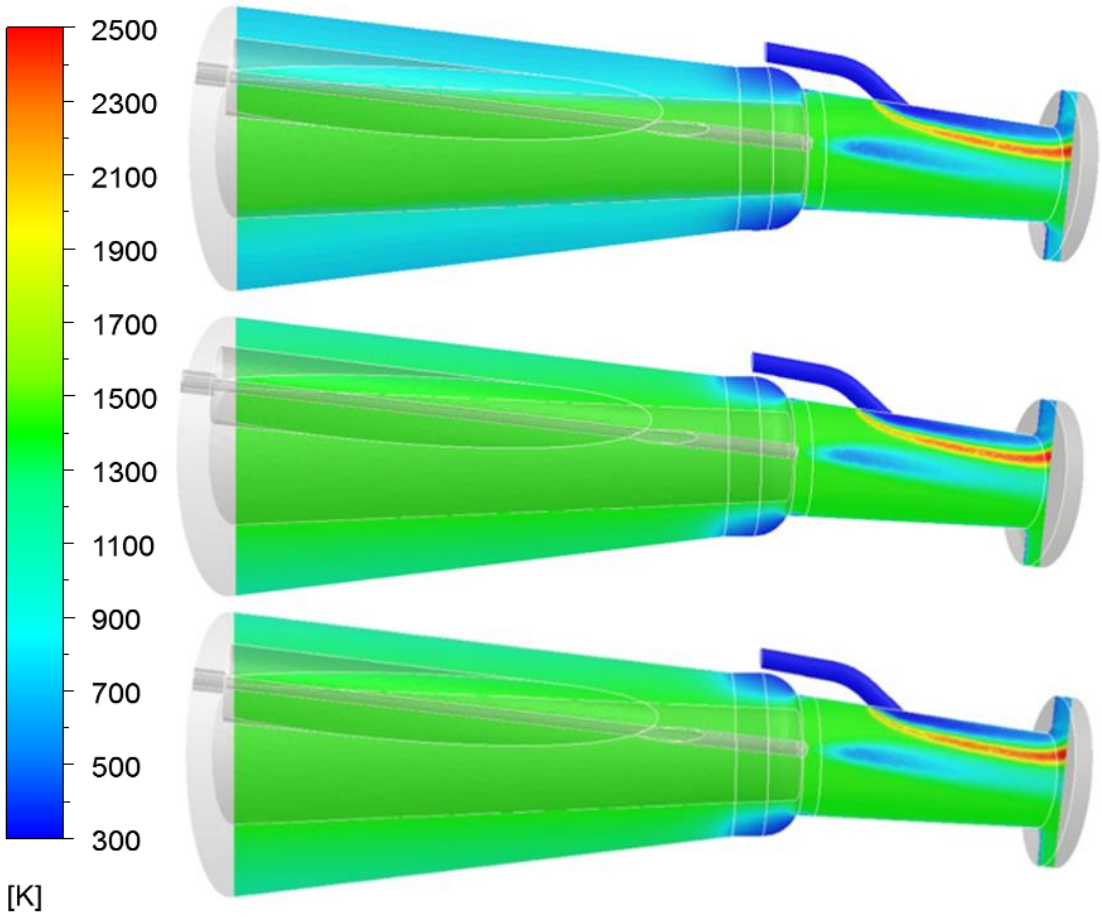

Figure 42. Contours of gas temperature inside the blowpipe/tuyere region for case 1 (top), the baseline case (middle), and case 2 (bottom).

The changes to blast flow rate have a more significant influence on the furnace raceway. Changes to the total wind rate alter the tuyere velocity and mass flow rate, and hence change the size and shape of the raceway envelope. Temperature distributions remain almost identical, however, the raceway is smaller in case 1 compared to the other two cases, and oxygen does not penetrate as far into the raceway coke bed. As expected, reducing the wind rate also reduces total fuel burnout in the absence of other factors. The total fuel burnout rate in case 1 is 69.8%, compared with 70.7% in the baseline case and 73.0% in case 2. The gas velocity distributions in the raceway region, as well as the relative raceway sizes for each case are shown in Figure 43.

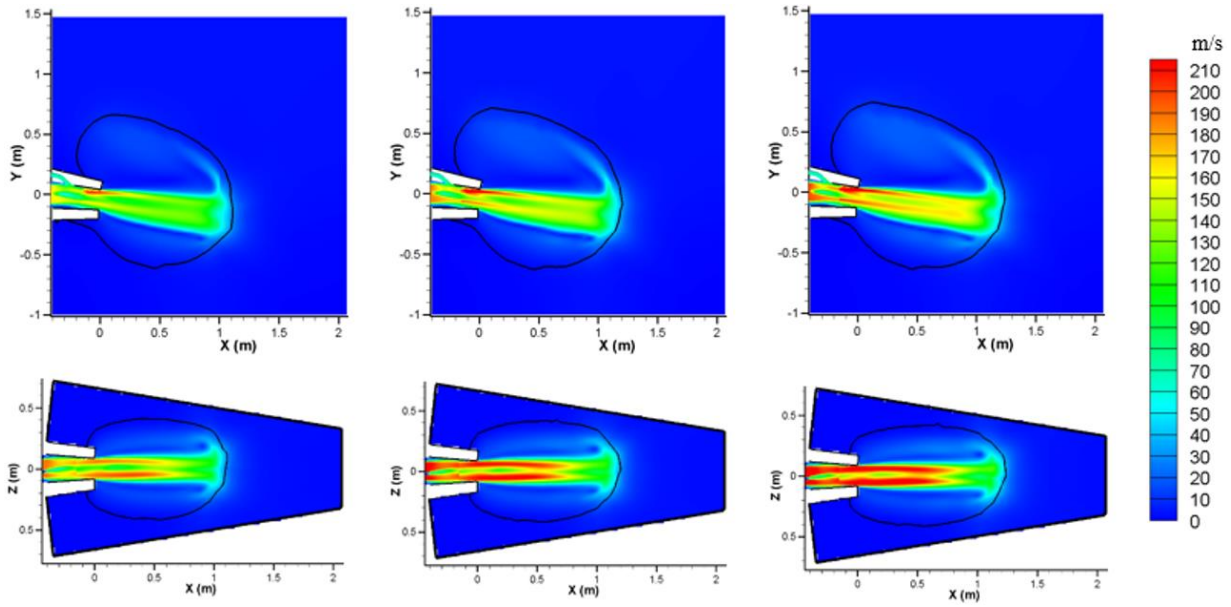

Figure 43. Contours of gas velocity on section A-A (top) and section B-B (bottom) in the raceway region for case 1 (left), the baseline case (middle), and case 2 (right).

These trends are also observed in cases 10 and 11, cases 14 and 16, and cases 15, 17, and 18. The total fuel burnout rate is 93.8% for case 10, 91.3% for case 11, 83.3% for case 14, 81.2% for case 16, 96.7% for case 15, 94.5% for case 17, and 100% for case 18.

4.1.3.3 Effects of Oxygen Enrichment

Hot blast oxygen enrichment was also examined in this research, expressed as a percentage of the blast furnace wind. Furnace operating parameters are once again held constant at a wind rate of 199,020 Nm^3/hr, hot blast temperature of 1,408 K, 85 kg/MTHM of PCI, and 65 kg/MTHM of natural gas. Oxygen enrichment total was varied from 11% (case 3) to 13.5% (baseline case) to 15% (case 4).

Similar to the effects of blast furnace wind rate, the variations in oxygen enrichment generated little predicted variation in gas combustion within the tuyere. There is enough oxygen present in the hot blast flow to allow for complete natural gas combustion in all three cases and the temperature distributions within the tuyere are extremely similar between the three cases. The most obvious difference between these cases is an increase in raceway average temperature, as seen in Figure 44.

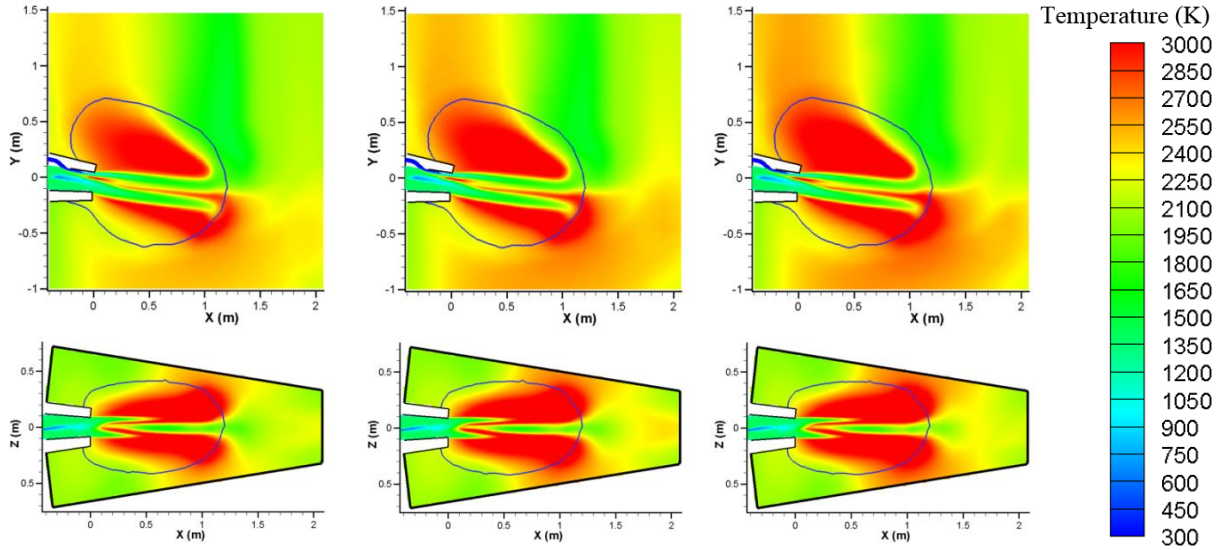

Figure 44. Contours of gas temperature on section A-A (top) and section B-B (bottom) in the raceway region for case 3 (left), the baseline case (middle), and case 4 (right).

The other result of import from this variation of parameters is an observed increase in predicted fuel burnout over the raceway, as seen in Figure 45. This increase corresponds with increased raceway temperatures and total oxygen enrichment. As previously mentioned, the burnout ratio in the baseline case is 70.7%. Decreasing oxygen enrichment to 11% reduces the burnout ratio to 67.3% (case 3), while increasing oxygen enrichment to 15% leads to a burnout ratio of 73.3% (case 5).

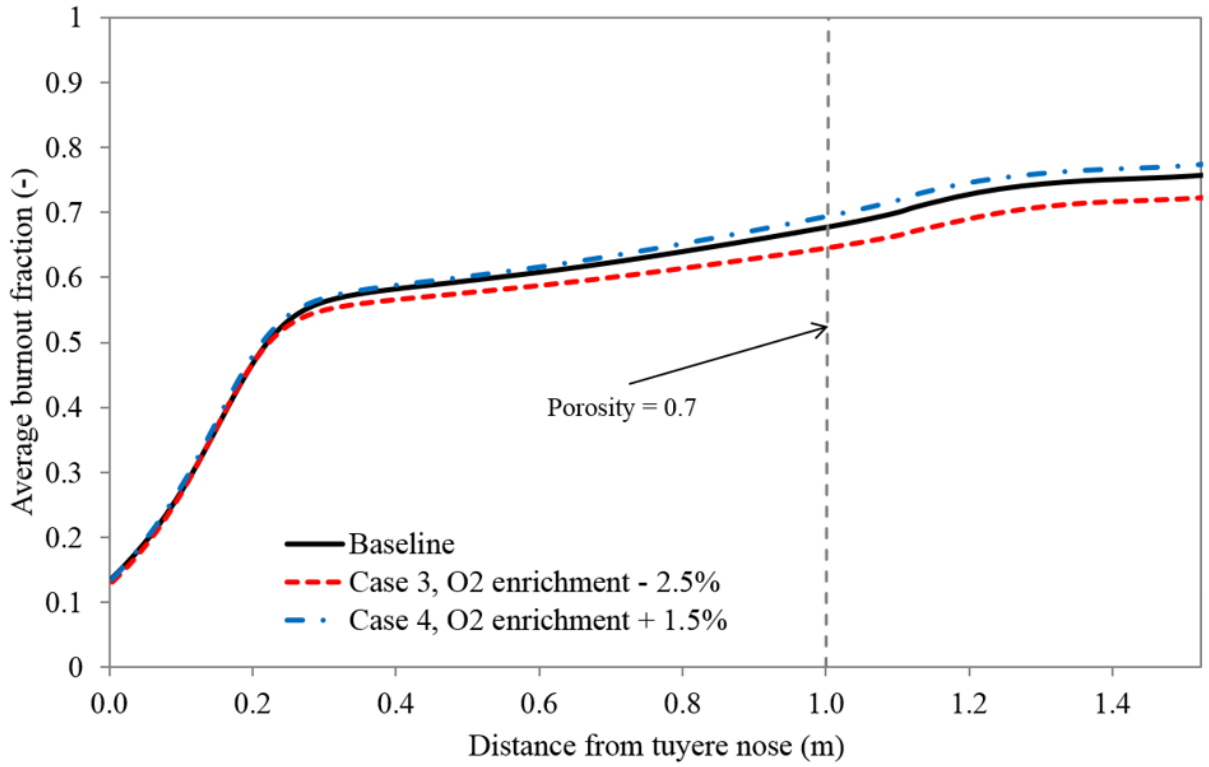

Figure 45. Fuel burnout vs. horizontal distance from tuyere nose in raceway region.

4.1.3.4 Effects of Hot Blast Temperature

To study the effects of hot blast temperature on raceway combustion characteristics, all parameters were fixed at the baseline conditions, while the hot blast temperature was varied between 1450 K (case 5), 1310 K (case 6), and 1120 K (case 9). Temperature distributions are mostly unaffected by these alterations, both in the tuyere and raceway regions, as seen in Figure 46.

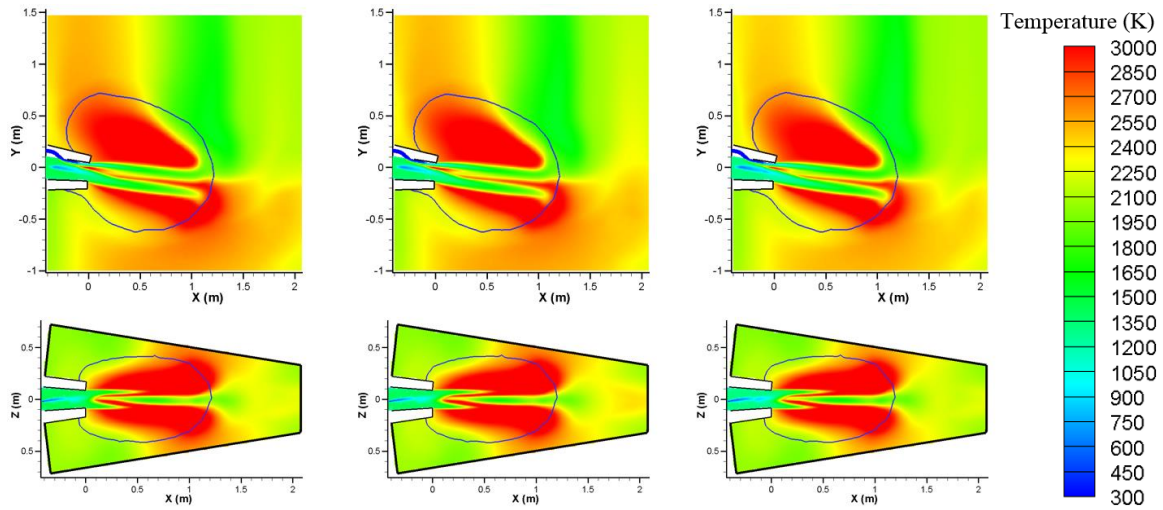

Figure 46. Contours of gas temperature on section A-A (top) and section B-B (bottom) in the raceway region for case 5 (left), the baseline case (middle), and case 6 (right).

However, hot blast temperature does have an influence on devolatilization speed inside the tuyere. The percentage of volatile matter released by the end of the tuyere in the baseline case is 13.2%, compared to 14.2% in case 5 and 9.5% in case 6. Increasing the hot blast temperature contributes to heating of injected pulverized coal particles and hastens devolatilization in the tuyere region.

4.1.3.5 Variation of PCI and Natural Gas Injection Rates

In recent years, the price of natural gas in North America has fallen rapidly due to a supply abundance generated by fracking. For this reason, gaining an understanding of the effects of varied fuel injection rates and ratios in co-injection systems has become extremely important. Cases were simulated at baseline conditions and the standard injection design at the Dearborn Works furnace, with a varied ratio between PCI and natural gas injection. The baseline case injection rates were 85 kg/MTHM of PCI and 65 kg/MTHM of natural gas. Two modified cases were modeled, one using 107.5 kg/MTHM of PC and 47.5 kg/MTHM of natural gas (case 7) and one using 67.5 kg/MTHM of PCI and 77.5 kg/MTHM of natural gas (case 8).

Modifying the ratio of natural gas to pulverized coal injected into the furnace can have a significant influence on combustion characteristics in the tuyere and raceway. One obvious factor is the mass and momentum of injected pulverized coal particles. Operation with an increased PCI rate requires more energy to heat and accelerate pulverized coal particles, as well as to begin the devolatilization

process. As the compared cases all utilized the baseline injection design, any additional natural gas supplied through the tuyere port will not combust immediately in the tuyere, rather it will combust and decompose in the raceway. Figure 47 shows a comparison between temperature and velocity distributions in the tuyere region for the modified injection ratio cases.

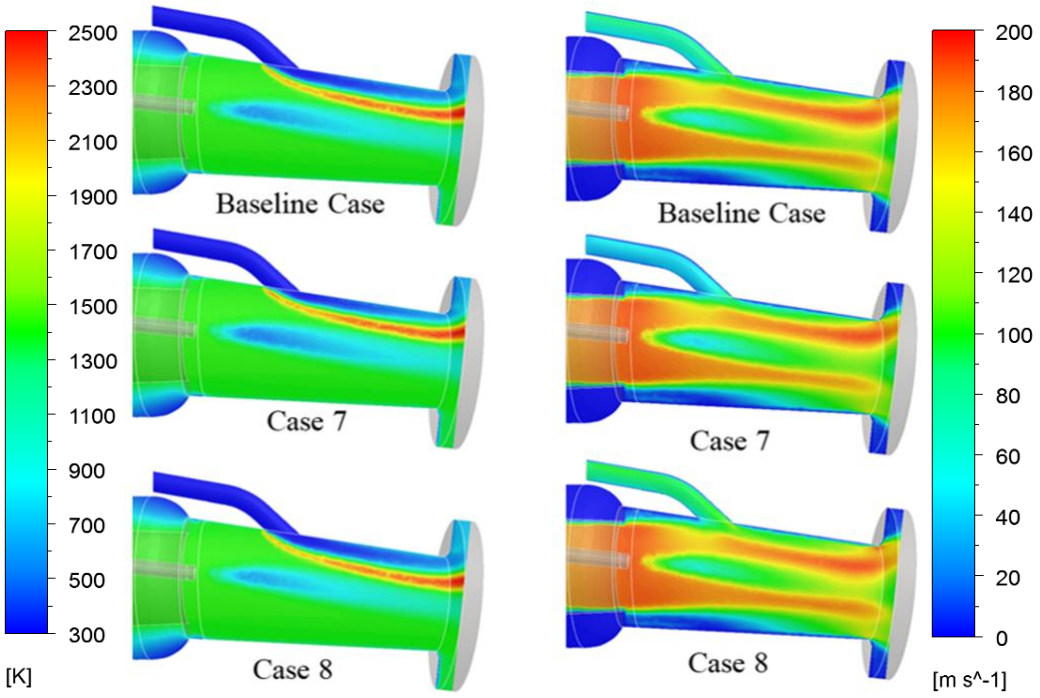

Figure 47. Contours of gas temperature (left) and gas velocity (right) in the tuyere for the modified auxiliary fuel injection ratio cases.

The reduced PCI mass in case 8 leads to a higher fuel burnout of 75.8%, 5% higher than the baseline case. This occurs primarily due to the reduced mass of pulverized coal particles heating and mixing with oxygen faster in the identical hot blast conditions. The reverse is true in case 7, with the increased PCI rate leading to a lower total fuel burnout of 66.8%. Case 7, with a higher PCI rate and a reduced natural gas injection rate, results in a RAFT analogue of 2,270 K (±4%). Case 8, with an increased natural gas injection rate and a reduced PCI rate results in a RAFT analogue of roughly 2,230 K (±4%). Overall, this results in a 1.2% increase in gas temperature in Case 7, and a 0.6% decrease in gas temperature in Case 8 when compared to the baseline conditions.

This can also be observed in Figure 48, wherein the gas temperature in case 8 is higher than both the baseline and case 7 for the first 0.2 meters inside the raceway. However, after the natural gas

has completed reacting with oxygen, the reaction products will then consume heat, reducing the raceway flame temperature. By contrast, in case 7, the additional pulverized coal combustion serves to increase raceway temperatures, as more heat is released in total despite the lower burnout rate.

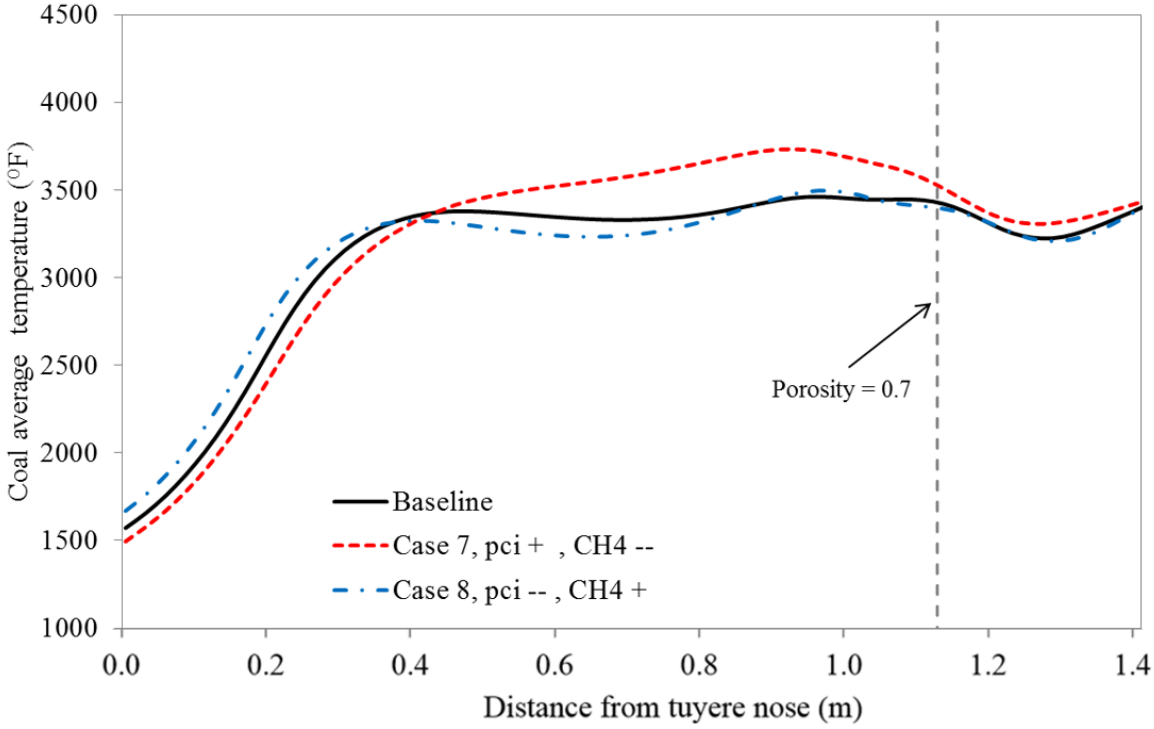

Figure 48. Coal temperature vs. horizontal distance from the tuyere nose in the raceway region.

In general, the gas temperature distribution remains similar between these cases. Species distribution along the flow path of gases through the raceway is also essentially identical. This has to do in part with the location of the natural gas injection port on the tuyere upper surface. The byproducts of natural gas combustion are concentrated in a similar region in all three cases.

Another case (Case 25) using only natural gas injection was also examined as part of this research. This case is intended to represent a scenario under which furnace operators are unable to utilize pulverized coal for a given period of time, for either economic or practical reasons. In an effort to avoid increasing the furnace coke rate, which is a costly and time consuming process, additional natural gas becomes necessary to supply the remainder of the necessary reducing gases previously

generated by pulverized coal. In this case, natural gas was injected through a lance at 150 kg/MTHM, a rate near the upper end of potentially feasibility. Injection conditions were otherwise identical, and production rates were assumed to be the same in Case 25 as in the baseline operation scenario.

Figure 49 compares contours of gas temperature, CH_4 mass fraction, and H_2O mass fraction in the raceway region for Case 25. Figure 50 compares the TOFT between baseline operating conditions and Case 25. The differences between the gas temperature distribution in a natural gas-only operating scenario and the standard co-injection case are immediately apparent.

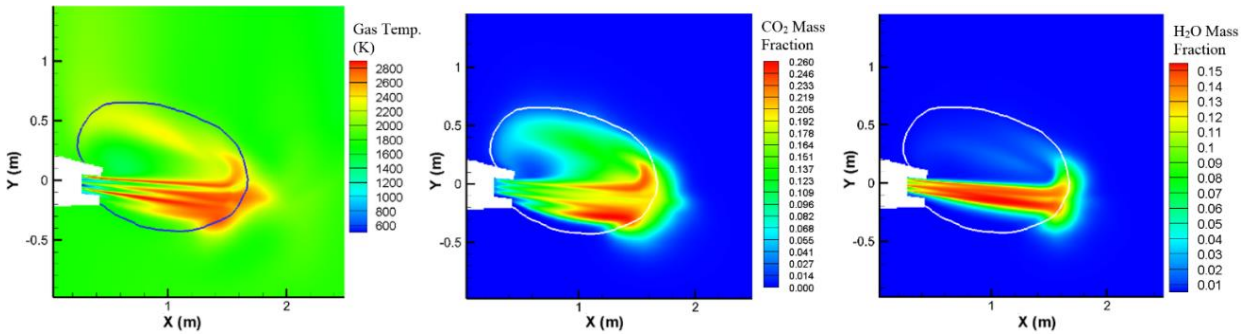

Figure 49. Contours of gas temp. (left), CO2 mass fraction (middle), and H2O mass fraction (right) for Case 4.

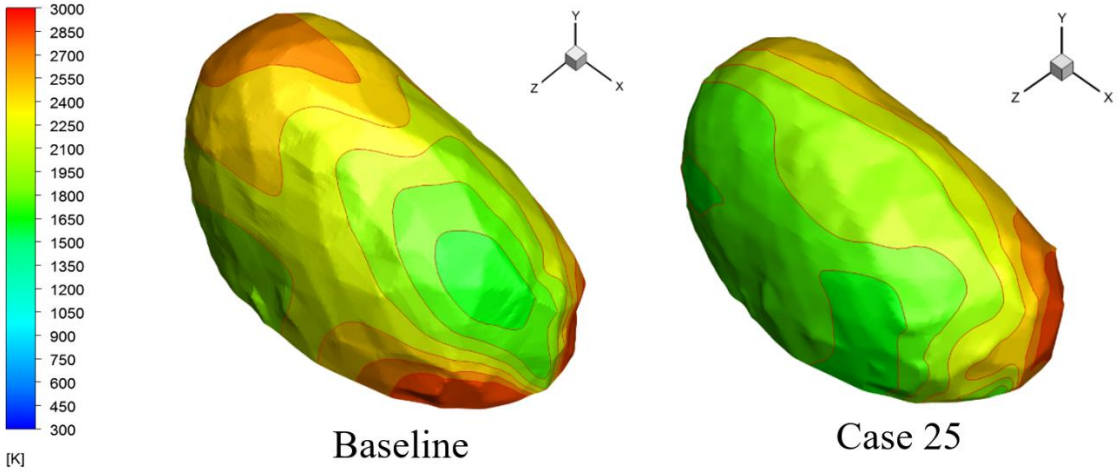

Figure 50. Comparison of TOFT between the baseline case (left) and Case 25 (right).

The tuyere jet is the primary reaction region, producing heat through combustion of CH_4. The byproducts of this combustion (CO_2 and H_2O) then make contact with the coke bed, and endothermic reactions reduce them into CO and H_2. However, with no pulverized coal to increase temperatures further, the furnace gases immediately begin to lose heat to the endothermic reactions of natural gas combustion byproducts. In this scenario, instead of coke or pulverized coal combusting with hot blast O_2, the only method through which reducing gases can be produced is through the endothermic reactions of CO_2 and H_2O with coke and the cracking of any un-combusted CH_4. Gas species distribution can be observed in Figure 51, showing a plot of mass fractions along the centerline of the tuyere jet.

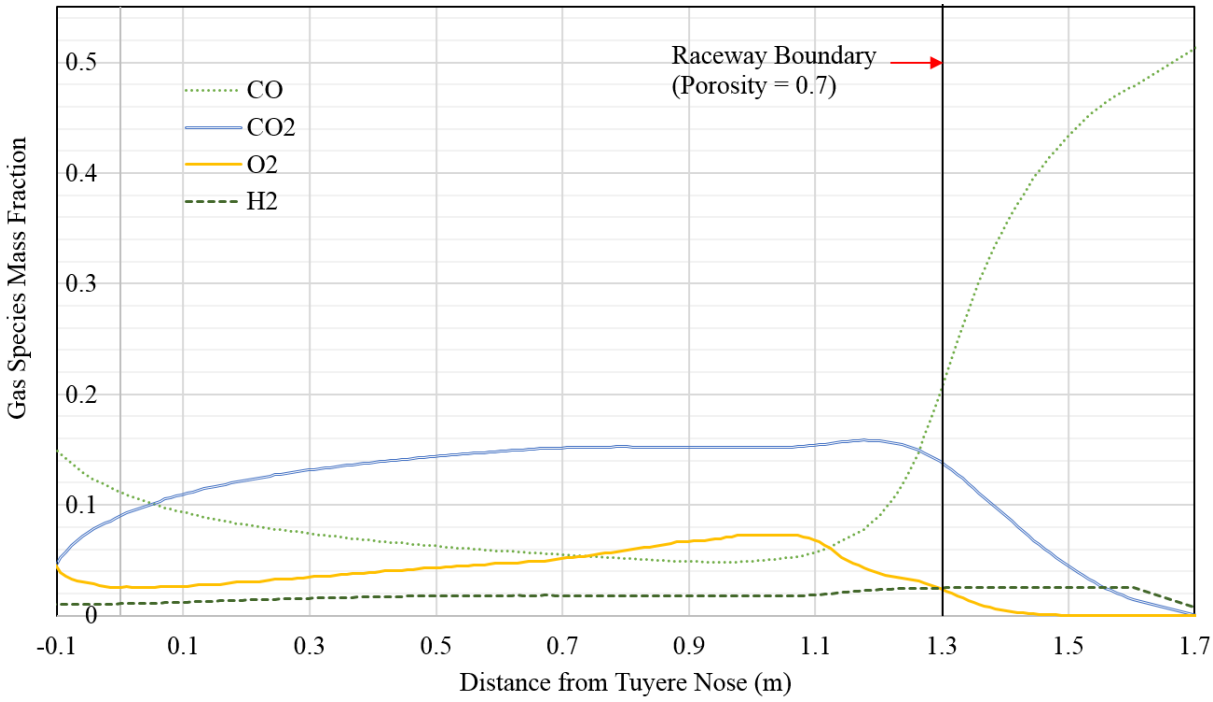

Figure 51. Species mass fractions of CO, CO_2, O_2, and H_2, plotted along the center of the tuyere jet for Case 4.

In this scenario, almost all injected fuel is consumed within the raceway, yet the RAFT analogue in Case 25 is significantly lower than any of the previous cases, falling to approximately 2,000 K (±4%), an 11.1 % decrease compared to the baseline case. This reduction in flame temperature, owed in entirety to the removal of heat from pulverized coal combustion and the increase in endothermic reactions between coke and the products of natural gas combustion, clearly indicates the fundamental reasons why increased natural gas injection rates often result poor furnace stability.

It is also worth noting that there is a significant change in temperatures in the lower regions of the furnace, particularly near the furnace wall directly above the tuyere. This would likely result in lower overall heat loading and reduced wear from an operational perspective.

Together, the cases examined in this section provide a unique view of the conditions within the blast furnace raceway region, as well as data corresponding to the general quenching effect of natural gas upon the flame temperature. The simulations clearly illustrate the effects of increased natural gas injection rates upon raceway gas temperatures. As shown in Figure 52, increasing the injection rate of natural gas can significantly reduce gas temperatures, leading to a unique environment in the blast furnace that must be carefully monitored by operators. One factor that is crucial here is the quenching effect of natural gas injection. The 11% decrease in flame temperature from the baseline case to the high-rate natural gas injection scenario could present difficulties in maintaining stable furnace operation.

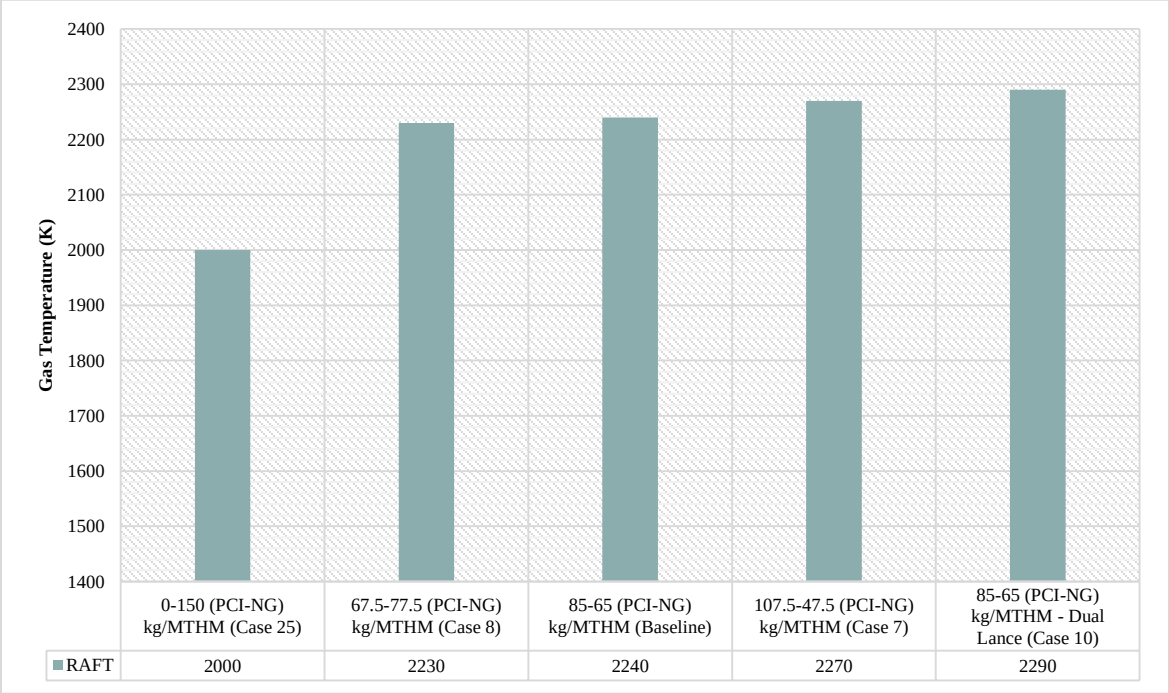

Figure 52. RAFT analogue for the baseline case and Cases 7,8,10, and 25 (±4%).

This quenching effect remains one of the primary reasons why extremely high natural gas rate operation remains limited in application, despite the obvious economic advantages of replacing coke with low cost North American natural gas. While it is somewhat unclear as to the exact lower

limit of flame temperature for stable furnace operation, recent research has documented the fact that most North American blast furnaces operate in a range of flame temperatures over 2,020 K [85]. The modeling in the scenario of Case 25 predicts a RAFT analogue slightly below that value, placing these conditions squarely at the onset of potential instability. It is clear that attempts to increase injected natural gas levels further without also adjusting other furnace operating parameters may introduce significant operational concerns.

Generally, the quenching effect can be counteracted by increasing the O_2 content in the furnace hot blast, allowing for additional heat generation via combustion with coke. However, in addition to increasing furnace coke consumption, this increase in O_2 can also lead to decreasing gas temperatures at the top of the furnace, causing potential condensation. Working within these constraints, there exists a theoretical upper limit to natural gas injection rates of somewhere around 150–160 kg/THM. There have been efforts to push this limit, as well as conceptual methods for expanding the window in which stable furnace operation can be achieved [85]. However, few research projects have fully explored these concepts, and there exists the possibility for significant future improvements to the process of blast furnace natural gas injection.

4.1.3.6 Effects of Natural Gas Injection Location

The final parameters varied in this research examine the effects of modifying the injection location of natural gas in a co-injection environment with pulverized coal. The baseline case (using a tuyere port to inject natural gas) was compared to case 10 (identical operating conditions, modified with the proposed dual lance injection design). Additionally, simulations were conducted comparing case 1 (using the natural gas port) to case 11 (using the dual lance design) at an increased wind rate of 176,550 Nm^3/hr. A general layout of the dual-lance design along with temperature contours for case 10 are shown below in Figure 53.

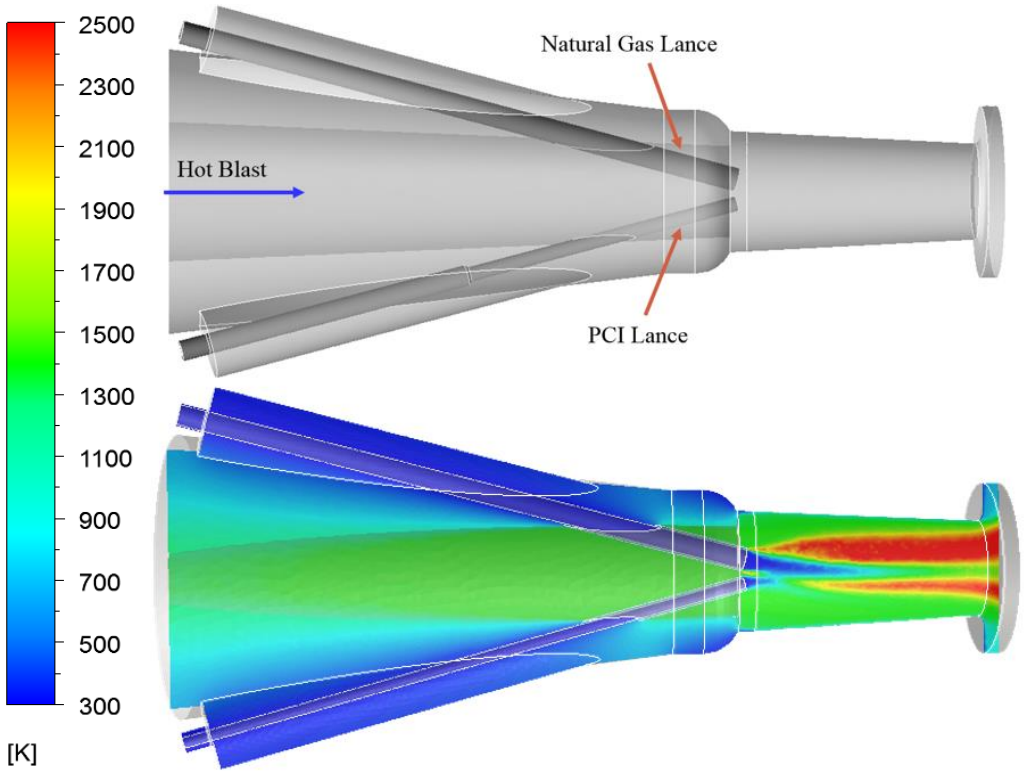

Figure 53. Proposed dual lance injection design (top) and temperature contours in tuyere and blowpipe (bottom).

In this injection apparatus, natural gas combustion inside the tuyere contributes a significant amount of heat to the pulverized coal particles. Downstream of the injection site, gas and coal particles increase rapidly. Additionally, the momentum of the natural gas injection has a significantly higher gas mass flow rate compared to the pulverized coal carrier gas (0.22 kg/s of natural gas vs. 0.03 kg/s of nitrogen). This helps to disperse the pulverized coal plume as it leaves the PCI lance and enhance mixing of both auxiliary fuels with available oxygen in the tuyere and blowpipe. Other published studies on coal particle combustion inside the raceway region have indicated that coal particle dispersion can enhance auxiliary fuel combustion and furnace performance [34]. Figure 54 shows path lines of coal particles inside the tuyere, colored by particle temperature.

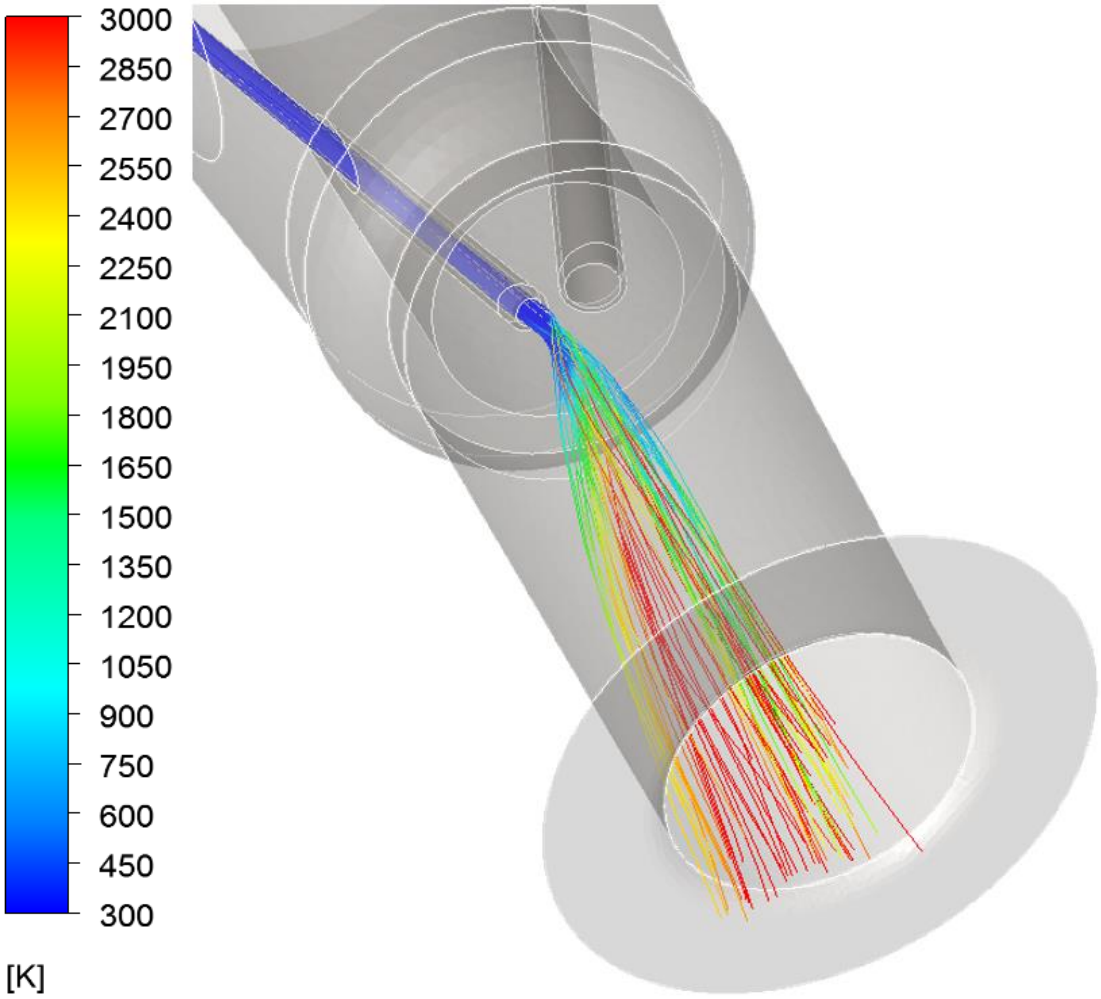

Figure 54. Coal particle path lines drawn in the tuyere, colored by particle temperature.

The increased coal particle plume dispersion is immediately obvious, and the comparison of gas temperature along the tuyere centerline between the baseline case and the dual lance design in Figure 55 highlights the enhanced heating.

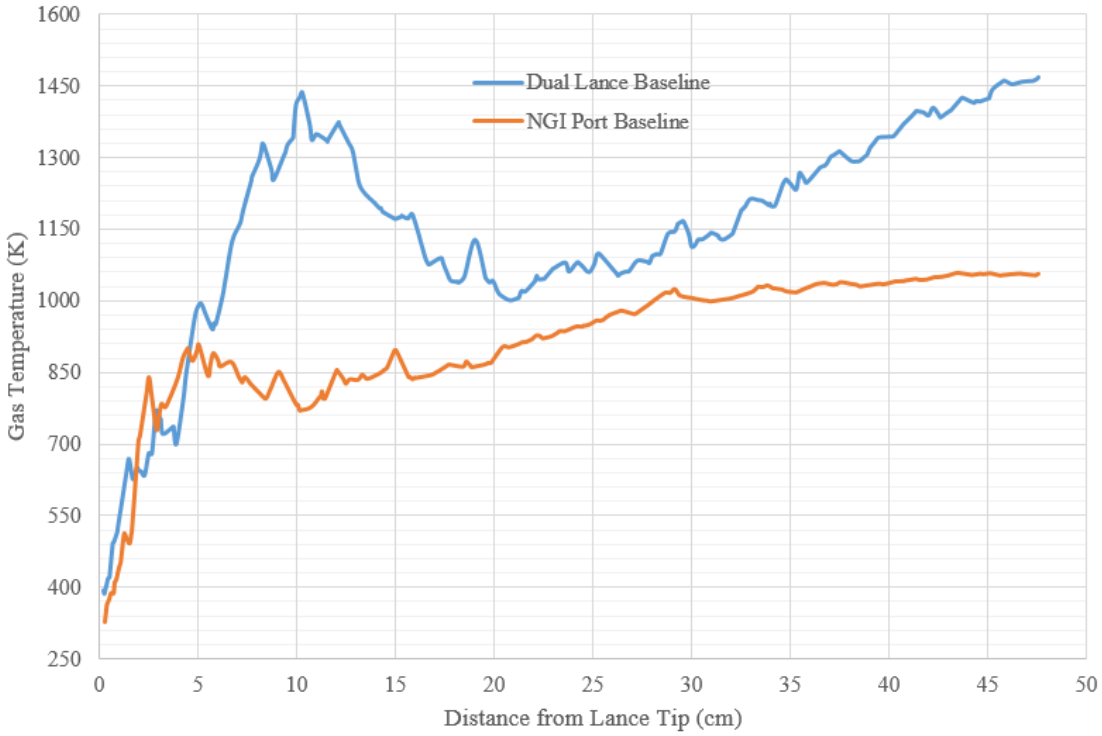

Figure 55. Gas temperature plotted along the tuyere centerline from the PCI lance tip to the tuyere outlet.

Examining coal particle devolatilization inside the tuyere provides similar results. Figure 56 shows contours of volatile mass fraction on both top and side cross-sections through the tuyere. Devolatilization appears to be highest in the path of the natural gas plume, corresponding to the regions of high temperature gases generated by natural gas combustion. The devolatilization rate inside the tuyere in case 10 reaches 62%, a significant increase from the standard Dearborn Works furnace design results (13.2%).

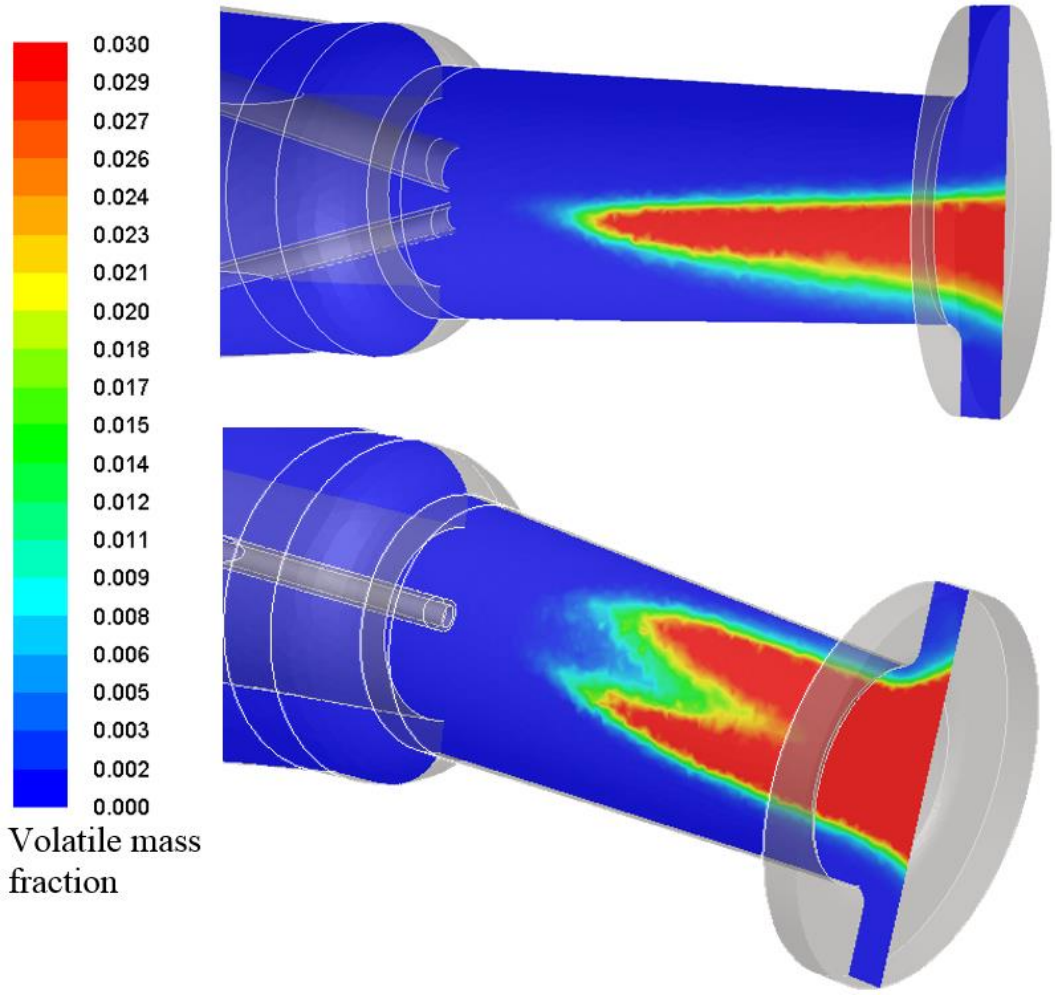

Figure 56. Contours of volatile mass fraction on horizontal (top) and vertical (bottom) cross-sections through the tuyere.

From this analysis, the primary predicted benefit of modifying the natural gas injection locations has to do with heating pulverized coal particles by natural gas combustion. As previously mentioned, in the baseline design, where natural gas is injected via a tuyere port, mixing of the natural gas and pulverized coal plumes is poor. Natural gas combusts only in the region where it mixes with oxygen from the hot blast, resulting in poor heating of the pulverized coal particles. However, the dual injection lance design places the natural gas and PCI locations immediately next to one another at the center of the tuyere. This results in better mixing of natural gas with the hot blast, better mixing of high temperature combusted gas with pulverized coal, and more rapid heating of pulverized coal. Figure 57 compares the temperature inside the blowpipe and tuyere region in the baseline case, case 1, case 10, and case 11. Modeling results predict that the total fuel

burnout rate in case 10 is increased to 89.7% from 70.7% in the original Dearborn Works design. A similar increase to 87.1% from 69.8% is predicted between case 11 and case 1.

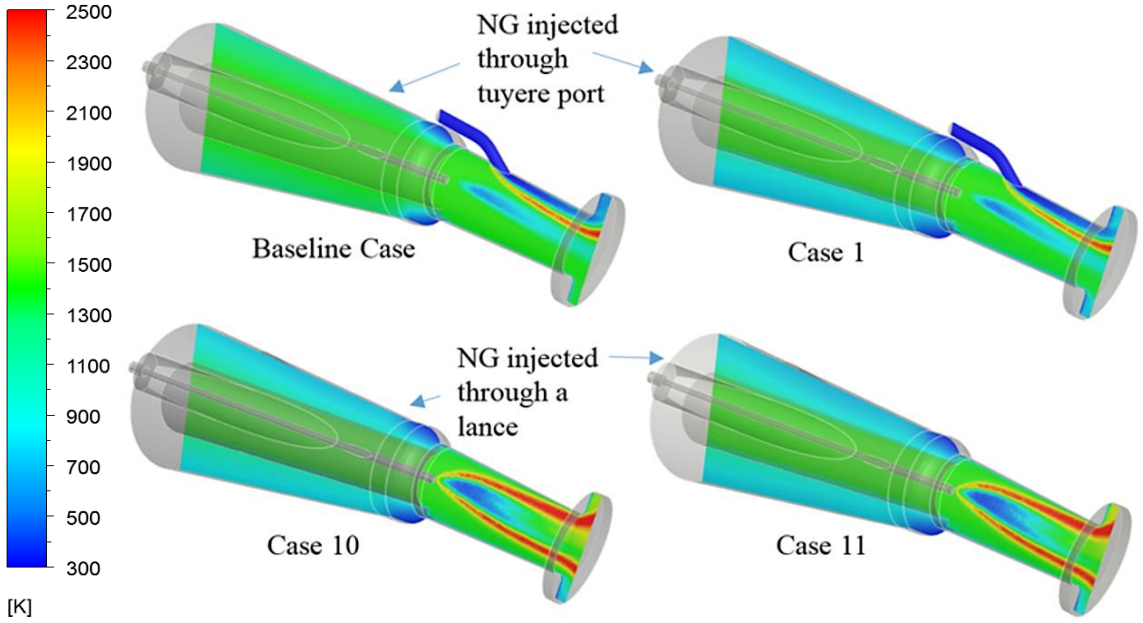

Figure 57. Contours of gas temperature on section A-A in the tuyere and blowpipe region for the altered lance design cases.

The natural gas injection location was further modified within the confines of the dual lance injection apparatus, and results were compared to case 10 (the baseline of the dual lance design). The natural gas lance was extended or retracted by 5.08 cm (two inches) along the axis of insertion. The results of this analysis provide insight into possible advantages presented by lance positioning for auxiliary fuel combustion efficiency inside the raceway. Case 21 (extended lance) and case 22 (retracted lance) use nitrogen as the carrier gas for PCI, while case 23 (extended lance) and case 24 (retracted lance) use natural gas as the PCI carrier. Figure 58 illustrates the lance positioning in all three geometries.

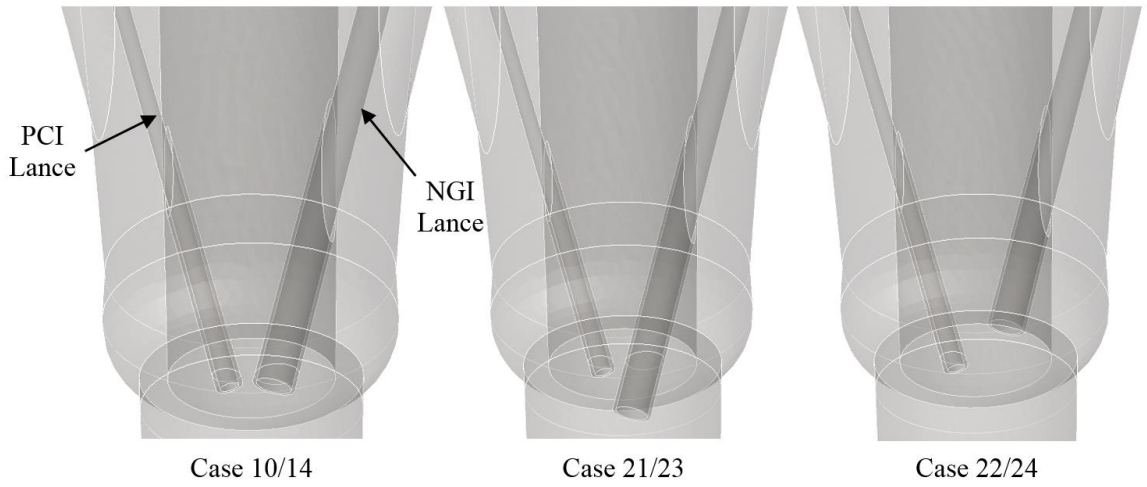

Figure 58. Geometry of proposed dual lance design (left), extended lance design (middle), and retraced lance design (right).

Simulations predict that modifying the natural gas lance position has a significant influence on combustion locations and flow phenomena inside the tuyere. Examination of Figure 59 reveals that extending and retracting the natural gas lance causes horizontal shifts in the high temperature gas regions resulting from combustion inside the tuyere. This phenomenon occurs primarily due to the impact on injected fuel momentum from the natural gas lance. As previously mentioned, changing the natural gas injection position from the tuyere port to a secondary lance led to significant changes in flow phenomena. Similarly, the movement of the natural gas lance along the axial direction also impacts the distribution and mixing of injected fuels in the tuyere.

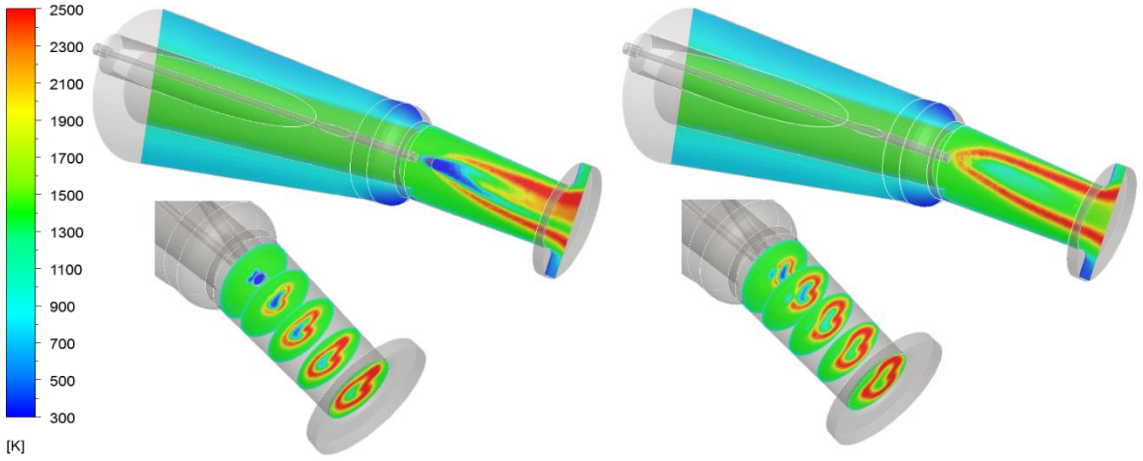

Figure 59. Gas temperature distributions inside the blowpipe and tuyere for case 21 (left) and case 22 (right).

In case 21, the incoming pulverized coal stream encounters interference due to the position of the natural gas lance, and is redirected in multiple directions towards the walls of the tuyere. This phenomenon is clearly illustrated in Figure 60.

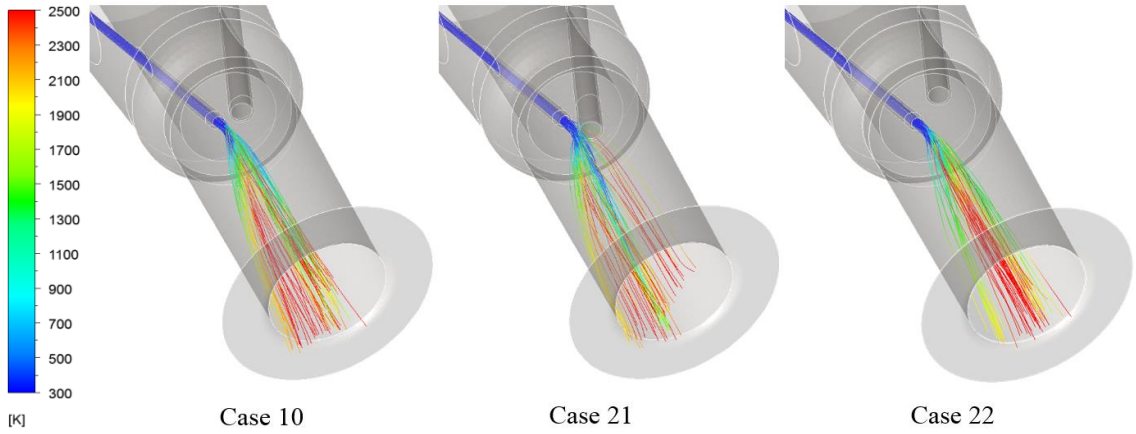

Figure 60. Comparison of coal particle path lines inside the tuyere, colored by temperature.

Coal particle dispersion is increased in Case 21, due to the impingement of coal on the natural gas lance. However, while this impingement assists in coal dispersion, the physical contact of the pulverized coal stream with the natural gas lance may introduce serious reliability issues. Solid particle impacts could result in erosion of the natural gas lance and a general degradation of operating conditions inside the tuyere, resulting in unplanned maintenance expenditures. Additionally, when natural gas is utilized as the carrier for PCI as in case 23, combustion serves to heat the natural gas lance tip, possibly resulting in significant thermal damage, as shown in Figure 61.

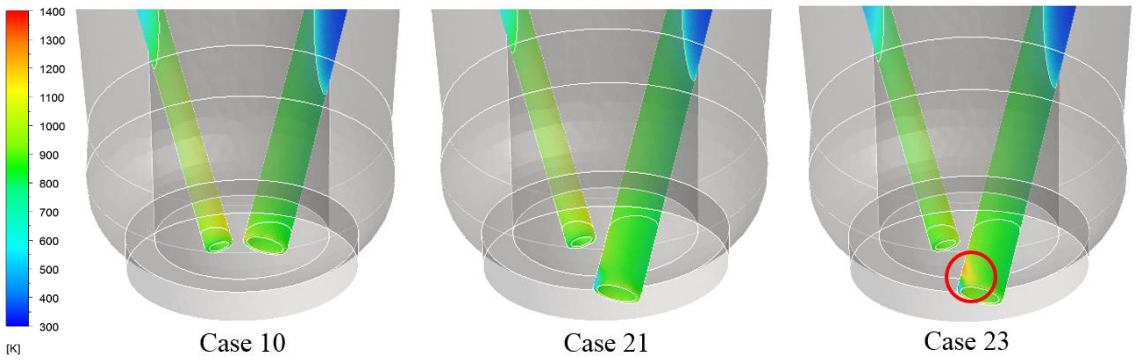

Figure 61. Comparison of lance tip surface temperature, with the high temperature zone observed in case 23 highlighted.

Devolatilization inside the tuyere is similar in case 10 and the retracted lance design (case 21), but is increased in the extended lance design (case 22). In case 21, 73.2% of available volatile matter is released inside the tuyere, compared to 62.0% for case 10 and 60.9% for case 22. However, simulations predict that case 22 provides the highest total fuel burnout of the cases simulated, at 96.7%. This compares favorably to case 10 (89.7%) and case 23 (76.8%). Figure 61 provides a comparison of volatile mass fractions inside the tuyere region for case 10, case 21, and case 22. In large part due to the flow obstruction generated by the natural gas lance, a significant amount of coal particles track through the higher temperature outer regions of the NG plume in case 21. These particles are nearer to the high temperature gases generated by natural gas combustion, leading to more rapid devolatilization. However, this design also results in lower total burnout due to poor mixing of oxygen, char, and volatiles.

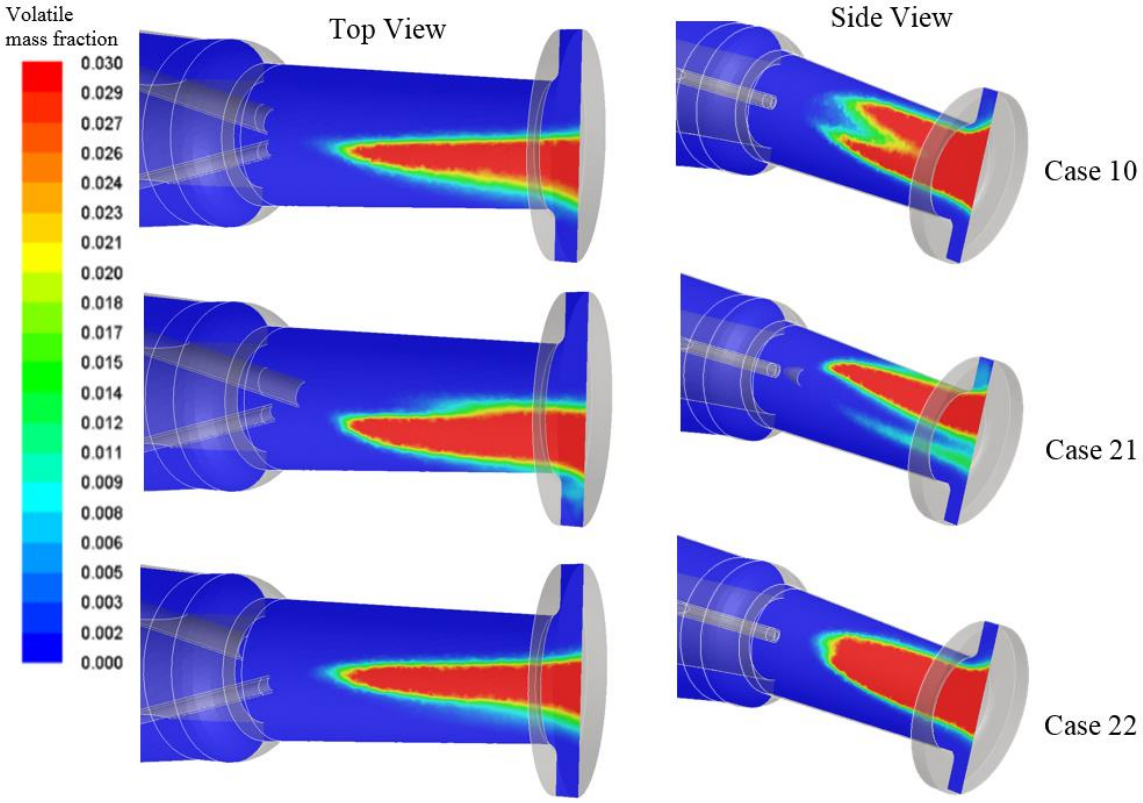

Figure 62. Contours of volatile mass fraction inside the tuyere for cases 10, 21, and 22.

As Figure 63 shows, the location of natural gas injection has a significant influence on combustion characteristics throughout the raceway. In case 10 (baseline dual lance design), coal burns gradually over the entirety of the raceway region, and consumption stops after all oxygen is

consumed from the hot blast. In both case 21 and case 22, initial coal burnout occurs more rapidly. However, conditions in case 21 result in pulverized coal particles experiencing reagent starvation, resulting in a lower maximum burnout value. In case 22, the total fuel burnout is enhanced due to improved mixing of the hot blast, injected natural gas, and injected pulverized coal.

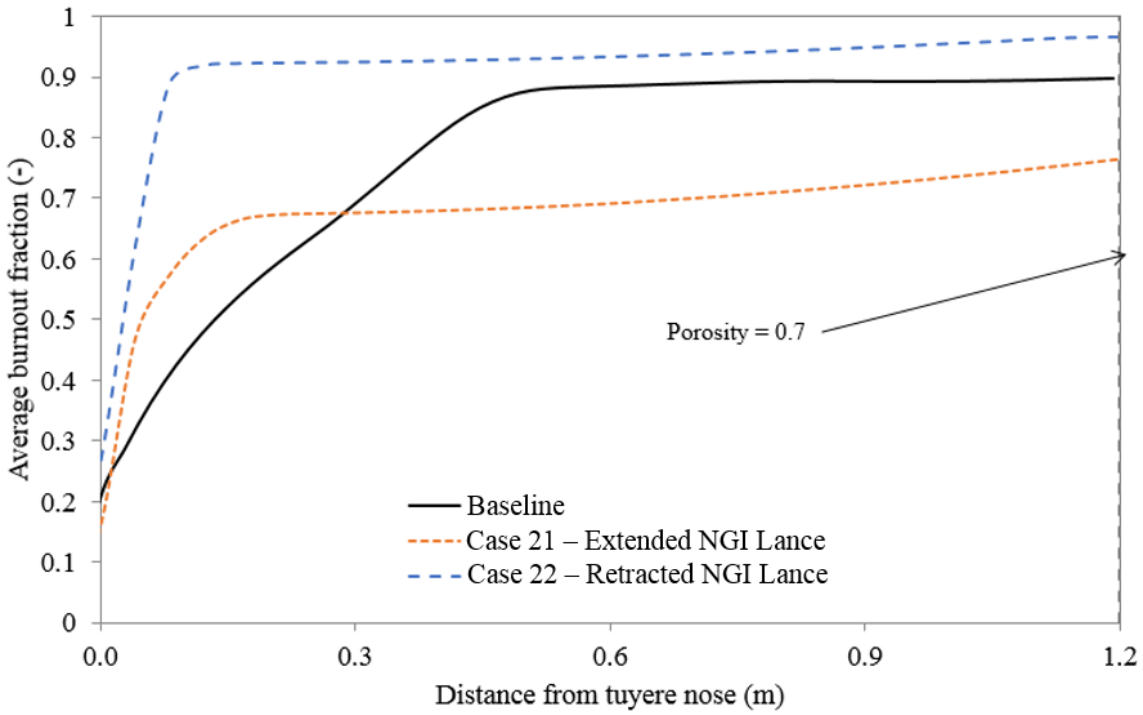

Figure 63. Comparison of fuel burnout along the raceway for case 10 (Baseline), case 21, and case 22.

4.1.3.7 Summary of Simulation Results

As predicted by other simulation models, increased devolatilization in the tuyere does not always directly correlate with an increased burnout rate throughout the raceway system. The parametric studies undertaken in the project indicate that the proposed concept of switching the PCI carrier gas from nitrogen to natural gas enhances total fuel burnout in all simulated cased. Additionally, while other operating parameters have minor effects on total auxiliary fuel burnout, adjusting the natural gas injection location has significant effects on the burnout rate. Regardless of the carrier gas used, injecting natural gas downstream of pulverized coal reduced the total burnout rate, while injecting it upstream of the coal increased total burnout. The final results for all cases run, focusing on combustion characteristics, are summarized in Table 6.

Table 6. Combustion results of parametric study simulations.

Scenario	Volatile Released in Tuyere	Total Burnout Rate Across the Raceway
Baseline	13.2%	70.7%
Case #1	11.7%	69.8%
Case #2	14.1%	72.9%
Case #3	13.5%	67.3%
Case #4	13.4%	73.3%
Case #5	14.2%	75.4%
Case #6	9.5%	72.3%
Case #7	12.6%	66.8%
Case #8	18.3%	75.8%
Case #9	4.2%	76.0%
Case #10	62.0%	89.7%
Case #11	60.1%	87.1%
Case #12	70.4%	97.0%
Case #13	69.7%	90.1%
Case #14	92.1%	86.8%
Case #15	26.4%	95.7%
Case #16	88.2%	71.4%
Case #17	19.0%	88.7%
Case #18	36.8%	100.0%
Case #19	33.1%	95.6%
Case #20	35.2%	98.9%
Case #21	73.2%	76.8%
Case #22	60.9%	96.7%
Case #23	65.5%	93.1%
Case #24	29.3%	100.0%
Case #25	N/A	N/A

The cases modeled in this simulation study provide an overview of a wide range of operating conditions for the Dearborn Works blast furnace. Within the scope of the study, novel injection methods were examined, including the effects of changing the carrier gas for PCI from nitrogen to natural gas (Case 14). Results indicate that this switch can provide a significant improvement to injected fuel burnout, increasing volatile release in the tuyere by nearly 600% and increasing fuel burnout by approximately 23%. Simulations also predicted that modifying the injection location of natural gas significantly improves total fuel burnout through enhancing the mixing of auxiliary fuels and hot blast. Specifically, the highest predicted burnout rate (96.7%) under standard

operating conditions at the Dearborn Works furnace was achieved with a modified dual lance injection design (case 22), a 36.7% increase compared to the baseline case. Modifications to the furnace wind rate and oxygen enrichment allowed the simulation model to predict 100% fuel burnout, however, these alterations in operating conditions may lead to unwanted changes in total production rate or increases in raceway flame temperature to unsustainable levels.

In a similar vein, cases testing variations in the ratio between injected natural gas and pulverized coal caused shifts in the gas species concentrations of CO_2 and H_2O, leading to additional endothermic reactions which may decrease raceway flame temperature. Detailed examination of these results confirmed the limitations of natural gas injection and highlighted the need for techniques to increase flame temperature without further oxygen enrichment, such as pre-heating injected natural gas.

4.1.3.8 Industrial Implementation of Design and Operational Improvements

Simulation modeling indicates that process efficiency could be enhanced by altering the configuration and operational conditions of the furnace co-injection apparatus at AK Steel Dearborn works. However, industrial implementation of these results presents additional difficulties. The simplest modification to the injection apparatus (modifying the natural gas injection location from a tuyere port to a secondary lance) would require changing all blowpipe and tuyere stock to accommodate the new design. Plant engineers also suggest that this modification could present additional difficulties with maintenance scheduling. The modification process to alter the injection apparatus is currently in progress, however, the timing of the changeover depends heavily on operational considerations. If restricted to the expected life cycle of tuyeres currently in use on the furnace, the time required to execute this modification would be nearly 450 days. Installing the modifications on all tuyeres at once would increase expenditures considerably.

Switching the PCI carrier gas from nitrogen to natural gas is an even more complex proposition. Plant engineers suggest that a re-design of the PCI system between the pulverized coal feed tanks and the transport line would be necessary, focusing on the mixing tee where carrier gas is introduced to the coal particles. A natural gas supply line would also need to be introduced into

the pulverized coal storage area, and the process would need to be controlled carefully to ensure safe operation. Further experimental and modeling work may also be necessary regarding the gas flow rates of the carrier gas, due to changes in solids loading and the shift deeper into the dense phase range, as seen in Figure 64.

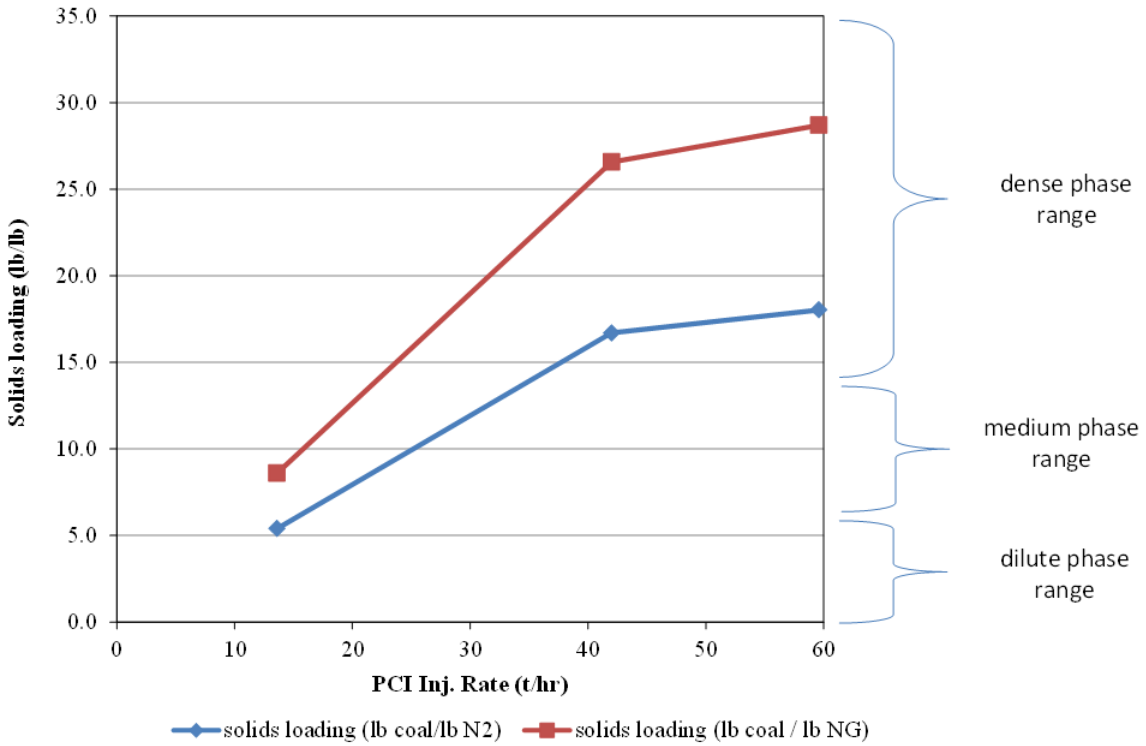

Figure 64. Influence of PCI carrier gas type and injection rate on solids loading of the PCI system.

Trials are expected to be run on an injection test rig on a small scale, allowing PCI to be performed using natural gas as the carrier in a select number of tuyeres. Still, full industrial implementation is likely necessary to verify the significant benefits predicted by industrial-scale simulation results, including increased coke replacement ratios, improved furnace stability, increased furnace productivity levels (nearly 2.5% improvement), and a reduction in nitrogen gas consumption of roughly 12% for the entirety of AK Steel Dearborn Works.

Additionally, examining results from these simulations provided valuable insight into industrial operational observations, including questions as to why difficulties exist in maintaining coal injection stability during unplanned reduced stove operation at the Dearborn Works furnace. This

type of operation typically occurs at PCI rates, reduced wind rates, and reduced hot blast temperatures. Observations at the Dearborn Works furnace indicated that these scenarios present difficulties in maintaining injection on lances due to decreased combustion and darker coal plumes. The light detection system on the furnace will then shut down coal injection, interpreting the darker coal plume as a possible blocked tuyere, which can present significant safety concerns in furnace operation.

4.2 Investigation of Natural Gas Injection Lance Designs

The blast furnace at the Stelco Inc. Lake Erie Works plant, located in Nanticoke, Ontario, has operated entirely using natural gas injection. Plant operation focused on the utilization of high rate natural gas injection to reduce overall furnace coke consumption in recent years. In order to optimize injected fuel combustion under different operating conditions, three different natural gas injection lance designs were modeled. Initially, a multi-ported ‘fast lance’ with a complex geometry containing several points of egress for gas flow was utilized in the furnace. During furnace outages, these lances were modified by boring out the tip region to generate a more simplistic geometry, known as the ‘bored lance.’ A final modification was a shift to simple straight pipe lances for natural gas injection. This portion of the research explores the influence of these three lance designs on the combustion characteristics of natural gas within the blast furnace tuyere and raceway, with an eye toward furnace operational efficiency and stability [86].

4.2.1 Simulation Geometry

This study is concerned with the effects of lance design on the combustion of natural gas injected into the tuyere and raceway of the Lake Erie Works furnace. The simulation domain modeled includes the blowpipe, natural gas injection lance, and the raceway. As previously mentioned, three lance designs were modeled, the details of which are shown in Figure 65.

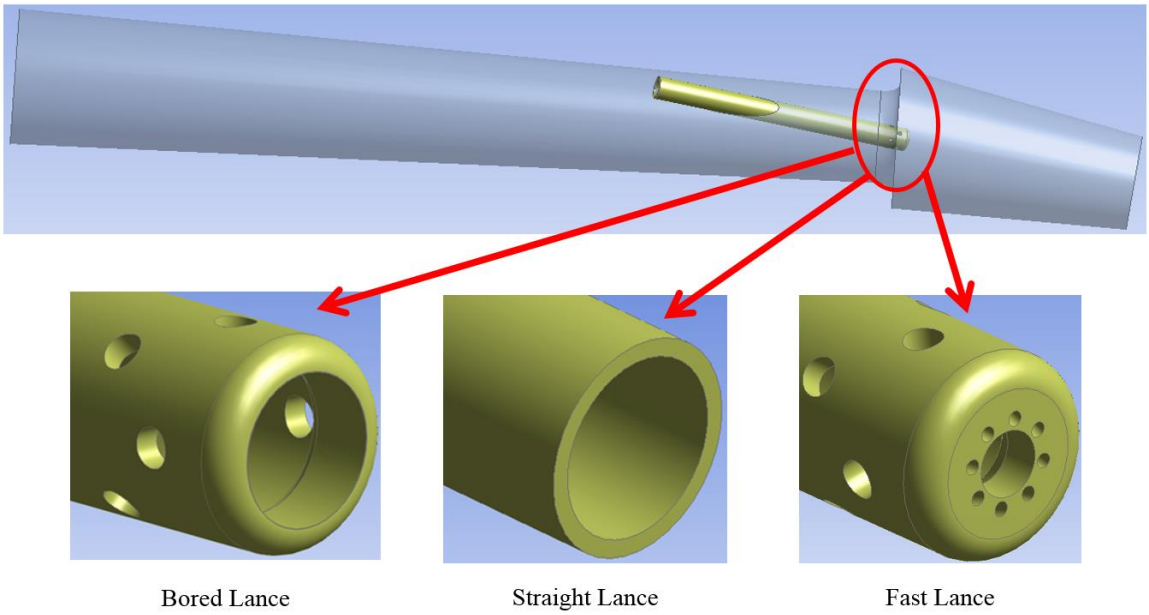

Figure 65. Geometry of blowpipe and tuyere region in the Lake Erie Works furnace (top) and natural gas lance tip designs (bottom).

The tuyere outlet is defined as an outflow boundary condition. Natural convection acting upon thermal insulation is applied as the boundary condition at the domain walls of the blowpipe. The inner surface of the tuyere is cooled via a water cooling system, which is modeled through a constant heat flux assumption. All three lance designs were simulated at identical conditions, with a hot blast temperature of 1420 K, a hot blast flow rate of 4.01 kg/s per tuyere, 30.9% oxygen in the hot blast, an operating pressure of 347 kPa, and a natural gas flow rate of 0.2686 kg/s per tuyere at 300 K.

4.2.2 Results of Simulations

Gas combustion within the tuyere is heavily dependent upon the injection lance design. When using the fast lance, natural gas is dispersed much more rapidly and more evenly throughout the tuyere, resulting in enhanced mixing with hot blast oxygen and increased combustion. The bored lance tip also enhances mixing, though to a significantly lower degree than the fast lance design. Combustion rates inside the tuyere are lowest in the straight lance case, as fuel mixing is not enhanced through additional injection ports as in the other two cases. This phenomenon can be observed in Figures 66 and 67.

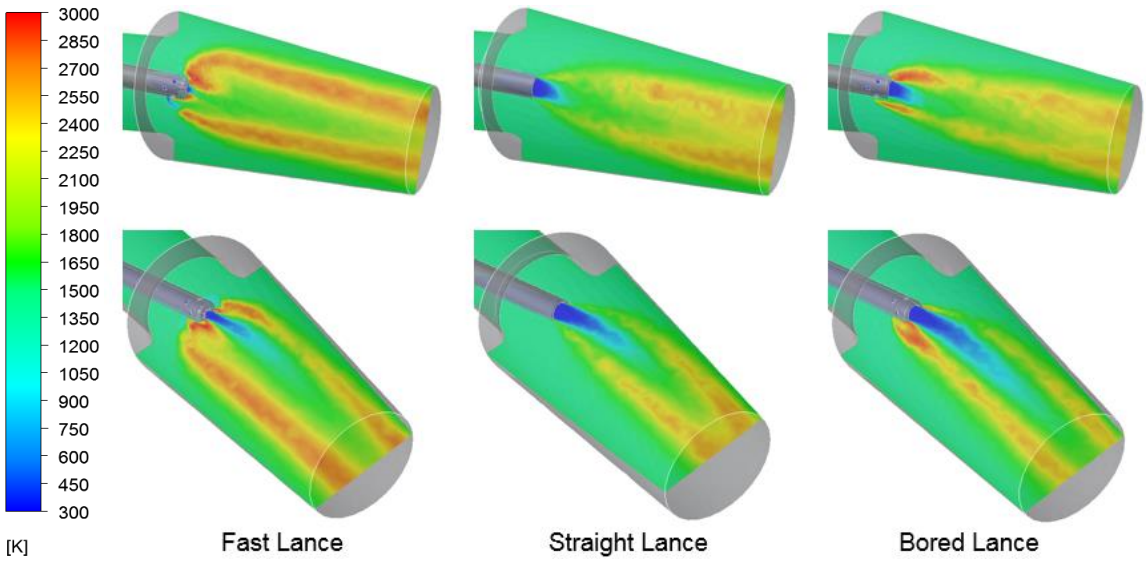

Figure 66. Gas temperature distributions within the tuyere along cross-sectional planes parallel to the flow direction.

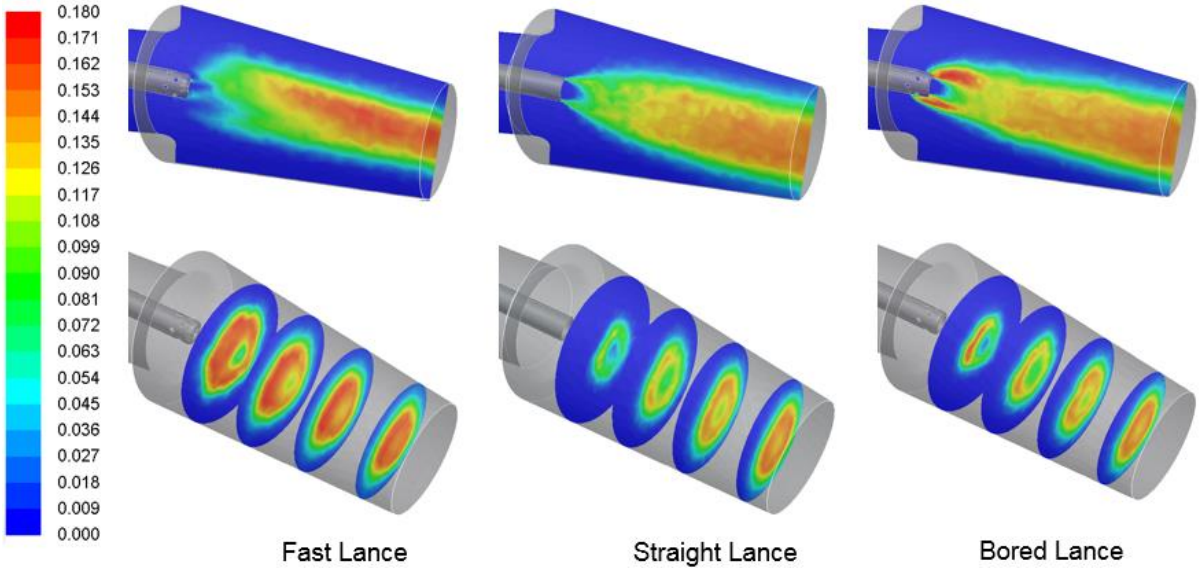

Figure 67. CO_2 mass fraction distributions within the tuyere along cross-sectional planes parallel to the flow direction.

Additionally, the enhanced combustion and increased gas temperatures when using the fast lance design also increase average gas velocity at the tuyere outlet due to thermal expansion. The gas velocity in the straight lance and bored lance cases is similar, while the increased thermal expansion in the fast lance case results in an 8.5% increase in gas velocity at the tuyere outlet (nearly 40 m/s), as seen in Figure 68.

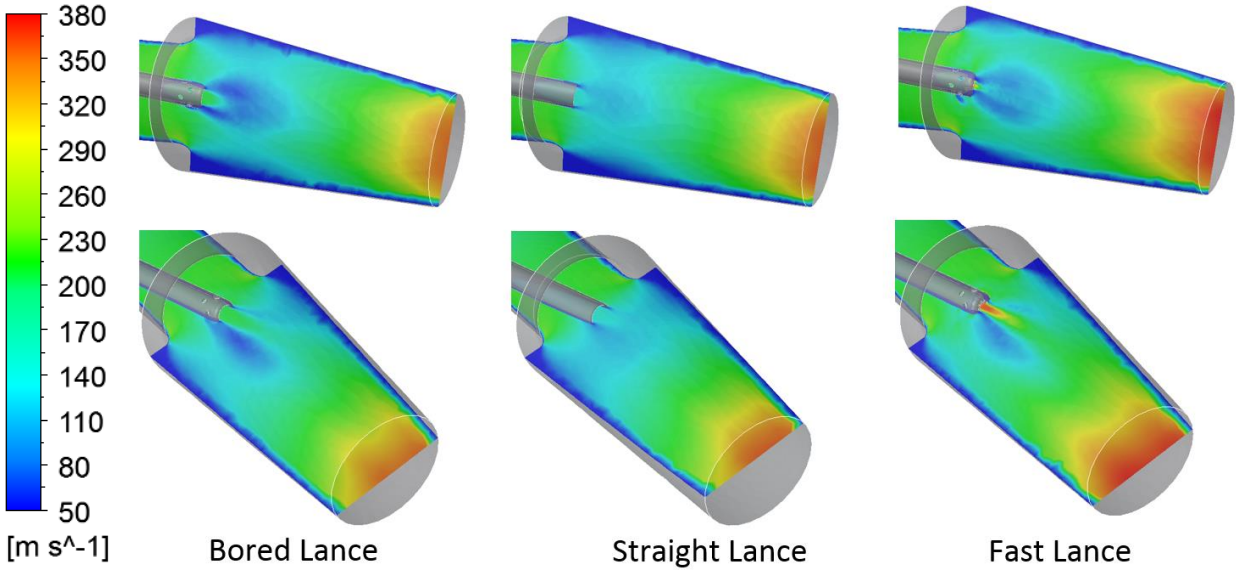

Figure 68. Gas velocity distributions within the tuyere along cross-sectional planes parallel to the flow direction.

Operators at the Lake Erie Works blast furnace indicated that high pressure drops were observed in the furnace at high natural gas injection rates during the use of the fast lance tips, limiting the maximum wind rate and furnace production rate. Simulation results appear to provide an explanation for this phenomenon, as evidenced by Figure 69.

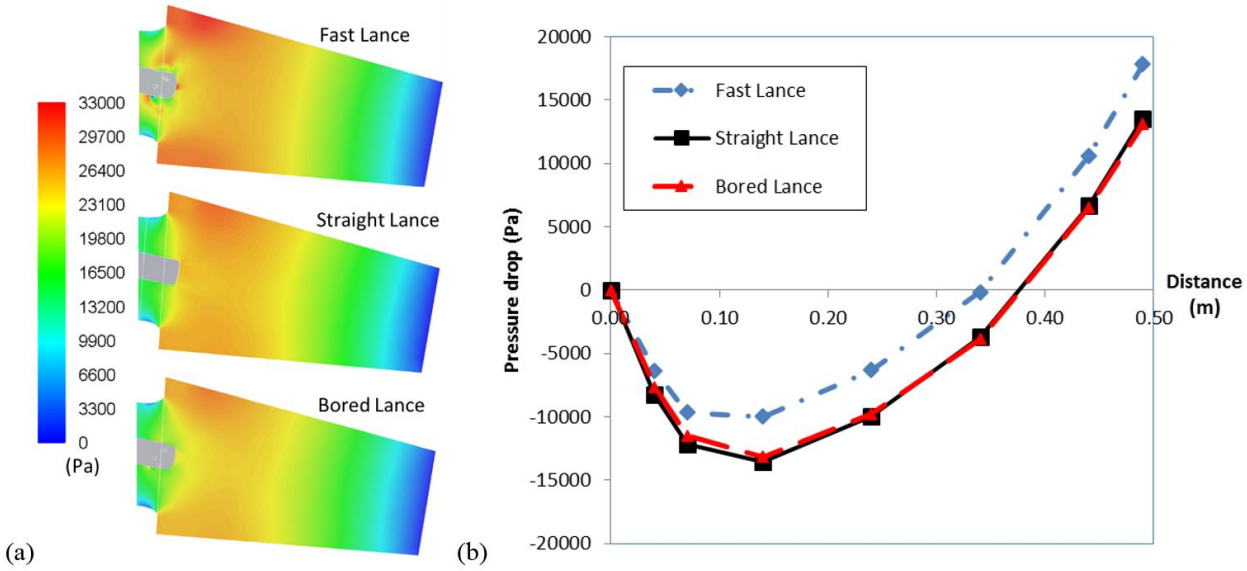

Figure 69. Static gauge pressure distribution on a vertical center plane through the tuyere (a) and average static pressure drop plotted along the tuyere (b).

Pressure contours predicted in the fast lance case show a pressure spike near the side vents of the lance. Examination of mass flow rates indicate that nearly 60% of the natural gas injected through the lance flows through the side ports in this design, leading to high combustion and thermal expansion in these regions. Overall the simulation model indicates that the pressure drop experienced in the fast lance case is nearly 4.3 kPa higher than when the straight or bored lance tips are used. This occurs due to the intensified combustion in the fast lance case, resulting in lower gas densities, higher gas velocities at the tuyere outlet, and a higher total pressure drop across the tuyere.

Raceway modeling was also undertaken for each of these cases. The shape and size of the raceway in all three cases is fairly similar, however, there is significant variation in gas temperature and species distributions throughout the raceway region. From the gas temperature distributions shown in Figure 70, it can be observed that the high temperature regions are shifted toward the side of the raceway opposite from the natural gas plume. This occurs due to the asymmetric nature of gas injection inside the tuyere. Natural gas consumes more oxygen to the right side of the tuyere jet (when viewed from the inside of the furnace looking back at the tuyere).

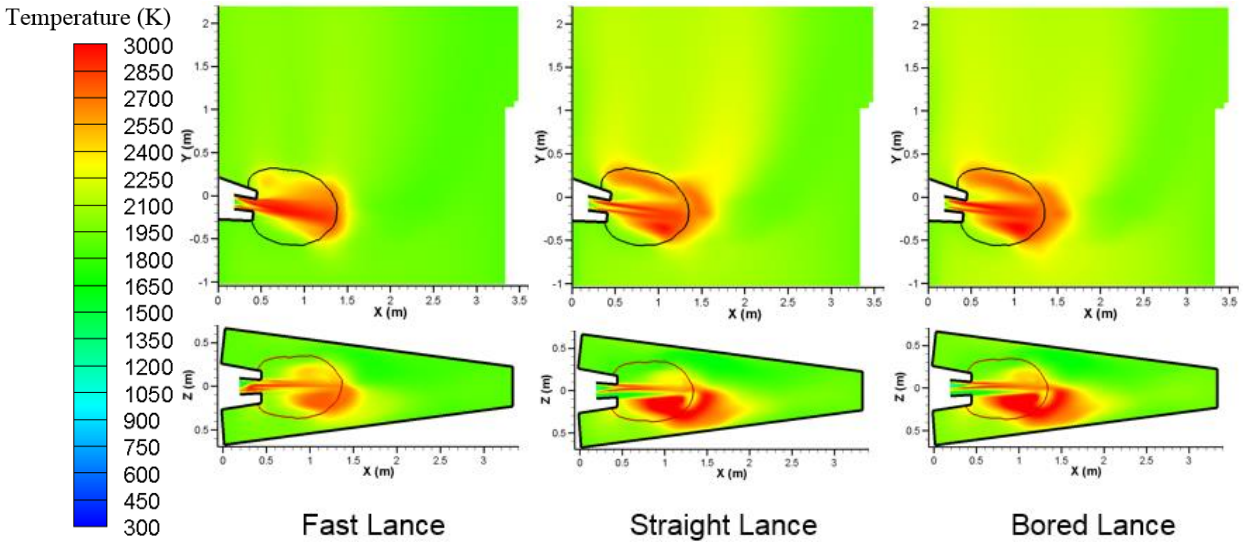

Figure 70. Gas temperature distributions inside the raceway from a side view (top) and a top view (bottom) for all three cases.

As observed in Figure 71, the free oxygen remaining on the left side (opposite the natural gas plume) reacts with coke and combusts rapidly, generating significant heat, while the products of

CH_4 combustion undergo endothermic reactions, generating hydrogen gas and carbon monoxide. This leads to the primary differences between the fast, straight, and bored lance cases. More rapid natural gas combustion consumes more oxygen, leaving less available to react with coke in the raceway, and reducing the raceway average temperature.

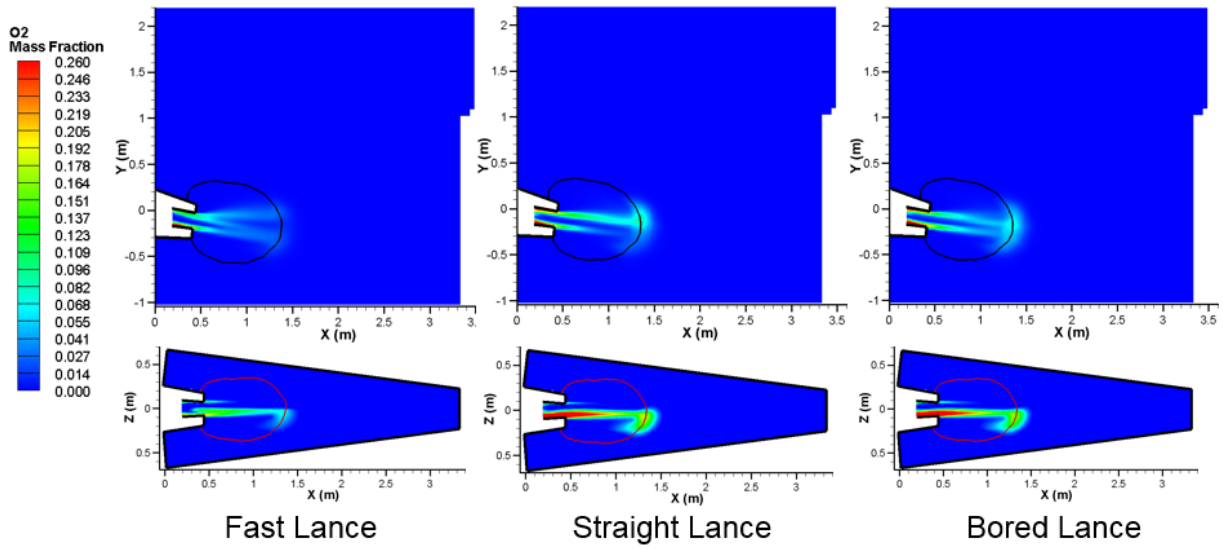

Figure 71. Oxygen distribution inside the raceway from a side view (top) and a top view (bottom).

These results indicate that while the lance type has little influence on the size and shape of the raceway, lance designs that serve to enhance combustion can have a significant influence on gas species distribution. This in turn can have an effect upon the gas utilization of the upper regions of the furnace. The primary finding from this study was the effect of lance design on furnace pressure drops. At lower production rates, many blast furnaces undertake efforts to maintain blast velocity, often by plugging tuyeres. However, this study indicates that under lower production rate conditions where wind rates are also lower, lance designs that enhance gas combustion in the tuyere can provide extra tuyere jet velocity and maintain raceway stability without forcing the plant to undertake the costly process of plugging and unplugging tuyeres. Results also indicate that too much combustion in the tuyere can lead to high tuyere pressure drops, which can lead to problems at high production rate conditions under which blast furnace wind rates are at peak plant capacity.

In addition to the specific focus on tuyere pressure drops and stable operation, research was also conducted to examine the RAFT analogue for the furnace in the fast lance case, as the simulated scenarios utilized only natural gas injection. As previously mentioned, gas is supplied at a rate of 100 kg/MTHM, and while this is significantly lower than the theoretical maximum value of 150 kg/MTHM explored in the scenarios using the AK Steel Dearborn Works blast furnace, the furnace experiences much lower gas temperatures in the raceway region, with a RAFT analogue of roughly 1,950 K (±4%). This value is nearly 100 K below the average minimum RAFT for North American blast furnaces. Production rates at the Lake Erie Works furnace are lower than those at the AK Steel Dearborn Works plant, and oxygen enrichment in the blast is far higher to compensate for these conditions. However, due to the heavy economic incentive to use natural gas as opposed to pulverized coal, these conditions were maintained. Further research could explore the effects of pre-heating the injected natural gas to increase the furnace flame temperatures.

Additionally, as seen in Figure 72, the Topographical Flame Temperature of the Fast Lance case indicates that the gas temperatures above the raceway are significantly different from results observed in co-injection furnaces utilizing both PCI and natural gas injection. High gas temperatures are concentrated near the nose of the raceway, in the plume of heat generated by natural gas combustion.

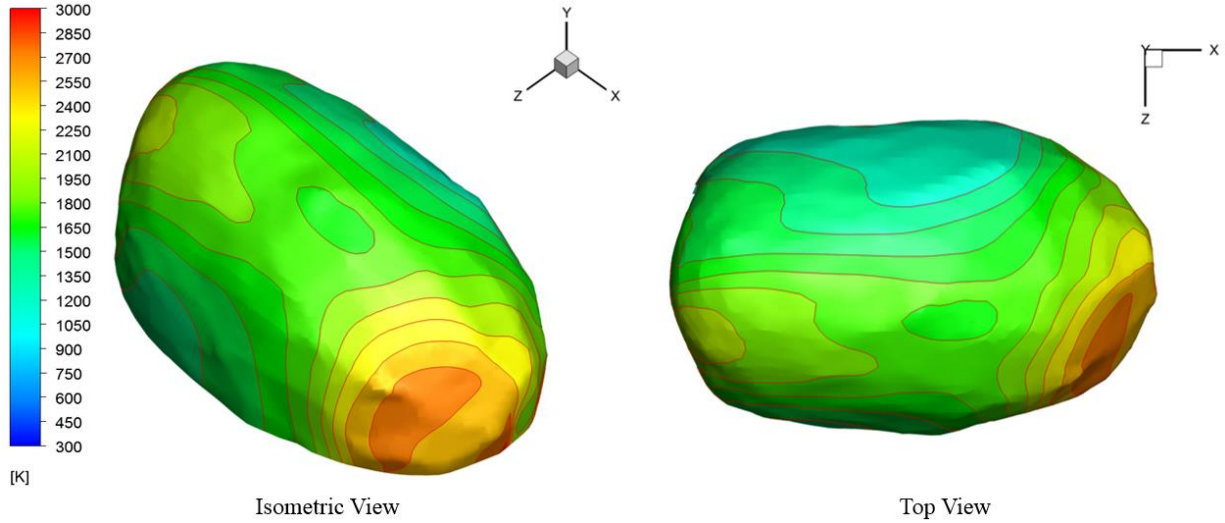

Figure 72. TOFT at the LEW furnace raceway upper surface.

Distributions of gas temperature at the surface of the raceway vary slightly between the three cases examined in this research, however, the fast lance case best illustrates the reduced temperatures generated via reaction of CH_4 combustion products with coke in the raceway region, as a much greater fraction of injected natural gas has burned in the tuyere. It is clear that the combustion of natural gas itself has led to the variations in local temperature, as natural gas does not linger in the raceway region in the same manner as pulverized coal and coke particles. Additionally, these conditions make clear the necessity of increased oxygen enrichment when operating at high natural gas injection rates, both to increase furnace heat and improve thermal uniformity through the combustion of coke with oxygen in the hot blast.

4.3 Investigation of Effects of PCI on Combustion and Injection Lance Wear

U.S. Steel's Gary Works facility, located in Gary, IN, operates several large-scale blast furnaces. The #14 blast furnace is the largest at the plant, capable of producing 8,350 metric tons of pig iron per day. It is supplied hot blast by 34 tuyeres around the furnace annulus. This portion of the research endeavors to examine the effects of design and operating parameters on combustion characteristics and injection lance wear in the Gary Works #14 blast furnace [87].

4.3.1 Simulation Geometry

The modeled portion of the #14 blast furnace contains a single tuyere (representative of all tuyeres operating within the furnace), including a natural gas injection lance and a pulverized coal injection lance, as well as the raceway generated by standard operating conditions at the furnace. Boundary conditions used for the model include an outflow boundary at the outlet of the tuyere (with radiation heat flux considered based on estimated internal emissivity and black body temperature of the blast furnace raceway). The outer walls of the domain include heat flux boundary conditions to model heat loss due to cooling water passing over the tuyere, and natural convection to ambient air outside the thermal insulation on the blowpipe shell is simulated. Material properties and ambient temperatures are gathered from plant data. The geometry of the blowpipe and tuyere region modeled in this study is shown in Figure 73.

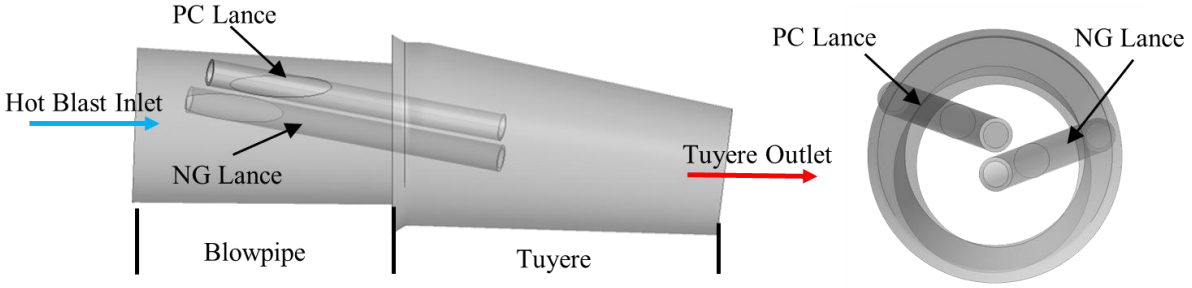

Figure 73. Tuyere and blowpipe region geometry with auxiliary fuel injection lances.

The operating conditions simulated for the baseline case of this study were selected based on typical operation at the Gary Works #14 furnace. Process parameters were a wind rate of 284,000 Nm^3/hr, a hot blast temperature of 1470 K, 124 kg/MTHM of PCI, and a natural gas flow rate of 5,600 Nm^3/hr.

4.3.2 Baseline Case

Injection lances at the Gary Works #14 furnace are arranged in such fashion that auxiliary fuels enter the tuyere in two plumes directly atop one another. Natural gas combustion begins almost immediately after the fuel leaves the lance, producing a plume of high temperature gas within the tuyere. Based on previous analyses, it would be expected that these high temperature gases would assist in the heating of pulverized coal, however, as the injection lances are staggered and enter from opposite sides of the tuyere, very little mixing occurs between the gas plume and the pulverized coal stream. Figures 74 and 75 show the distribution of gas temperature and released volatile mass fraction within the tuyere respectively.

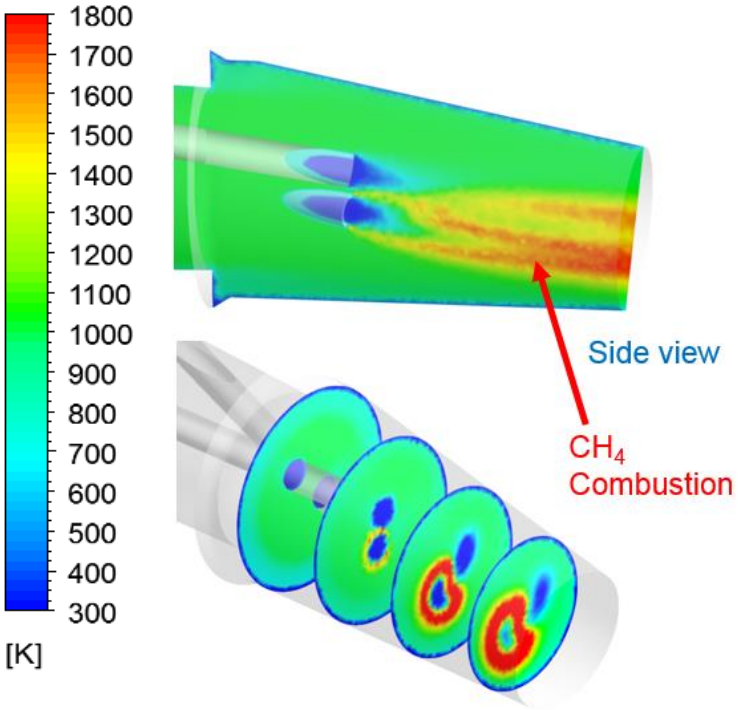

Figure 74. Gas temperature distribution inside the tuyere.

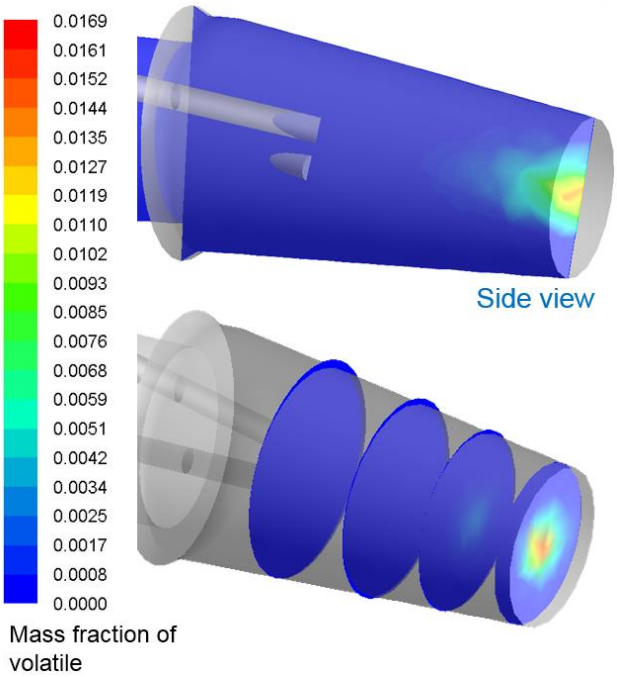

Figure 75. Released volatile mass fraction distribution inside the tuyere.

The average gas temperature at the outlet of the tuyere increases by roughly 200 K from the hot blast temperature, to 1,670 K (±4%). The average gas velocity at the tuyere exit is approximately

190 m/s (±4%). Examination of the pulverized coal particles at the tuyere outlet reveals that roughly 7% of volatile matter has been devolatilized. Figures 76 and 77 help to illustrate the cause of this phenomenon. As previously mentioned, the injection apparatus results in little mixing between the two fuel streams. Results in this study appear similar to the results of previous studies in which poor mixing between the natural gas plume and the pulverized coal stream resulted in low devolatilization in the tuyere.

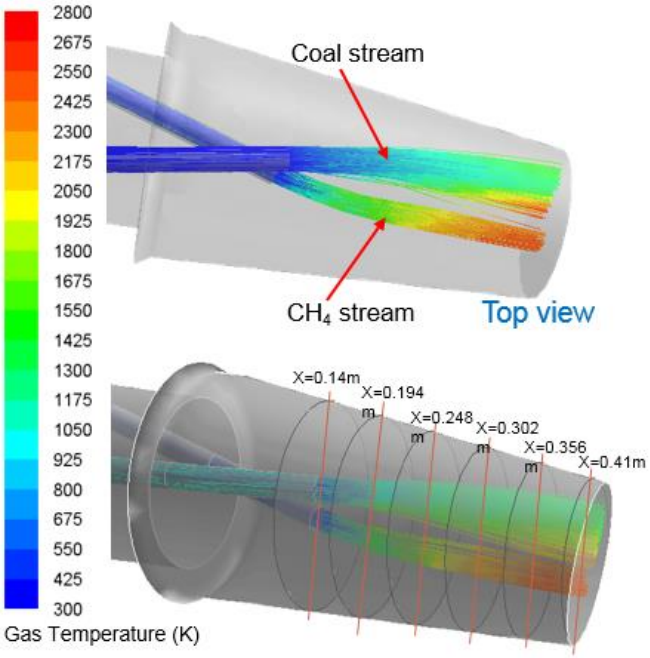

Figure 76. Streamlines of natural gas flow and path lines of pulverized coal particles, colored by temperature.

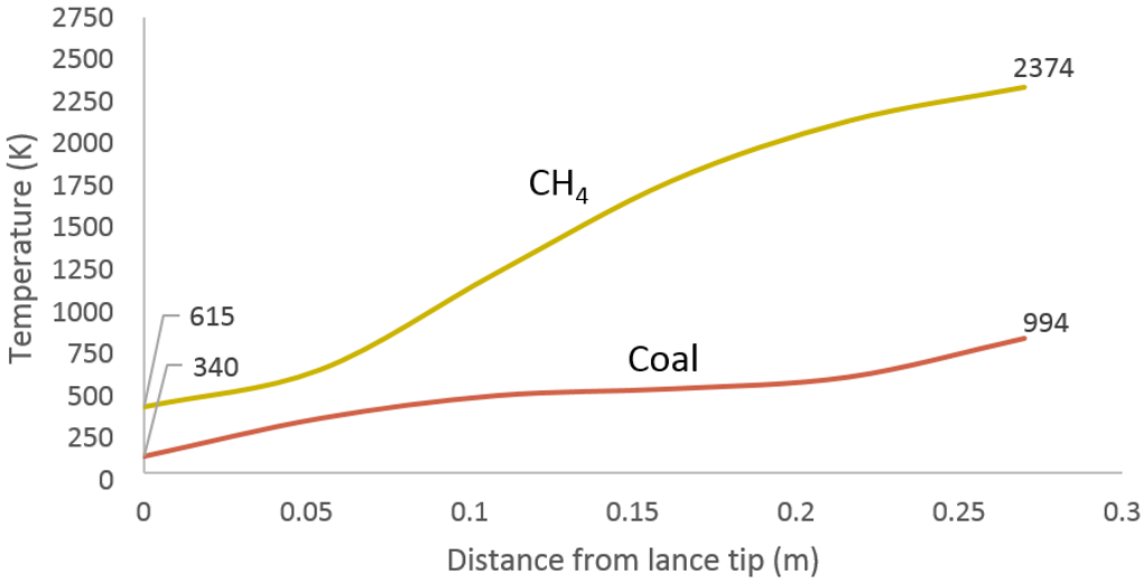

Figure 77. Average natural gas and pulverized coal temperatures plotted inside the tuyere.

Results from raceway modeling show standard jet flow leaving the tuyere, forming recirculation regions inside the raceway and generating reducing gases through the reaction of oxygen, injected fuels, coke, and combustion products. Gas flow patterns and temperature distributions inside the raceway are shown in Figure 78, while gas species distributions inside the raceway are shown in Figure 79.

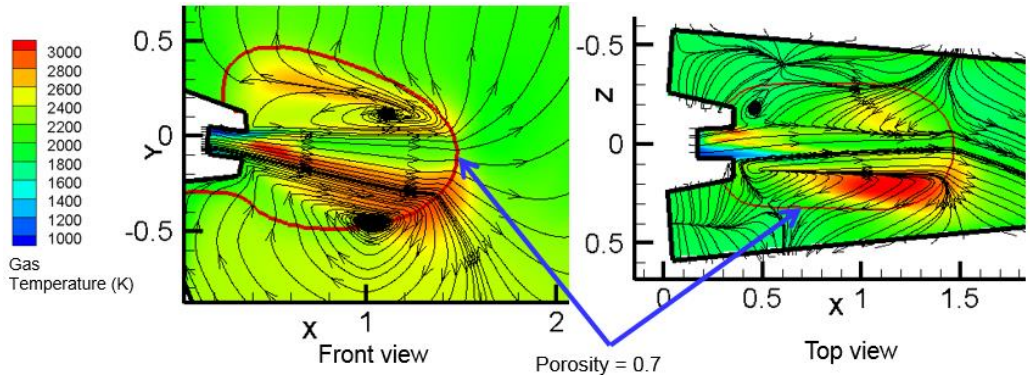

Figure 78. Gas temperature distributions and streamlines inside the raceway for the baseline case.

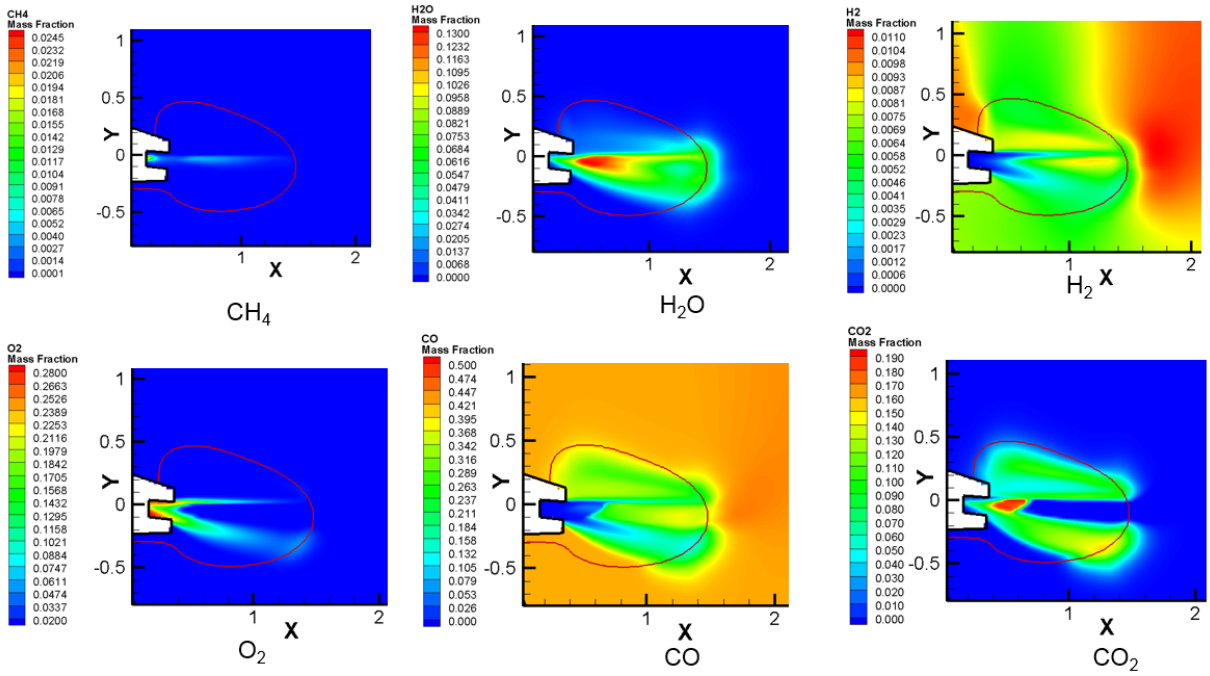

Figure 79. Predicted gas species distributions on a vertical cross-section of the raceway for the baseline case.

4.3.3 Investigation of Injection Lance Design

The primary focus of this study was the effects of injection lance design and location on co-injection combustion phenomena within the tuyere region. Two design modifications were tested. The first utilized an extended PCI lance with a cut tip angled to 45 degrees. In the second injection apparatus design modification, the auxiliary fuel injection lances were retracted by 6.35 cm (2.5 in) along their axes. The geometries used in the simulation of both of these cases are compared to the baseline geometry in Figure 80.

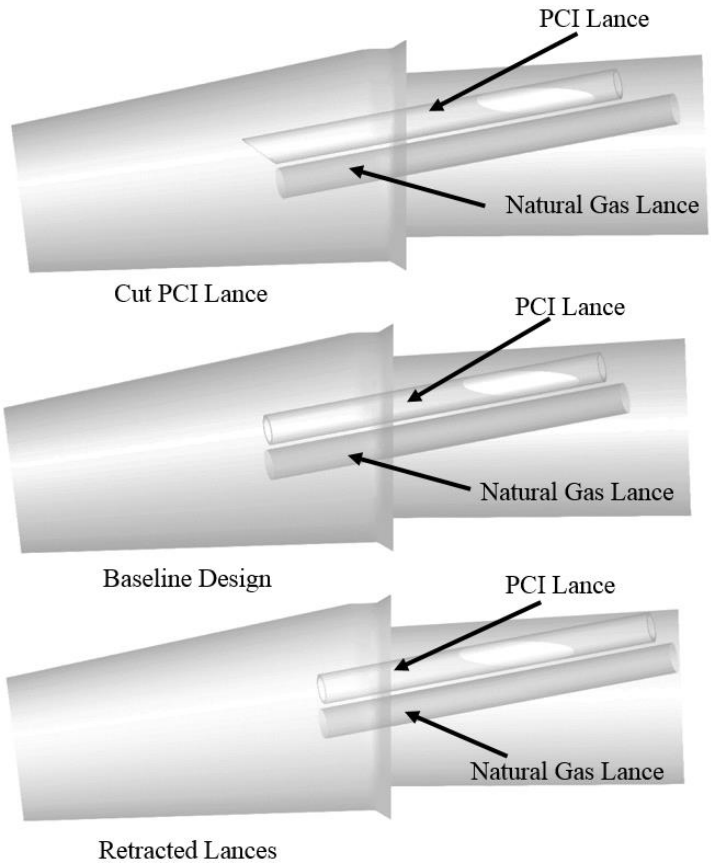

Figure 80. Geometry of tuyere injection region for the baseline design, cut PCI lance design, and retracted lance design.

Flow patterns inside the tuyere vary most between the baseline and retracted lance cases. Adjusting the entry position of both auxiliary fuels into the tuyere region leads to improved mixing of the natural gas flow and pulverized coal stream, and higher dispersion of pulverized coal particles throughout the tuyere. This phenomenon is detailed in Figure 81.

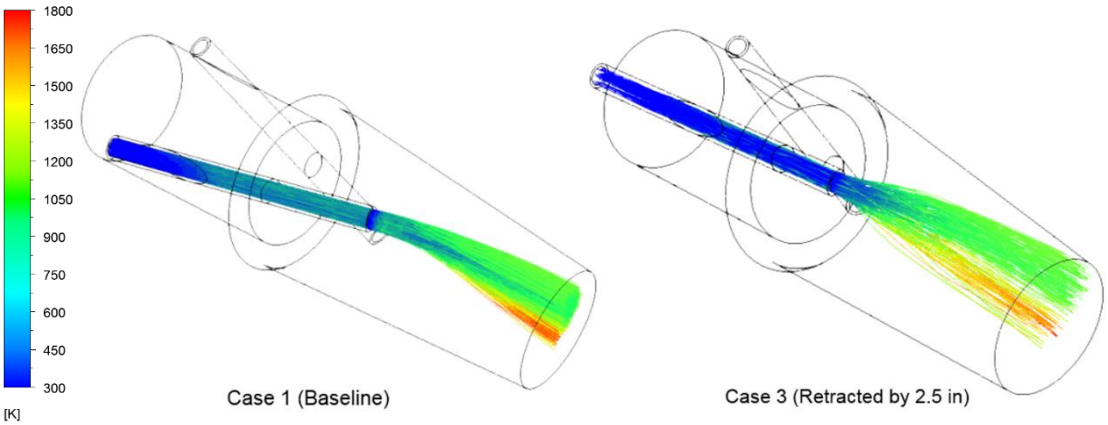

Figure 81. Path lines of coal particles through the tuyere, colored by temperature.

Table 7 details the combustion characteristics inside the tuyere for the three cases simulated.

Table 7. Comparison of tuyere combustion characteristics for Gary Works #14.

Case	Average Outlet Gas Temp (K) (±4%)	Natural Gas Consumption	Volatile Release Fraction
Case 1 (Baseline)	1580	36.1%	7.0%
Case 2 (Cut PCI lance)	1620	39.9%	9.0%
Case 3 (Retracted by 2.5 in)	1630	45.3%	33.0%

There are apparent advantages to retracting both lances, including an increase in devolatilization of nearly 20% compared to the baseline case. This increase is primarily due to rapid pre-heating of the pulverized coal particles through better mixing with the natural gas plume. However, these adjustments in injection design also present some potential drawbacks related to PCI lance reliability. When the design modifications proposed in case 2 (the cut tip lance) were implemented at the blast furnace, some PCI lances began to exhibit failures and cracks located roughly 19 cm from the lance tip. Examining the simulation results for case 2 provided possible explanations for the damage. Modifications in the lance geometry led to a minor increase in total convective and radiative heat transfer to the PCI lance surface in the location where the plant lances failed, as observed in Figure 81.

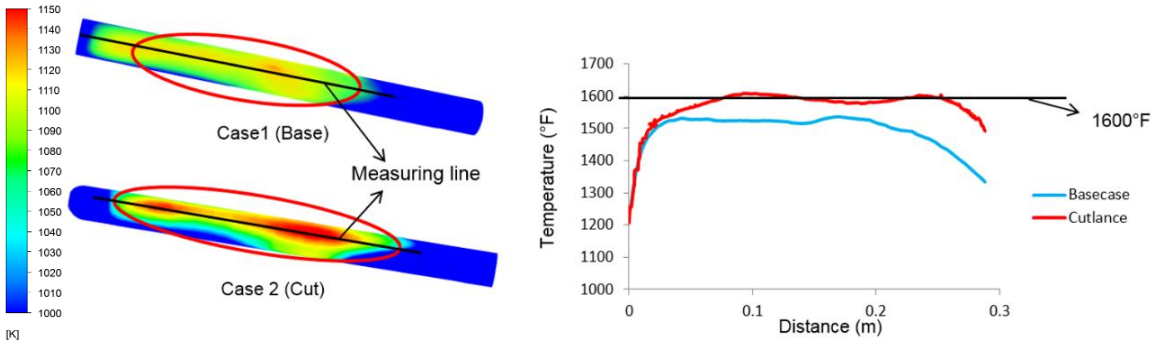

Figure 82. Contours of lance surface temperature (left) and lance surface temperature plotted along the measuring line (right).

The higher temperature region that resulted from this phenomenon, combined with the increased possibility for physical lance damage during the modification process likely led to the lance failures observed at U.S. Steel Gary Works.

4.3.4 Investigation of PCI Rate

In addition to the comparison of injection lance apparatus design, simulations of varied coal injection rates were performed to gain a better understanding of pulverized coal combustion characteristics under high injection rate conditions. With a fixed natural gas injection rate, five different PCI rates were compared through simulations in this study. In addition to the baseline case (124 kg/NTHM), simulations were conducted using injection rates of 100, 137.5, 150, 162.5, and 175 kg/NTHM. All cases utilized the standard injection apparatus design. As expected, Figure 82 and Table 8 indicate that gas temperature distributions, natural gas combustion rates, and devolatilization rates inside the tuyere do not vary significantly between cases.

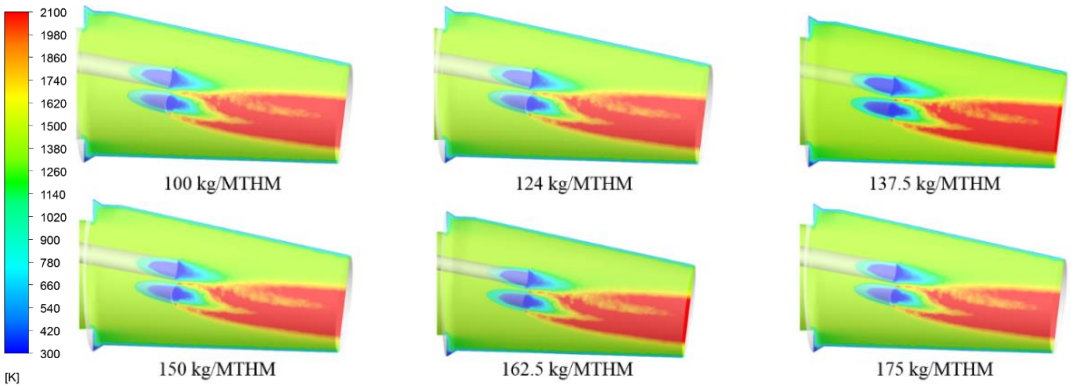

Figure 83. Gas temperature distribution on the tuyere center plane for each PCI rate case.

Table 8. Comparison of combustion properties for varied injection rate cases (tuyere).

Case	PCI rate (kg/mthm)	Average Outlet Temp (K) (±4%)	Natural Gas Consumption	Devolatilization
Case 4	100	1580	33.9 %	4.1 %
Case 1	124 (Baseline)	1580	33.7 %	4.2 %
Case 5	137.5	1575	33.4 %	4.0 %
Case 6	150	1575	33.5 %	4.2 %
Case 7	162.5	1575	33.2 %	4.1 %
Case 8	175	1575	33.3 %	4.1 %

More variation between cases becomes apparent through analysis of raceway combustion results, listed in Table 9. Simulations predict that fuel burnout rate over the raceway decreases as the PCI rate is increased from 100 to 150 kg/MTHM. Beyond 150 kg/MTHM, it appears that the fuel burnout rate reaches a plateau at the upper range of feasible injection conditions.

Table 9. Comparison of combustion properties for varied injection rate cases (raceway).

Case	PCI rate (kg/mthm)	Volatile burnout ratio	Char burnout rate	Total burnout rate
Case 4	100	50.9%	78.6%	68.0%
Case 1	124 (Baseline)	69.6%	64.3%	66.3%
Case 5	137.5	55.4%	57.6%	56.6%
Case 6	150	53.3%	47.6%	49.8%
Case 7	162.5	51.1%	46.6%	49.1%
Case 8	175	48.0%	50.1%	49.3%

The results from these simulations provide some basis for general industry experience indicating that most blast furnaces begin to encounter operational instability when striving for higher pulverized coal injection rates. These simulations indicate that insufficient mixing of pulverized coal with oxygen from the hot blast results in a significant fraction of the injected pulverized coal going unconsumed in the raceway. As previously mentioned, this can lead to poor coke bed permeability in the lower regions of the furnace, increased pressure drops, burden hanging, and other damaging phenomena. In order to achieve higher PCI rates, industry operators will need to explore adoption of new methods and designs, like those detailed throughout this research, including lance positioning, lance tip design, co-injection of natural gas, and other novel concepts. These methods can increase the combustion efficiency of injected fuels, improving furnace stability, increasing production rates, and reducing total furnace fuel consumption and operating expenditures.

CHAPTER 5. CONCLUSION AND FUTURE RESEARCH

5.1 Conclusion

5.1.1 CFD Model and Methodology Development

A multi-component 3-D CFD model for simulating gas flow and raceway formation under different hot blast and injection conditions and furnace geometries has been developed, calibrated, and implemented for the analysis of several industry-scale blast furnaces. This process consists of several sub-models, one for modeling the tuyere and blowpipe region, another for modeling the formation of the raceway, and a final model for combustion within the raceway. The entire raceway simulation methodology includes representations of the major flow and chemical reaction phenomena within the blast furnace raceway, including gas-solid combustion, devolatilization, solid particle motion, turbulence, heat and mass transfer, and raceway formation. Additionally, these models were validated against industrial measurement data and observations for multiple operating blast furnaces. The following list details the major model revisions and developments of this research.

1. A revised computational model for raceway formation has been developed through the course of this research. The formulation for interphase momentum exchange has been enhanced to better account for the high relative velocities between the tuyere jet and coke particle phase during the raceway formation simulation. This is accomplished via a revised calculation of particle drag coefficient to take into account the shifts in drag force and particle terminal velocity at high Reynolds numbers. The raceway size and shape match well with theoretical correlations as well as comparisons with industrial observations. Additionally, a new solver methodology for this model has been developed in FORTRAN. This development will allow the formation and combustion models to be seamlessly interfaced in a single, integrated solver. In this way, the two solvers can now utilize the same computational grid, and the total time necessary for computational simulation is significantly reduced. As an aside, this solver can be expanded upon in future research to develop a parallelized integrated blast furnace raceway model, further increasing

computational efficiency and expanding the range and breadth of conditions that could be modeled.

2. A methodology was developed for the calculation of a **RAFT analogue** from CFD simulation data. This value is calculated by taking a mass-weighted average of temperature for CO, H_2, and N_2, the final reducing gases produced after the reaction of all carbon, oxygen, and water vapor have reacted in the raceway and nearby coke bed. This RAFT analogue can be utilized to directly compare CFD predictions of raceway conditions with calculated RAFT values (based on mass and energy balance for a given set of operating conditions) utilized by furnace operators in the field. The computational RAFT analogue compared favorably to RAFT values from typical conditions at an industrial blast furnace, with a total variance of less than **2%.** The RAFT analogue both allows for extremely useful validation of CFD blast furnace modeling, and presents further opportunities to illuminate one of the most significant factors in blast furnace operation.

3. The distribution and combustion of injected fuels has a significant influence upon the corresponding distribution of gas temperatures in the raceway region. As previously mentioned, RAFT is traditionally calculated as a single uniform value for a given raceway. In the past, when blast furnace operation relied primarily on coke combustion with oxygen from the hot blast, this single value average was often acceptable. However, with the rise of injected fuels, combustion across the furnace raceway is often no longer uniform and symmetric. Modeling and visualization has indicated that there exist significant variations in gas temperature. With this in mind, this research has developed a new method to portray these variations in a manner useful to industrial furnace operators, referred to as the **Topographical Flame Temperature (TOFT)**. The TOFT presents previously unavailable information regarding furnace gas temperature distributions, helping to highlight the fundamental causes behind furnace wear, instability, and other factors. Additionally, the TOFT could be expanded into a kind of uniformity index to provide a single value by which the distribution of raceway gas temperature could be examined.

5.1.2 Research Findings

In this research, these CFD models were combined and utilized in conjunction with a unique analysis methodology to analyze and optimize operating conditions and designs of injection apparatuses for several blast furnaces through numerical simulation by varying auxiliary fuel injection rates, lance tip designs, injection position within the tuyere, and injection methods. Findings have been validated against industrial operations data and observed conditions within multiple furnaces. The major findings of the research studies conducted using this simulation methodology follow.

1. The **novel fuel injection techniques** explored in this research, primarily the alteration of PCI carrier gas from nitrogen/air to natural gas may present an as yet untapped method of enhancing injected auxiliary fuel combustion. Simulations have indicated that improved mixing and enhanced heat transfer under these conditions could increase fuel burnout rates by as much as **23%**. In addition, due to the removal of nitrogen as the carrier gas for pulverized coal, there is the potential for an increase in furnace production rate by nearly **2.5%**. This switch may present difficulties in industrial implementation; however, the potential benefits to fuel combustion within the raceway presents significant potential.

2. Utilizing the **Topographical Flame Temperature** distribution and **RAFT Analogue**, research regarding the effects of high-rate natural gas injection was conducted. While there are obvious benefits to NGI operation, including cost savings and reduction in char loading on the furnace, increased natural gas combustion leads to additional endothermic reactions within the raceway, consuming heat energy. The results of simulation studies clearly indicate an inverse correlation between the natural gas injection rate and a RAFT analogue, as well as a significant shift in the gas temperature distributions throughout the lower parts of the furnace. These changes could be exploited to improve campaign life, or they could lead to potential furnace instability due to reduced available heat. Regardless, it is crucial for operators in the field be aware of the potential effects of auxiliary fuel injection conditions, regardless of the economic incentives supporting natural gas injection.

3. When operating a pulverized coal injection system, careful attention must be paid to dispersion of the pulverized coal plume in order to ensure sufficient mixing of coal particles with oxygen. High plume dispersion, generated either through specific design modifications or through impingement of gas flows, typically results in better mixing between coal particles, carrier gas, and the hot blast air. Low plume dispersion can result in slower particle heating. This, in turn, may lead to low fuel burnout rates, and reduced furnace efficiency. Pulverized coal plume size can be monitored in the field through currently available methods such as tuyere cameras or peep-sight observation.

4. Related to finding 5, attempting high pulverized coal injection rates using standard lance injection techniques often presents serious difficulties for blast furnace stability due to low burnout rates. High PCI rates often lead to poor plume dispersion, resulting in poor heating of pulverized coal particles, low volatile release rates, and less oxygen/coal mixing. Unburned pulverized coal particles present significant potential detriments to furnace operation, as they enter the coke bed and decrease permeability. This reduction in permeability can lead to other concerns such as burden hanging, high pressure drops, and an increased possibility for blocked tuyeres. The modeling techniques utilized in this study can adequately predict pulverized coal burnout, however, further development may be necessary to accurately capture the movement of unburned particulates in the coke bed beyond the raceway, as well as any interactions they may have with the densely packed coke bed in the lower portions of the furnace.

5. Simulation studies have indicated that novel lance tip designs have a significant influence on gas flow distribution inside the tuyere, and can greatly improve the speed at which injected fuels are combusted. As previously mentioned, lances that can enhance gas mixing and pulverized coal plume dispersion can greatly assist improving reaction rates and fuel combustion in the raceway. Improved lance designs have potential for both pulverized coal and natural gas lances, with a focus on gas and coal plume dispersion in future research.

6. The simulations undertaken in this research indicate that there are significant potential benefits to modifying the natural gas injection position relative to the PCI location. Placing

the natural gas injection point upstream of the pulverized coal injection location in the tuyere can serve to enhance mixing of natural gas and pulverized coal, as well as dramatically increase devolatilization due to increased heat transfer. These phenomena result in an increase in injected fuel burnout in the range of **27%**, depending on operating conditions and specific furnace tuyere region design. However, it is noted that this modification should not be undertaken without first examining the potential impacts upon the PCI lance. As observed both in simulation results generated by this research work and previously published literature, natural gas combustion can lead to thermal damage to the pulverized coal lance, such as burning, sagging, and cracks. This damage can lead to unexpected shutdowns and capital expenditures, negating potential advantages gained through the enhanced combustion efficiency.

5.2 Future Research

Future research includes several areas of focus. These include the analysis of the combustion characteristics of natural gas and pulverized co-injection inside a CFD model of an industry operated test rig, exploration of the potential behind pre-heated natural gas injection in industrial blast furnaces, and further work to integrate existing models of the blast furnace shaft with the newly improved raceway formation simulation model detailed in this research.

Comparisons of the tuyere and blowpipe region model with experimental test runs at a Praxair facility are currently in progress as a part of work within the Steel Manufacturing Simulation and Visualization Consortium (SMSVC). Simulations will strive to further calibrate the CFD model, test the effects of various coal blends on combustion performance, and examine the impacts of new pulverized coal lance designs on combustion within the both CFD modeling and physical testing environments. These comparisons will also allow for a detailed study of any unique phenomena present in a physical test rig when compared to the CFD model.

Further research into the potential for pre-heating natural gas before injection into the tuyeres will be undertaken in the future. Theoretically, this approach could provide enough supplemental heat energy to operate the blast furnace raceway at higher natural gas injection levels without reducing gas temperatures in the furnace to levels below safe values for stable operation. Additionally, the

newly developed TOFT could be utilized to examine temperature distributions above the raceway to better quantify the causes of heavy wear on the furnace bosh and other regions. The TOFT may also be related to furnace operational stability, and further studies could seek to investigate whether large variations in temperature across the raceway relate to unstable furnace operation in practice.

Further upgrades to both the in-house raceway and shaft models could improve computational efficiency by allowing for automatic data transmission from the raceway to the shaft. Ongoing collaborative projects with Lawrence Livermore National Laboratory aim to parallelize both in-house CFD codes, allowing for the application of high performance computing to enhance the simulation process. Such efforts will be key to further progress in blast furnace modeling, as increased computational speed brings modeling closer to real-time analysis, potentially providing operators with new tools for analyzing individual furnaces under unique conditions.

REFERENCES

[1] Geerdes, M., Toxopeus, H., & van der Vliet, C. (2009). Modern Blast Furnace Ironmaking: An Introduction. Amsterdam: IOS Press.

[2] Suzuki, T., Smoot, L. D., Fletcher, T. H., & Smith, P. J. (1986). Prediction of High-Intensity Pulverized Coal Combustion. Combustion Science and Technology, 167-183.

[3] Poos, A., & Ponghis, N. (1990). Potentials and Problems of High Coal Injection Rates. 49th Ironmaking Conference Proceedings. Detroit, U.S.A.

[4] Lherbier, L. W., & Ricketts, J. A. (2015). Ironmaking in North America. Proceedings of AISTech 2015, (pp. 1443-1451). Cleveland, U.S.A.

[5] Wijayanta, A. T., Alam, M. S., Nakso, K., Fukai, J., Kunitomo, K., & Shimizu, M. (2014). Numerical Study on Pulverized Biochar Injection in Blast Furnace. ISIJ International, 1521-1529.

[6] Babich, A., Senk, D., & Gudenau, H. W. (2016). Ironmaking. Dusseldorf: Verlag Stahleisen GmbH.

[7] Babich, A., Gudenau, H. W., Senk, D., Formoso, A., Menedez, J. L., & Kochura, V. (2002). Experimental Modelling and Measurements in the Raceway when Injecting Auxiliary Substances. Proceedings of the International Blast Furnace Lower Zone Symposium, (pp. 16.1-14). Wollongong, Australia.

[8] Tada, S., Yabata, T., & Uehara, T. (1990). Coal Injection in the Blast Furnace. Future Ironmaking Processes Conference Proceedings. Hamilton, Canada.

[9] Ariyama, T., Sato, M., Yamakawa, Y., Yamada, Y., & Suzuki, M. (1994). Combustion Behavior of Pulverized Coal in Tuyere Zone of Blast Furnace and Influence of Injection lance Arrangement on Combustibility. ISIJ International, 476-483.

[10] Babich, A., Yaroshevskii, S., Formoso, A., Isidro, A., Ferreria, S., Cores, A., & Garcia, L. (1996). Increase of Pulverized Coal Use Efficiency in Blast Furnace. ISIJ International, 1250-1258.

[11] Sakurai, M., Mori, K., Cheng, A., Fanning, D., & Jere, T. (1998). Process Consideration for Coal Injection at National Steel's Great Lakes D-4 Blast Furnace. ICSTI/Ironmaking Conference Proceedings, (pp. 425-430). Toronto, Canada.

[12] Ponghis, N. (1998). Reduction of Blast Furnace Coke Rate: Coal Injection. ICSTI/Ironmaking Conference Proceedings, (pp. 365-372). Toronto, Cananda.

[13] Hur, N. S., Cho, B. R., Kim, H. D., & Heor, K. S. (1998). Reduction of Coke Rate to 310 kg/THM under the High Productivity at the Kwangyang No. 4 Blast Furnace. ICSTI/Ironmaking Conference Proceedings, (pp. 373-378). Toronto, Cananda.

[14] StaRosa, D., Fanning, D., Cheng, A., Sakurai, M., & Smith, N. (1998). Pulverized Coal Injection Start Up at National Steel's Great Lakes Division. ICSTI Ironmaking Conference Proceedings, (pp. 379-394). Toronto, Canada.

[15] Babich, A., Yaroshevskii, S., Formoso, A., Cores, A., Garcia, L., & Nozdrachev, V. (1999). Co-injection of Noncoking Coal and Natural Gas in Blast Furnace. ISIJ International, 229-238.

[16] Geerdes, M. (2015). Coal-Gas Co-Injection in Blast Furnaces: Are There Hidden Benefits. Proceedings of AISTech 2015, (pp. 908-816). Cleveland, U.S.A.

[17] Agarwal, J. C., Brown, F. C., Chin, D. L., & Stevens, G. S. (1999). Coinjection of Natural Gas and Pulverized Coal at High Levels: Field Test Results at USS/Gary. ISS Ironmaking Conference Proceedings, (pp. 105-134).

[18] Lherbier, L. W., & Riley, M. F. (2013). Fundamental Evaluation of Natural Gas Co-Injection with Coke Over Gas or Coal. Proceedings of AISTech 2013, (pp. 559-572). Pittsburgh, U.S.A.

[19] Holmes, D. J., Trenkinshu, S., & Zuke, D. A. (2013). Co-Injection of Pulverized Coal and Natural Gas on IH7 Blast Furnace. Proceedings of AISTech 2013. Pittsburgh, U.S.A.

[20] Feshchenko, S. A., Pleshkov, V. I., Lizunov, B. N., Lapshin, A. A., Sovelko, K. N., Loglnov, V. N., & Vasil'ev, L. E. (2007). Making Blast-Furnace Smelting More Efficient Through the Injection of Heated Natural Gas. Metallurgist, 605-611.

[21] Takeda, K., & Lockwood, F. C. (1997). Integrated Mathematical Model of Pulverized Coal Combustion in a Blast Furnace. ISIJ International, 432-440.

[22] Jamaluddin, A. S., Wall, T. F., & Truelove, J. S. (1986). Mathematical Modeling of Combustion in Blast Furnace Raceways, including injection of Pulverized Coal. Ironmaking and Steelmaking, 91-99.

[23] Nogami, H., Miura, T., & Furukawa, T. (1992). Simulation of Transport Phenomena around Raceway Zone in the lower part of the Blast Furnace. Tetsu-to-Hagane, 1222-1229.

[24] Guo, Y. C., Chan, C. K., & Lau, K. S. (2003). Numerical Studies of Pulverized Coal Combustion in a Tubular coal Combustor with Slanted Oxygen Jet. Fuel, 893-907.

[25] Picard, M. (2001). Pulverized Coal Combustion in the Blast Furnace Raceway, using a 3D Numerical Simulation. ISS Ironmaking Conference Proceedings, (pp. 229-239).

[26] de Castro, J. A., Nogami, H., & Yagi, J.-I. (2002). Numerical Investigation of Simultaneous Injection of Pulverized Coal and Natural Gas Injection with Oxygen Enrichment to the Blast Furnace. ISIJ International, 1203-1211.

[27] Gu, M., Chen, Z., Huang, D., Chaubal, P., & Zhou, C. Q. (2006). Heat Transfer, Devolatilization and Combustion of Injected Coal before Entering Raceways. Proceedings of AISTech 2006, (pp. 345-355). Cleveland, U.S.A.

[28] Guo, B., Zulli, P., Rogers, H., Mathieson, J. G., & Yu, A. (2005). Three-dimensional Simulation of the Combustion Behavior of Pulverized Coal Injection. Proceedings of the 5th International Symposium on Multiphase Flow, Heat Mass Transfer and Energy Conversion. Xi'an, China.

[29] Shen, Y., Yu, A., & Zulli, P. (2011). CFD Modelling and Analysis of Pulverized Coal Injection in Blast Furnace: An Overview. Steel Research International, 532-542.

[30] Pomeroy, D., & Morson, M. (2003). Mathematical Modeling of Blast Furnace Oil Injection. Proceedings of ISSTech 2003, (pp. 241-247).

[31] Walker, W., Gu, M., Selvarasu, N., D'Alessio, J., Macfadyen, N., & Zhou, C. Q. (2007). Numerical Study of Pulverized Coal Injection with Natural Gas Co-Injection in a Blast Furnace. Proceedings of AISTech 2007. Indianapolis, U.S.A.

[32] Walker, W., Gu, M., Selvarasu, N., D'Alessio, J., Macfadyen, N., & Zhou, C. Q. (2008). Simulation of Natural Gas and Pulverized Coal Combustion in a Blast Furnace and their Effects on Coke Consumption in the Raceway. Proceedings of AISTech 2008. Pittsburgh, U.S.A.

[33] Maldonado, D., Austin, P. R., Zulli, P., & Guo, B. (2008). Modelling Coal Combustion Behaviour in an Ironmaking Blast Furnace Raceway - Model Development and Applications. Proceedings of AISTech 2008. Pittsburgh, U.S.A.

[34] Austin, P. R., Chew, S. J., Maldonado, D., Mathieson, J. G., Pinson, D. J., Rogers, H., . . . Zulli, P. (2011). PC Injection Studies at Bluescope Steel. Proceedings of the 6th European Coke Ironmaking Congress.

[35] Shen, Y., & Yu, A. (2015). Characterization of Coal Burnout in the Raceway of an Ironmaking Blast Furnace. Steel Research International, 604-611.

[36] Majeski, A., Runstedtler, A., D'Alessio, J., Macfadyen, N., Ferron, K. J., & Zhao, Y. (2012). The Effects of Lance Positioning and Design on the Co-Injection of Pulverised Coal and Natural Gas into Blast Furnace. Proceedings of the 9th Intl. Conf. on CFD in the Minerals and Process Industries.

[37] Majeski, A., Runstedtler, A., D'Alessio, J., & Macfadyen, N. (2015). Injection of Pulverized Coal and Natural Gas into Blast Furnaces for Iron-making: Lance Positioning and Design. ISIJ International, 1377-1383.

[38] Schott, R. (2015). Optimization Strategies for Pulverized Coal Injection into the Blast Furnace. METEC and 2nd ESTAD Conference. Dusseldorf, Germany.

[39] Maier, C., Jordan, C., Feilmayr, C., Thaler, C., & Harasek, M. (2015). Numerical Analysis of Injection of Liquid Hydrocarbons, Processed Waste Plastics and Pulverized Coal into Blast Furnace Raceway. Proceedings of AISTech 2015, (pp. 1569-1580). Cleveland, U.S.A.

[40] Rajneesh, S., Sarkar, S., & Gupta, G. S. (2004). Prediction of Raceway Size in Blast Furnace from Two Dimensional Experimental Correlations. ISIJ International.

[41] Gupta, G. S., & Rudolph, V. (2006). Comparison of Blast Furnace Raceway size with Theory. *ISIJ International*, 195-201.

[42] Flint, P. J., & Burgess, J. M. (1992). A Fundamental Study of Raceway Size in Two Dimensions. Metallurgical Transactions B, 267-283.

[43] Szekely, J., & Poveromo, J. J. (1975). A Mathematical and Physical Representation of the Raceway Region in the Iron Blast Furnace. Metallurgical and Materials Transactions B, 119-130.

[44] Mondal, S. S., Som, S. K., & Dash, S. K. (2005). Numerical Predictions on the Influence of the Air Blast Velocity, Initial Bed Porosity and Bed Height on the Shape and Size of Raceway zone in a Blast Furnace. Journal of Physics: Applied Physics, 1301.

[45] Selvarasu, N. K., Gu, M., Zhou, C. Q., & Zhao, Y. (2007). Computer Modeling of Blast Furnace Raceway Formation Kinetics. Proceedings of AISTech 2007. Indianapolis, U.S.A.

[46] Versteeg, H. K., & Malalasekera, W. (1995). An Introduction to Computational Fluid Dynamics. London: Prentice Hall.

[47] Launder, B. E., & Spalding, D. B. (1972). Lectures in Mathematical Models of Turbulence. New York, U.S.A.: Academic Press.

[48] Kobayashi, H., Howard, J. B., & Sarofim, A. F. (1976). Coal Devolatilization at High Temperatures. 16th Symposium (Int.) on combustion.

[49] Ubhayakar, S. K., Stickler, D. B., Von Rosenberg Jr., C. W., Gannon, R. E. (1977). Rapid Devolatilization of Pulverized Coal in Hot Combustion Gases. Symposium (Int'l) on Combustion, 427-436.

[50] Baum, M. M., & Street, P. J. (1971). Predicting the Combustion Behavior of Coal Particles. Combustion Science and Technology, 231-243.

[51] Field, M. A. (1969). Rate of Combustion of Size-Graded Fraction of Char from a Low Rank Coal between 1200K-2000K. Combustion and Flame, 237-252.

[52] Magnussen, B. (1981). On the Structure of Turbulence and a Generalized Eddy Disspation Concept for Chemical Reaction in Turbulent Flow. 19th Aerospace Sciences Meeting. St. Louis, MO, U.S.A.

[53] Jazbek, M., Fletcher, D. F., & Haynes, B. S. (2000). Simulation of the Ignition of Lean Methane Mixtures using CFD Modeling and a Reduced Chemistry Mechanism. Applied Mathematical Modelling, 689-696.

[54] Syamlal, M., Rogers, W., & O'Brien, T. J. (1993). MFIX Documentation: Volume 1, Theory Guide. Springfield, VA, U.S.A.: National Technical Information Service.

[55] Ogawa, S., Umemura, A., & Oshima, N. (1980). On the Equation of Fully Fluidized Granular Materials. Journal of Applied Mathematics and Physics.

[56] Lun, C. K., Savage, S. B., Jeffrey, D. J., & Chepurniy, N. (1984). Kinetic Theories for Granular Flow: Inelastic Particles in Couette Flow and Slightly Inelastic Particles in a General Flow Field. Journal of Fluid Mechanics, 223-256.

[57] Gidaspow, D., Bezburuah, R., & Ding, J. (1992). Hydrodynamics of Circulating Fluidized Beds, Kinetic Theory Approach. Fluidization VII: Proceedings of the 7th Engineering Foundation Conference on Fluidization, (pp. 75-82). Brisbane, Australia.

[58] Ding, J., & Gidaspow, D. (1990). A Bubbling Fluidization Model Using Kinetic Theory of Granular Flow. AIChE Journal, 523-538.

[59] Chapman, S., & Cowling, T. G. (1990). The Mathematical Theory of Non-Uniform Gases. Cambridge, England: Cambridge University Press.

[60] Alder, B. J., & Wainwright, T. E. (1960). Studies in Molecular Dynamics II: Behaviour of a Small Number of Elastic Spheres. Journal of Chemical Physics.

[61] Wadell, H. (1943). The Coefficient of Resistance as a Function of Reynolds Number for Solids of Various Shapes. Journal of the Franklin Institute, 459-490.

[62] Liao, C. M., Lin, W. Y., & Zhou, L. X. (1997). Simulation of Particle-fluid Turbulence Interaction in Sudden-Expansion Flows. Powder Technology, 29-38.

[63] Halim, K. S. (2007). Effective Utilization of Using Natural Gas Injection in the Production of Pig Iron. Materials Letters, 3281-3286.

[64] Zhou, L. X. (1993). Theory and Numerical Modeling of Turbulent Gas-Particle Flows and Combustion. New York, U.S.A.: Science Press & CRC Press.

[65] Spalding, D. B. (1971). Mixing and Chemical Reaction in Steady Confined Turbulent Flames. *Symposium (Int.) on Combustion*, 649-657.

[66] Magnussen, B. F., & Hjertager, B. H. (1977). On Mathematical Modeling of Turbulent Combustion with Special Emphasis on Soot Formation and Combustion. *Symposium (Int.) on Combustion*, 719-729.

[67] Yan, R., Nader, M., & Norman, F. (2007). Kinetic Model for the Combustion of Coke Derived at Different Coking Temperatures. Energy & Fuels, 82-87.

[68] Zhou, L. X. (1986). *Combustion Theory and Chemical Fluid Dynamics.* Moscow, Russia: Science Press.

[69] Peters, N. (1979). Premixed Burning in Diffusion Flames - The Flame Zone Model of Libby and Economos. International Journal of Heat and Mass Transfer, 691-703.

[70] Bueters, K. A., Cogoli, J. G., & Habelt, W. E. (1974). Performance Prediction of Tangentially Fired Utility Furnaces by a Computer Model. Fifteenth Symposium (Intl.) on Combustion (pp. 1245-1260). Pittsburgh, PA, U.S.A.: The Combustion Institute.

[71] Lowe, A., Stewart, I. M., & Wall, T. F. (1978). The Measurement and Interpretation of Radiation from Fly Ash Particles in Large Pulverized Coal Flames. Seventeenth Symposium (Intl.) on Combustion (pp. 105-114). Pittsburgh, PA, U.S.A.: The Combustion Institute.

[72] Fiveland, W. A. (1991). The Selection of Discrete Ordinate Quadrature Sets for Anisotropic Scattering. *Fundamentals of Radiation Heat Transfer*, 89-96.

[73] Nogami, H., Yamaoka, H., & Takatani, K. (2004). Raceway Design for the Innovative Blast Furnace. ISIJ International, 2150-2158.

[74] Zhou, C. Q. (2008). CFD Modeling for High rate Pulverized Coal Injection (PCI) to Blast Furnaces. U.S. Dept. of Energy.

[75] Chen, Y., Silaen, A., Zhao, J., Zhao, Y., D'Alessio, J., Capo, J. C., & Zhou, C. Q. (2015). Simulation of Natural Gas Combustion Liftoff and Blowout Phenomenon in Blast Furnace. TMS Summit 2015.

[76] Celik, I. B., Ghia, U., Roache, P. J., & Freitas, C. J. (2008). Procedure for Estimation and Reporting of Uncertainty Due to Discretization in CFD Applications. *ASME Journal of Fluids Engineering*, p.4.

[77] Patankar, S. V. (1980). Numerical Heat Transfer and Fluid Flow. New York: Hemisphere Publishing Corporation.

[78] Vasquez, S. A., & Ivanov, V. A. (2000). A Phase Coupled Method for Solving Multiphase Problems on Unstructured Meshes. ASME 2000 Fluids Engineering Division Summer Meeting. Boston.

[79] Copeland, C., & Street, S. (2013). A Practical Engineering Approach to Improving the Reliability of Blast Furnace Tuyeres. Iron and Steel Technology, 47-62.

[80] Babich, A., Gudenau, H. W., Mavrommatis, K., Froehling, C., Cores, A., & Garcia, L. (2002). Choice of Technological Regimes of a Blast Furnace Operation with Injection of Hot Reducing Gases. Revista De Metallurgia, 288-305.

[81] Okosun, T., Street, S. J., Zhao, J., Wu, B., & Zhou, C. Q. (2017). Influence of Conveyance Methods for Pulverized Coal Injection in a Blast Furnace. Ironmaking and Steelmaking, 513-525.

[82] Okosun, T., Street, S. J., Chen, Y., Zhao, J., Wu, B., & Zhou, C. Q. (2015). Investigation of Co-Injection of Natural Gas and Pulverized Coal in a Blast Furnace. Proceedings of AISTech 2015 (p. 14). Cleveland: AIST.

[83] Okosun, T., Street, S. J., Zhao, J., Wu, B., & Zhou, C. Q. (2016). Investigation of Dual Lance Designs for Pulverized Coal and Natural Gas Co-Injection. Proceedings of AISTech 2016 (pp. 581-594). Pittsburgh: AIST.

[84] Zhou, D., Cheng, S., Zhang, R., Li, Y., Chen, T. (2017). Uniformity and Activity of Blast Furnace Hearth by Monitoring Flame Temperature of Raceway Zone. *ISIJ International*, 1509-1516.

[85] Pistorius, P. C., Gibson, J., & Jampani, M. (2017). Natural Gas Utilization in Blast Furnace Ironmaking: Tuyere Injection, Shaft Injection and Prereduction. *Applications of Process Engineering Principles in Materials Processing, Energy and Environmental Technologies*, 283-292.

[86] Silaen, A. K., Okosun, T., Chen, Y., Wu, B., Zhao, Y., D'Alessio, J., . . . Zhou, C. Q. (2015). Investigation of High Rate Natural Gas Injection through Various Lance Designs in a Blast Furnace. Proceedings of AISTech 2015 (p. 10). Cleveland: AIST.

[87] Okosun, T., Liu, X., Silaen, A. K., Barker, D., Dybzinksi, D. P., & Zhou, C. Q. (2017). Effects of Blast Furnace Auxiliary Fuel Injection Conditions and Design Parameters on Combustion Characteristics and Injection Lance Wear. Proceedings of AISTech 2017 (p. 12). Nashville: AIST.

VITA

Tyamo Okosun was born in Holland, MI. He received a Bachelor of Science in Mechanical Engineering in May of 2009 from Purdue University Northwest (formerly Calumet), in Hammond, IN. He then went on to obtain a Master of Science in Mechanical Engineering in August of 2012 from Purdue University, in West Lafayette, IN. He joined the research group at the Center for Innovation through Visualization and Simulation (CIVS), directed by Professor Chenn Q. Zhou at Purdue University Northwest (formerly Calumet) in 2011. He began work on his Ph.D. in Mechanical Engineering at Purdue University in West Lafayette in 2012. He expects to be granted his Doctor of Philosophy in Mechanical Engineering in May of 2018.

Through the course of his studies, he has written two journal papers directly based upon this research, one pending publication review, and one currently published in the journal *Ironmaking and Steelmaking*. Additionally, he has published and presented three conference papers based on this research at AISTech, the Iron and Steel Technology Conference. A complete list of his current publications is included on the following page. Publications based directly on this research have won the following awards.

- 2016 Josef S. Kapitan Award for Ironmaking – Awarded to: *Investigation of Co-Injection of Natural Gas and Pulverized Coal in a Blast Furnace*
- 2017 Josef S. Kapitan Award for Ironmaking – Awarded to: *Investigation of Dual Lance Designs for Pulverized Coal and Natural Gas Co-Injection*
- 2017 Hunt-Kelly Outstanding Paper Award (AIME) – Awarded to: *Investigation of Co-Injection of Natural Gas and Pulverized Coal in a Blast Furnace*

PUBLICATIONS

T. Okosun, X. Liu, A. K. Silaen, D. Barker, D. P. Dybzinksi, C. Q. Zhou, "Effects of Blast Furnace Auxiliary Fuel Injection Conditions and Design Parameters on Combustion Characteristics and Injection Lance Wear," Proceedings of AISTech 2017, 11 p., 2017

T. Okosun, S. J. Street, J. Zhao, B. Wu, C. Q. Zhou, "Influence of Conveyance Methods for Pulverized Coal Injection in a Blast Furnace," *Ironmaking and Steelmaking*, p. 513–525, 2017

T. Okosun, S. J. Street, J. Zhao, B. Wu, C. Q. Zhou, "Investigation of Dual Lance Designs for Pulverized Coal and Natural Gas Co-Injection," Proceedings of AISTech 2016, p 581–594, 2016

T. Okosun, A. K. Silaen, G. Tang, B. Wu, C. Q. Zhou, "CFD Analysis of Blast Furnace Operating Conditions Impacts on Operational Efficiency," *CFD Modeling and Simulation in Materials Processing*, p.75, 2016

D. Wang, W. Zhang, D. Liu, X. Chen, G. Tang, T. Okosun, B. Wu, C. Q. Zhou, "CFD Simulation of a 6-Cylinder Diesel Engine Intake and Exhaust Manifold," ASME International Mechanical Engineering Congress and Exposition, Proceedings (IMECE), v 7B, 2015

T. Okosun, C. Q. Zhou (2015) "Computational Examination of Utility Scale Wind Turbine Wake Interactions," Journal of Fundamentals of Renewable Energy and Applications, Vol. 5, Issue 4, July 14, 2015

T. Okosun, X. Liu, Y. Liu, J. Dekker, J. Moreland, C. Q. Zhou, "Development of a Wake Simulator for Wind Energy Analysis," Proceedings of the 47th Summer Computer Simulation Conference, SCSC 2015, *Simulation Series*, v 47, n 10, p. 88–94, 2015

T. Okosun, S. J. Street, Y. Chen, J. Zhao, B. Wu, C. Q. Zhou, "Investigation of Co-Injection of Natural Gas and Pulverized Coal in a Blast Furnace," Proceedings of AISTech 2015, p. 1581–1594, 2015

A. K. Silaen, T. Okosun, Y. Chen, B. Wu, J. Zhao, Y. Zhao, J. D'Alessio, J. C. Capo, C. Q. Zhou, "Investigation of High Rate Natural Gas Injection Through Various Lance Designs in a Blast Furnace," Proceedings of AISTech 2015, p. 1536–1549, 2015

B. Wu, G. Tang, X. Chen, C. Q. Zhou, C. P. Colella, T. Okosun, "Optimization of a Urea Decomposition Chamber using CFD and VR," Applied Thermal Engineering, v 70, n 1, p 827 – 837, 2014

J. Moreland, S. Dubec, T. Okosun, X. Wang, C. Q. Zhou, "A 3D Wind Turbine Simulator for Aerodynamics Education," ASME International Mechanical Engineering Congress and Exposition, Proceedings (IMECE), v 5, 2013

N. Yan, T. Okosun, S. K. Basak, D. Fu, J. Moreland, C. Q. Zhou, "Numerical Simulation and Virtual Reality Visualization of Horizontal and Vertical Axis Wind Turbines," Proceedings of the ASME Design Engineering Technical Conference, v 2, PARTS A AND B, p 1507–1514, 2011